

BUILDING OF
THE 21CM FRONT END RECEIVER
FOR
THE GIANT METREWAVE RADIO TELESCOPE

THESIS
SUBMITTED TO THE
BANGALORE UNIVERSITY
FOR THE DEGREE OF
M.Sc Engg. (BY RESEARCH)

BY
A.RAGHUNATHAN

CS&IS

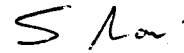
RAMAN RESEARCH INSTITUTE
Bangalore - 560080, INDIA
January 2000

CERTIFICATE

We certify that this thesis submitted by Sri. **A. RAGHUNATHAN** is based on the work carried out by him under our guidance. It is also certified that this thesis or any other part of it has not been previously submitted for any other degree or diploma to this university or any other university.



(Dr. A. SRINIVASAN, GUIDE)
Professor (PG Studies) & PG
Co-ordinator
Dept. of PG Studies
B.M.S College of Engineering
Bangalore-19



(Dr. RAVI SUBRAHMANYAN, GUIDE)
Scientist
RAMAN RESEARCH INSTITUTE
Bangalore-80

Date : - - 1999
Bangalore -85

DECLARATION

The work presented in this thesis is carried out by me in Raman Research Institute, Bangalore, India. I hereby declare that the results embodied therefo are bonafide and has not been previously submitted for any other degree or diploma either in this University or any other University.



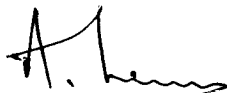
(A. RAGHUNATHAN)

ENGINEER

RAMAN RESEARCH INSTITUTE

BANGALORE-85

CERTIFIED



(Dr. A. SREENIVASAN)

Dr. A. SREENIVASAN

Professor (P.G. Studies) & P.G. Co-ordinator

Dept. of Post Graduate Studies

B.M.S. College of Engineering

BANGALORE-560019



(DR. RAVI SUBRAHMANYAN)

Date : - - 1999

Bangalore -85

ACKNOWLEDGEMENTS

I thank Prof. N.Kumar - Director of Raman Research Institute for giving me an opportunity to carry on the work on GMRT 21 cm receiver in the Radio Astronomy Laboratory. I sincerely thank Prof. N.V.G. Sarma for his guidance on several aspects of this project.

I thank my advisers Dr. Ravi Subrahmanyan and Dr. A. Sreenivasan for their help in the matter related to this thesis. I take this opportunity to express my gratitude to Ravi Subrahmanyan for having taught me the techniques of radio astronomy.

I remain indebted to Dr. D.K.Ravindra without whose help I would not have been able to do this project. His constant encouragement enabled me to carry on the project quite successfully.

I thank Prof. V.Radhakrishnan, Dr.A.A. Deshpande and Dr. N.Udaya Shankar for their useful comments and suggestions on several aspects of my work on microwave background temperature measurements.

Building of 21cm front end receiver is the team work of several people in the Radio Astronomy Laboratory. Prof. Sarma is the driving force in every aspect of this project. He developed the broad band feed assembly for this 21cm front end receiver. Dr. Vivek Dhawan developed a total power test receiver to characterise the GMRT dish. Shaji and Smiles did some initial work in the design and building of the feed. Sarabagopalan's painstaking work on optimising the dimensions of the probes in the orthomode transducer helped in increasing the bandwidth of the feed assembly with good VSWR. Seetha, Sadik and Verghese developed the uncooled low noise amplifier. Imtiyaz designed and built both narrow and wide bandpass filters required for the receiver. Girish with great patience characterised most of the receivers with well documentation. Kasthuri, Sandhya and Raghavendra built and tested several rf modules used in this receiver. I thank all the above persons for their monumental contributions to this project.

I thank Ateequlla, Manohar, Gangadhar and their group members for getting done all the necessary fabrications in the workshops.

I thank Dr. Ratnakar and his colleagues for having helped me at all the times during my literature survey in the library.

I thank the photographer Raju Verghese for the excellent colour photographs of the system.

I thank all the people at Gauribidanur for providing me all the necessary help during the time of my observation.

Finally I thank all the staff members once again who have directly or indirectly helped me in completing this project.

BUILDING OF 21CM FRONT END RECEIVER FOR GIANT METRE WAVE RADIO TELESCOPE

SYNOPSIS

Giant metre wave radio telescope is a national facility available for the research work in the field of radio astronomy. It is a fourier synthesis array of 30 parabolic dish antennae each of 45 m diameter. Each antenna consists of six receivers for the observation at 50 MHz, 150 MHz, 233 MHz, 327 MHz, 610 MHz and 1420 MHz. The receiver for the frequency 1420 MHz - more generally called 21cm receivers are built for radio observations in the frequency range 1000 to 1450 MHz. These receivers are constructed for the astronomical observations of hydrogen gas in our galaxy and external galaxies. This is achieved by receiving the spectral line emissions from neutral hydrogen atoms. The receiver is made wide band so as to enable the observation of red shifted hydrogen lines originating from hydrogen gas a very large distance from us. The red shifting of the radiation implies that the signal associated will be observed at lower frequencies. The feeds are designed to be of prime focus type and hence the receivers containing them are mounted at the prime foci of the GMRT antennae.

Cosmology is the study of the properties and evolution of the universe including the galaxies and their distribution structure. Among several theories put forward for the study of the evolutionary process, BIG BANG theory enjoys much of support from the observational basis. This theory predicts that there should be a thermal radiation in the universe originating from the explosive expansion that took place millions of years of ago while forming the universe. It also says that the present day radiation temperature must be about 3K. This temperature is measured using the 21cm front end receiver built for GMRT after incorporating suitable modifications to it.

Chapter I of this thesis describes mainly the terminologies, basic concepts and techniques associated with the radio telescopes, chapter II describes the design and construction and measurement of 21cm receiver built for Giant metrewave radio telescope (GMRT), chapter III describes the cosmic microwave background radiation temperature measurement experiment conducted using the receiver built for GMRT.

CONTENTS

	Page No.
CHAPTER 1. RADIO ASTRONOMY TELESCOPES	
1.1 FLUX DENSITY	1
1.2 BRIGHTNESS AND BRIGHTNESS TEMPERATURE	1
1.3 RESOLVING POWER OF THE ANTENNA	2
1.4 APERTURE EFFICIENCY	3
1.5 ANTENNA POLARIZATION	4
1.5.1 STOKES PARAMETERS	
1.6 ANTENNA TEMPERATURE	5
1.7 RECEIVER TEMPERATURE	7
1.8 MINIMUM DETECTABLE TEMPERATURE (SENSITIVITY)	8
1.9 EFFECT OF SYSTEM INSTABILITY ON THE SENSITIVITY	9
1.10 CALIBRATION OF THE RECEIVER	10
REFERENCES	12
CHAPTER 2. 21 CM RECEIVER FOR THE GIANT METER WAVE RADIO TELESCOPE	 13
2.1 CORRUGATED HORN	18
2.1.1 FLARE ANGLE ($2\theta_0$)	18
2.1.2 DISTANCE BETWEEN THE PHASE CENTRE AND THE LAST CORRUGATION (R)	19
2.1.3 THE DIMENSIONS OF CORRUGATIONS	19
2.2 ORTHOMODE TRANSDUCER (OMT)	21
2.2.1 DESIGN OF OMT	22
2.2.2 PERFORMANCE CHARACTERISTICS OF HORN AND OMT	25
2.2.2.1 MEASUREMENT OF THE RADIATION PATTERN	27
2.2.2.2 VSWR MEASUREMENT OF OMT	27
2.2.2.3 MEASUREMENT OF THE INSERTION LOSS OF THE OMT	28
2.3 LOW NOISE AMPLIFIER (LNA)	29
2.3.1 ANALYSIS	29
2.3.2 TOTAL GAIN OF THE LNA	29
2.3.3 NOISE FIGURE OF AN AMPLIFIER	33
2.3.4 USE OF FEEDBACK TECHNIQUE	34

2.3.5	MEASUREMENT OF THE PERFORMANCE CHARACTERISTICS OF THE LNA	37
2.3.5.1	MEASUREMENT OF THE GAIN AND RETURN LOSS OF THE LNA	37
2.3.5.2	MEASUREMENT OF THE NOISE FIGURE OF THE LNA AND THE STRENGTH OF THE CALIBRATION SIGNAL	40
2.4	POST AMPLIFIER	41
2.4.1	DESIGN OF THE POST AMPLIFIER	41
2.5	PHASE SWITCH BOX	43
2.5.1	DESIGN OF PHASE SWITCH BOX	46
2.5.2	PERFORMANCE CHARACTERISTICS OF THE PHASE SWITCH	46
2.6	NARROW BAND PASS FILTERS	46
2.6.1	DESIGN OF THE NARROW BANDPASS FILTERS	49
2.6.2	PERFORMANCE CHARACTERISTICS OF THE NARROW BANDPASS FILTERS	49
2.7	WIDE BANDPASS FILTERS	49
2.8	NOISE GENERATOR	53
2.8.1	DESIGN OF THE NOISE GENERATOR MODULE	53
2.9	POWER SUPPLY FOR THE 21 CM FRONT END RECEIVER	58
2.10	RF MONITOR AND CONTROL CARD	58
2.11	MEASUREMENT OF SYSTEM TEMPERATURE	58
2.12	MEASUREMENT OF THE APERTURE EFFICIENCY	62
2.13	POLARISATION IN THE 21 CM FRONT END RECEIVER	63
	REFERENCES	64

CHAPTER 3. MEASUREMENT OF COSMIC MICROWAVE BACKGROUND TEMPERATURE USING THE GMRT 21 CM FRONT END RECEIVER

3.1	INTRODUCTION	65
3.2	DISTORTIONS IN THE COSMIC MICROWAVE BACKGROUND RADIATION SPECTRUM	67
3.3	MODIFICATIONS TO THE 21 CM FRONT END RECEIVER	68
3.3.1	MINIMIZATION OF THE GROUND LEAKAGE	71
3.3.1.1	DESIGN OF THE CORRUGATED PLATE	71
3.3.1.2	DESIGN OF THE ALUMINIUM SHIELD	75
3.4	CALIBRATION OF A PLATINUM RESISTANCE THERMOMETER	76
3.5	INTRODUCTION OF A CIRCULATOR BETWEEN THE OMT AND LNA	78
3.6	THE DATA ACQUISITION SYSTEM	80
3.7	MEASUREMENT OF THE RECEIVER TEMPERATURE (T_R) AND	

	CALIBRATION-SIGNAL TEMPERATURE (T_{cal})	81
3.8	MEASUREMENT OF THE REFLECTION COEFFICIENT (Γ) OF THE FEED ASSEMBLY	84
3.9	MEASUREMENT OF THE ABSORPTION COEFFICIENT OF THE FEED ASSEMBLY	86
3.10	ESTIMATE OF THE GALACTIC CONTRIBUTION (T_{Gal})	88
3.11	ESTIMATE OF THE ATMOSPHERIC CONTRIBUTION (T_{atm})	91
3.12	ESTIMATE OF THE GROUND CONTRIBUTION (T_{gnd})	92
3.13	MEASUREMENT OF THE COSMIC MICROWAVE BACKGROUND TEMPERATURE	93
3.14	COMPARISON WITH THE PREVIOUS MEASUREMENTS	96
	REFERENCES	97
	CONCLUSIONS	98

CHAPTER 1

RADIO ASTRONOMY TELESCOPES

Radio astronomy telescopes are the tools by which astronomers study the radio frequency electromagnetic radiation from celestial objects. The telescopes are expected to collect the electromagnetic radiation incident on an area of the ground and amplify them to detectable levels. The telescopes also focus the research by selectively collecting the electromagnetic radiation with specific polarization components from a required sky region and amplifying them. The quality of a receiver is its ability to reject unwanted and spurious electromagnetic radiation present in the environment and present the required signal with a high signal to noise ratio to the astronomer's detection apparatus.

The value of any celestial observation made with a receiver depends on the precision in the characterization and calibration of the receiver. These enable one to accurately relate the detected quantities to the celestial parameters and thereby quantify the astrophysical phenomena precisely.

The telescope essentially consists of an antenna element, a transducer, an associated network that couples polarization components to the transmission lines, amplifiers, filters and, perhaps, heterodyning systems to down convert the frequency band of interest to a particular frequency range in which it may be more convenient to construct and operate detectors.

This chapter is an introduction to the terminology, basic concepts and techniques associated with radio telescopes. References for further reading are provided at the end of the chapter.

1.1 FLUX DENSITY

The energy in electromagnetic radiation from a celestial object that is incident on a unit area per unit time is called the *flux*. The power per unit frequency interval is called the *flux density*. The unit in which the flux density is usually quoted is the Jansky which is equal to 10^{-26} Watts of power incident per square metre per Hertz bandwidth.

1.2 BRIGHTNESS AND BRIGHTNESS TEMPERATURE

When the antenna beam solid angle is smaller than the angular extent of the celestial source being observed, the antenna is said to have *resolved* the source. Celestial sources usually emit differently over various parts of their projected sky area. The *brightness* or specific intensity towards any sky position in a resolved celestial source is the flux density per unit solid angle that is received from an infinitesimal solid angle along the line of sight.

Brightness of the sky in any direction is usually measured in units of Watts per square metre per Hertz per steradian.

The brightness of the sky in any direction and at any particular frequency may be quoted in terms of the temperature of a black body that has an identical brightness at the same frequency. The brightness of a blackbody at any frequency depends only on its temperature and this relationship is given by the Planck's radiation law:

$$B(\nu) = \frac{2h\nu^3}{c^2(e^{\frac{h\nu}{kT}} - 1)}, \quad (1.1)$$

where ν is the frequency (Hz), T is the temperature of the blackbody (K), k is the Boltzmann's constant and h is the Planck's constant. This relation simplifies to

$$B(\nu) = \frac{2kT\nu^2}{c^2} \quad (1.2)$$

at frequencies where $h\nu \ll kT$; this asymptotic form of the radiation law is known as the Rayleigh-Jeans' approximation. The approximation is usually adopted as a law to quote the brightness of the sky at radio frequencies in a temperature scale. The equivalent temperature, as given by this 'formula', corresponding to the brightness of the sky at any frequency is called the *brightness temperature* of the sky. In other words, the brightness temperature towards any sky direction is the temperature T of a fictitious black body (whose brightness-temperature relation is given by equation 1.2 rather than 1.1) which would have the same specific intensity $B(\nu)$ at the frequency of observation as that towards the particular sky direction.

1.3 RESOLVING POWER OF THE ANTENNA

The resolving power of any antenna is determined by its radiation pattern which may be characterised in terms of the half power beam width or beam width between nulls. The *half power beam width* (HPBW) is defined as the angular size of the locus of directions at which the power transmitted will be half of the maximum power which is transmitted along the axis of the main lobe; if the locus is elliptic, the HPBWs are usually quoted along the major and minor axes. Similarly, the *beam width between nulls* is defined as the angular separation between the nearest directions on opposite sides of the main lobe axis at which zero power gets transmitted. The antenna is said to have a better resolving power if its HPBW is smaller.

The beam pattern can also be defined in terms of the beam solid angle (Φ_A) and main beam solid angle (Φ_M). They are defined by the expression

$$\Phi = \int P(\theta)d\Omega, \quad (1.3)$$

where $P(\theta)$ is the normalized power radiated per unit solid angle in any direction θ and in an infinitesimal solid angle $d\Omega$, with the normalization being the peak power radiated along

the axis of the antenna. When the integration is restricted to the main lobe, we get the *main beam solid angle* Φ_M and when the integration is over 4π steradians we get the *beam solid angle* Φ_A . The beam solid angle is the angle through which all the power from a given antenna gets transmitted if the power per unit solid angle were constant over this angle and equal to the maximum value. The main beam solid angle is the same as the beam solid angle except that the power transmitted is bounded by the first minima of the radiation pattern. Antennas with small main beam solid angles are highly directional: most of the radiated power is confined to a small solid angle. Conversely, a receiving radio astronomy antenna with a small main beam solid angle will primarily receive power from a small sky patch.

Main beam efficiency of an antenna is defined as the ratio of the main beam solid angle to the beam solid angle. It is a measure of its efficiency in transmitting the power fed to it in its main lobe when used as a transmitter. So a transmitter with high main beam efficiency will radiate most of the power through the main lobe and only a small percentage of it through side lobes and back lobes. When the antenna is used as a receiver, a poor main beam efficiency results in the pickup of undesired signals through side lobes along with the desired signal in the main lobe and this may worsen the signal to noise ratio.

$$\text{Main beam efficiency} = \left[\frac{\Phi_M}{\Phi_A} \right]. \quad (1.4)$$

1.4 APERTURE EFFICIENCY

A celestial radio source of a known flux density may be observed by a radio astronomy telescope by pointing its antenna towards the source. If the antenna beam well exceeds the angular extent of the source, the power available at the output terminals of the antenna will be proportional to the *effective area* of the antenna. The effective area of an antenna at any frequency mainly indicates its ability in collecting the sky radiation at that particular frequency. An exact relationship exists between Φ_A and the effective area A_e :

$$\Phi_A = \frac{\lambda^2}{A_e}, \quad (1.5)$$

where λ is the wavelength of operation. When the antenna consists of a concentrator (*e.g.* a parabolic reflector) along with a focal feed system (*e.g.* a horn), the effective area is usually less than the geometric area of the concentrator since the antenna surface is usually not uniformly illuminated by the feed: the antenna surface is illuminated in such a way that the power density at the edge is much smaller than the on-axis gain. This tapering of the illumination from on-axis to off-axis is called *edge taper* of an antenna. The amount of taper or, equivalently, the illumination pattern is selected on the basis of the amount of rejection one desires of the noise contribution from the earth through the side lobes of the feed pattern.

The aperture efficiency indicates how effectively the antenna is used in collecting the radiations coming from the sky. *Aperture efficiency* is defined as the ratio of effective collecting

area (A_e) to the physical collecting area (A_{phy}). Usually trade offs are made between S/N ratio and the aperture efficiency of the antenna. If one adopts a uniform illumination of the antenna surface, a high collecting area can be achieved. But at the same time the unwanted noise contributed by other sky sources, terrestrial interference and the ground gets received through the enhanced sidelobes and, consequently, the S/N ratio at the receiver input deteriorates. Therefore, the aperture is illuminated in such a way as to get minimum sidelobe level and a moderate collecting area.

$$\text{Aperture Efficiency} = \left[\frac{A_e}{A_{phy}} \right]. \quad (1.6)$$

Usually the effective collecting area is smaller than physical collecting area and the aperture efficiency is always less than 100%. It may be noted that these considerations are relevant only for compound antenna systems, *e.g.* secondary feeds illuminating primary apertures: a simple thin dipole, which is a non-filled type of an antenna, has its aperture efficiency greater than 100% since its effective aperture area is much greater than its physical area.

1.5 ANTENNA POLARIZATION

Celestial radio frequency radiation is, in general, polarised. Any antenna output terminal can be coupled only to one polarisation state of the incoming wave. Information or power in the orthogonal polarization mode will not be received and hence may be lost. Therefore, in order to receive the complete information in the sky signal, the antenna must be equipped to receive two orthogonal components of the incoming wave; these may be a pair of orthogonal linear polarization components or circularly polarised components or, in general, any pair of orthogonal elliptically polarized components of the incident wave. Astronomers usually describe the incoming radiation using Stokes parameters and may compute the degree of polarization, angle of polarization or the power in any polarization component from the Stokes parameters.

1.5.1 STOKES PARAMETERS

Adopting a right-handed cartesian coordinate system, the polarization state of any incident electromagnetic wave can be characterised with the help of two electric components (E_x and E_y) orthogonal to each other and to the direction of propagation of the wave (which is assumed to be along the z-direction). The resultant field vector ($E = E_x + E_y$) at any position in space traces an ellipse in the x,y-plane with time whose major axis subtends an angle τ w.r.t the x-direction. This angle is called the *Tilt angle* of the ellipse. The ratio of the major axis to the minor axis of the ellipse is called the *Axial ratio* (AR). ϵ is an alternate parameter used to describe the polarization ellipse and is defined as

$$\epsilon = \cot^{-1}(AR). \quad (1.7)$$

The power in the radiation components with fields along the x and y directions are given by

$$S_x = \frac{E_x^2}{Z} \quad \text{and} \quad S_y = \frac{E_y^2}{Z}, \quad (1.8)$$

where Z is the characteristic impedance of the medium.

A set of parameters (I , Q , U and V) are formed using the quantities S_x , S_y , ϵ and τ and these describe fully the polarization properties of the electromagnetic wave. These parameters are called Stokes parameters and are defined as:

$$I = S_x + S_y, \quad (1.9)$$

$$Q = S_x - S_y, \quad (1.10)$$

$$U = (S_x - S_y)\tan(\tau), \quad \text{and} \quad (1.11)$$

$$V = (S_x + S_y)\sin(2\epsilon) \quad (1.12)$$

where I represents the total flux density of the incoming wave, Q and U represent the linear polarization components of the wave and V represents the circular polarization component of the wave. All these Stokes parameters are measured by radio astronomers in units of flux density, the Jy.

Various polarization parameters of the incoming wave like the degree of polarization, angle of polarization, percentage of circular polarization etc. may be computed from the Stokes parameters:

$$\text{Degree of Polarization} = \frac{\sqrt{Q^2 + U^2 + V^2}}{I} \quad (1.13)$$

$$\text{Degree of Linear Polarization} = \frac{\sqrt{Q^2 + U^2}}{I} \quad (1.14)$$

$$\text{Degree of Circular Polarization} = \frac{V}{I} \quad (1.15)$$

$$\text{Angle of Polarization} = \frac{1}{2} \tan^{-1} \left[\frac{U}{Q} \right] \quad (1.16)$$

Using the above four Stokes parameters one can characterise any incoming wave which is arbitrarily polarized. The level of complexity involved in deriving the polarization characteristics of the incoming wave from antenna measurements depends on whether one uses linearly polarized or circularly polarised antenna feeds.

1.6 ANTENNA TEMPERATURE

The thermal noise power available at the terminals of a resistor which is at T K physical temperature is given by $P = kTB$ W, where B is the frequency bandwidth. In radio astronomy, it is customary to represent power in terms of temperature. So we simply indicate T K to imply a power per Hertz of value kT . Similarly, an *antenna temperature* of value T_a is used to imply that a power per Hertz of value kT_a is available at the antenna output terminals.

It may be noted that T_a is simply a measure of the power that appears at the antenna terminals and need have no relation to the physical temperature of the antenna. However, if the ideal antenna were enclosed in a blackbody cavity that is maintained at a temperature T , the power available at the antenna terminals would correspond to an antenna temperature T . It follows that if the antenna were lossless (zero ohmic losses and perfectly impedance matched to free space), the antenna temperature corresponds to the average brightness of the sky as seen by the antenna beam, where the averaging is weighted by the antenna power pattern.

Practical antennas are lossy. The loss is of two types: (i) reflective loss and (ii) Ohmic loss. The reflective loss occurs due to the impedance mismatch between the antenna and free space and the ohmic loss occurs due to the dissipation in the finite resistance of the antenna elements. In effect, both the above losses reduce the celestial power coupled by the antenna system to the antenna output terminals. Ohmic loss not only reduces the signal, but also worsens the signal-to-noise ratio at the antenna output because the lossy elements add their own thermal noise to the celestial signal.

We assume that

T_a'' is the sky signal incident on the antenna,

T_a' is the sky signal coupled into the antenna system,

T_a is the (sky + noise) signal present at the output terminals of the antenna,

α is the power absorption coefficient of the antenna due to its finite resistance,

γ is the voltage reflection coefficient of the antenna due to its impedance mismatch, and

T_{amb} is the ambient temperature = physical temperature of lossy antenna elements.

Because of the impedance mismatch between the sky and the antenna, not all the power T_a incident on the antenna will get into the system. Only a portion of it will be accepted and the rest will be reflected. The amount of power accepted by the system is given by

$$T_a' = (\text{Incident power} - \text{reflected power}) = (T_a'' - T_a''\gamma^2). \quad (1.17)$$

Similarly, due to the finite resistance of the antenna, some portion of the accepted signal will be absorbed and, in addition, thermal noise will be added to the signal by the resistance of the system. Therefore, the net sky signal power available will be $T_a'(1 - \alpha)$ and the net noise power will be $(T_{amb}\alpha)$. Hence, the total signal available at the output terminals of the antenna is given by

$$T_a = [T_a'(1 - \alpha) + T_{amb}\alpha] \quad (1.18)$$

or

$$T_a = T_a''(1 - \gamma^2)(1 - \alpha) + T_{amb}\alpha. \quad (1.19)$$

With respect to an antenna output terminal, any electromagnetic wave can be resolved into two components: (i) matched polarization component (S_p) and (ii) orthogonal unmatched polarization component (S_c). The total flux density S is always equal to the sum of the flux densities of the matched polarization component and that of the unmatched polarization component. If the incident radiation is unpolarised, then the flux density of the matched polarization component (S_p) will be equal to that of unmatched polarization component (S_c) and each of them will be equal to $S/2$.

An antenna having a single output is sensitive to only the matched polarization component of the incoming wave. If A_e is the effective area of the antenna, the power available at the input to the antenna system is

$$P = S_p B A_e = \left(\frac{S}{2}\right) B A_e, \quad (1.20)$$

where B is the frequency bandwidth; it is assumed that the incident radiation is unpolarised. Expressed in temperature units, the effective sky power, or the antenna temperature owing to the sky (T_a^{sky}) that is available at the output of the antenna system is

$$T_a^{sky} = \left(\frac{S}{2k}\right) A_e. \quad (1.21)$$

This net sky signal that is available from the antenna at the antenna output terminal has been previously expressed in terms of the sky power T_a'' as $T_a''(1 - \gamma^2)(1 - \alpha)$ and is dependent on its reflective and ohmic losses. Because both these losses decrease the amount of sky signal available at the antenna output terminal, these losses may also be viewed as decreasing the effective collecting area of the antenna system and, therefore, result in poorer aperture efficiency.

1.7 RECEIVER TEMPERATURE

The amplifier used for the amplification of the sky signal collected by the antenna itself contributes (adds) its own noise. This noise power is quantified by an equivalent noise temperature T_R . The *receiver temperature* of an amplifier may be defined as the noise power (in units of temperature) that must be added at the input terminal of an ideal noiseless amplifier with the same gain in order to produce the same noise power at its output. If the amplifier has a gain G , an amplifier with noise temperature T_R contributes an equivalent noise power kT_R per unit bandwidth referred to its input and a noise power GkT_R per unit bandwidth referred to its output.

Assume that a receiver has N amplifiers connected in series following the antenna feed system; these have gains G_1, G_2, \dots, G_N and their noise temperatures are $T_{R1}, T_{R2}, \dots, T_{RN}$. The net noise temperature as referred to the input of the first amplifier is given by

$$T_R = T_{R1} + \frac{T_{R2}}{G_1} + \frac{T_{R3}}{G_1 G_2} \dots \dots \dots + \frac{T_{RN}}{G_1 G_2 \dots G_N} \quad (1.22)$$

From the above relation it is clear that if the gain of the first stage amplifier (G_1) is sufficiently high, the noise temperature of the entire receiver chain will be mainly dependent on the noise temperature of the first stage amplifier alone. If the gain of first stage amplifier is very high, then the noise contributions of other amplifiers will be considerably reduced. Therefore, the first stage amplifier should be designed to have as low a noise temperature as possible along with a sufficiently high gain G_1 . This amplifier is usually designed to be a *Low Noise Amplifier*.

The *system temperature* T_{sys} of any receiver is defined to be the sum of the receiver temperature T_R and the antenna temperature T_a . As defined here, the system temperature is referred to the output terminal of the antenna which is the same as the input terminal of the low noise amplifier.

1.8 MINIMUM DETECTABLE TEMPERATURE (SENSITIVITY)

Any receiver which measures the total noise power from the antenna is called a 'Total Power Receiver'. The basic configuration of the total power receiver consists of an antenna connected to a low noise amplifier followed by other other amplifiers and filters whose output finally drives a square-law detector. The square law detector converts the power at its input into an equivalent dc output. Heterodyning may or may not be present in the receiver system.

We assume that

T_{sys} is the system temperature of the receiver,

T_n is the noise component, *i.e.* the system temperature excluding the power owing to the astronomical signal of interest,

ΔT is the antenna temperature due to the astronomical signal: this is to be detected and measured,

$\Delta \nu$ is the pre-detection bandwidth of the system,

τ is the post-detection integration time,

$\Delta \nu_{LF}$ is the post-detection bandwidth of the integrator, $\Delta \nu_{LF} \approx \tau^{-1}$

G is the total gain of the system,

V_{dc} is the total detector-integrator output voltage,

v_{dc} is the detector-integrator output voltage corresponding to the power ΔT .

The detector-integrator output voltage is proportional to the system temperature and is given by

$$V_{dc} = G[kT_{sys}\Delta\nu] = G[kT_n\Delta\nu + k\Delta T\Delta\nu]. \quad (1.23)$$

By applying a suitable bias at the output of the detector, the voltage due to the noise temperature T_n may be subtracted. Then the residual voltage v_{dc} at the detector-integrator output will be proportional to $(k\Delta T\Delta\nu)$. The corresponding power in this mean d.c. signal at the detector output is given by

$$P_{dc}(\text{mean signal}) \propto [k\Delta T\Delta\nu]^2. \quad (1.24)$$

This mean signal, whose value is to be determined as a measure of the power in the astronomical signal of interest, will fluctuate due to the stochastic nature of the pre-detection voltage corresponding to T_{sys} . The fluctuations at the output of the detector may be viewed as being due to beats between the different frequency components of the voltage waveform entering the detector. The variance in this fluctuation about the mean signal is given by

$$P_{dc}(\text{noise}) \propto [kT_{sys}]^2 \Delta\nu \Delta\nu_{LF}, \quad (1.25)$$

assuming that $\Delta\nu_{LF} \ll \Delta\nu$.

The *sensitivity*, or the *minimum detectable temperature* ΔT_{min} of any total power receiver is defined to be the signal noise temperature ΔT which produces at the detector-integrator output a dc power $P_{dc}(\text{mean signal})$ equal to the rms noise in the detector-integrator output: $P_{dc}(\text{noise})$.

From the above equations it follows that the receiver sensitivity

$$\Delta T_{min} = \left[\frac{T_{sys}}{\sqrt{\Delta\nu\tau}} \right]. \quad (1.26)$$

In practice, the telescope is pointed at the astronomical source and a $P_{dc}(\text{mean signal})$ corresponding to $T_{sys} = T_n + \Delta T$ is measured with an uncertainty given by ΔT_{min} given in equation (1.26). A separate measurement is made of the system noise part T_n by, *e.g.*, pointing the telescope off-source on the sky in a continuum measurement or, in the case of a spectral-line measurement, the observing band may be shifted off in frequency and away from a line feature that causes the ΔT ; the noise in the offset measurement is again given by equation (1.26). The separate measurements are then differenced to obtain the $P_{dc}(\text{mean signal})$ corresponding to ΔT . Simple difference measurements with a time τ devoted to integration at each measurement position would have a sensitivity that is factor $\sqrt{2}$ worse than that given by equation (1.26).

1.9 EFFECT OF SYSTEM INSTABILITY ON THE SENSITIVITY

A detector in a total power receiver cannot distinguish between an increase in the sky signal power and an increase in the total system gain. From equation (1.23) it is clear that the detector output voltage is proportional to T_{sys} . If V_D represents the detector output voltage due only to T_{sys} , then

$$V_D = G(KT_{sys}\Delta\nu). \quad (1.27)$$

If G , the total gain of the receiver, increases by a small factor f , then the above equation becomes

$$V_D = Gf(KT_{sys}\Delta\nu) \quad (1.28)$$

This may also be written as

$$V_D = G[K(fT_{sys})\Delta\nu] \quad (1.29)$$

which simply means that the effect of any increase in gain is the same as a rise in system temperature. The receiver output fluctuations due to gain variations are independent of the fluctuations resulting from the system temperature. Since the two variations are independent of each other, the net variation at the detector output will be the quadrature sum of the individual variations. Hence, the sensitivity of total power receiver may be stated as

$$\Delta T_{min} = T_{sys} \sqrt{\frac{1}{\Delta\nu\tau} + \frac{\Delta G^2}{G^2}}, \quad (1.30)$$

where ΔG is the rms variations in the total system gain G .

This necessitates a stabilization of the system gain in order to make the variance contribution from gain fluctuations ($\Delta G^2/G^2$) sub-dominant. The usual practice is to calibrate the receiver gain at frequent intervals of time.

1.10 CALIBRATION OF THE RECEIVER

A commonly adopted method of calibrating the system gain is to inject a certain amount of noise into the system close to its input and measure the system response. This is performed during the period of observation in order to remove the effects of system gain variations. The gain variations can also be calibrated out by Dicke switching in which case the receiver input is periodically switched between the antenna and a reference load which is at a standard temperature. Switching is done at a sufficiently high rate so that both the antenna and the reference load approximately see the same system gain during any switching period and, consequently, the gain variations do not limit the certainty in the power measurement.

To illustrate the effect of Dicke switching, let

T_c be the reference load temperature,

T_a be the antenna temperature,

V_1 represent the detected voltage of the receiver when connected to the antenna:

$$V_1 = G(T_R + T_a), \text{ and}$$

V_2 represent the detected voltage of the receiver when connected to the load:

$$V_2 = G(T_R + T_c).$$

The measured quantities V_1 and V_2 may be used to compute a gain-independent quantity:

$$x = \frac{V_1 - V_2}{V_2} = \frac{G(T_a - T_c)}{G(T_R + T_c)} = \frac{T_a - T_c}{T_c + T_R}. \quad (1.31)$$

Hence,

$$T_a = T_c + x(T_c + T_R). \quad (1.32)$$

From these considerations it is clear that if the receiver is switched sufficiently rapidly between a load and antenna, the antenna temperature may be measured unaffected by gain variations. This measurement requires stable and known reference load and receiver temperatures.

REFERENCES

Christiansen, W.N., Hogbom, J.A., 1985, Radio Telescopes, Cambridge University press, Cambridge.

Kraus, J.D., 1986, Radio Astronomy, Cygnus-Quasar Books, Ohio.

Steinberg, J.L., Lequeux, J., 1963, Radio Astronomy, translated by R.N. Bracewell, McGraw-Hill Book Company, New York.

CHAPTER 2

21 CM RECEIVER FOR THE GIANT METREWAVE RADIO TELESCOPE

The Giant Metrewave Radio Telescope (GMRT) is a Fourier synthesis array of 30 parabolic dish antennae each of 45 m diameter. The radio telescope is located near Khodad in Maharashtra. 21 cm front end receivers have been built for radio observations in the frequency range 1000 to 1450 MHz using the GMRT. These receivers were constructed for astronomical observations of Hydrogen gas in our Galaxy and in external galaxies by the reception of 1420.4 MHz spectral line emission from neutral Hydrogen atoms. Because external galaxies at increasing distances from our Galaxy appear to recede away from us with increasing line-of-sight velocities, the receivers have been constructed with a wide bandwidth so as to be able to detect the gas at extremely large distances from us: the line radiation from distant galaxies appear red-shifted to lower frequencies. The receivers are mounted at the prime focii of the GMRT antennae. The construction of these 30 receivers forms the major work carried out for this thesis. An outline of the receiver configuration is given in the following paragraph; details of the design and performance characteristics are given in the remainder of this chapter.

Figs. 2.0(a),2.0(b) show the block diagrams of the 21 cm front end receiver. The receiver has a corrugated horn to collect the radiation reflected from the parabolic dish. The radiation collected is routed through an orthomode transducer in which the waveguide mode of signal is converted into co-axial mode. In the orthomode transducer two linear components of the incoming signal are picked up in two perpendicular directions which are designated as V and H channels. Each of the two signals coming out in these two channels pass through identical electronics. The co-axial signal is then amplified by a low noise amplifier and further by a few post amplifiers. For the purpose of calibration of the receiver, four different levels (Low, Medium, High and Extra-High CAL) of noise may be injected from a noise generator module into the system. The noise injection is done at the input of the low noise amplifier. This noise signal injected for the purpose of calibration is usually called Calibration signal (CAL signal). The choice of the calibrator noise level may be made depending on the requirement: usually the CAL temperature is selected to be about 10% in power as compared to the total system temperature. For example, if the system temperature (T_{sys}) is very high while observing an extremely strong source like the Sun, then High CAL is selected. On the other hand, if a weak celestial source is being observed and T_{sys} is at its minimum, then Low CAL signal is selected for calibrating the system. The amplified signal is 0-180° phase modulated using Walsh functions in a phase switch module; this enables the rejection of any common mode coupling of spurious signals into the signal path following the phase-switch. The phase modulated rf signal passes through a narrow bandpass filter where it is band limited to 120 MHz. Then it passes through another wide band pass filter having 3 dB bandwidth of

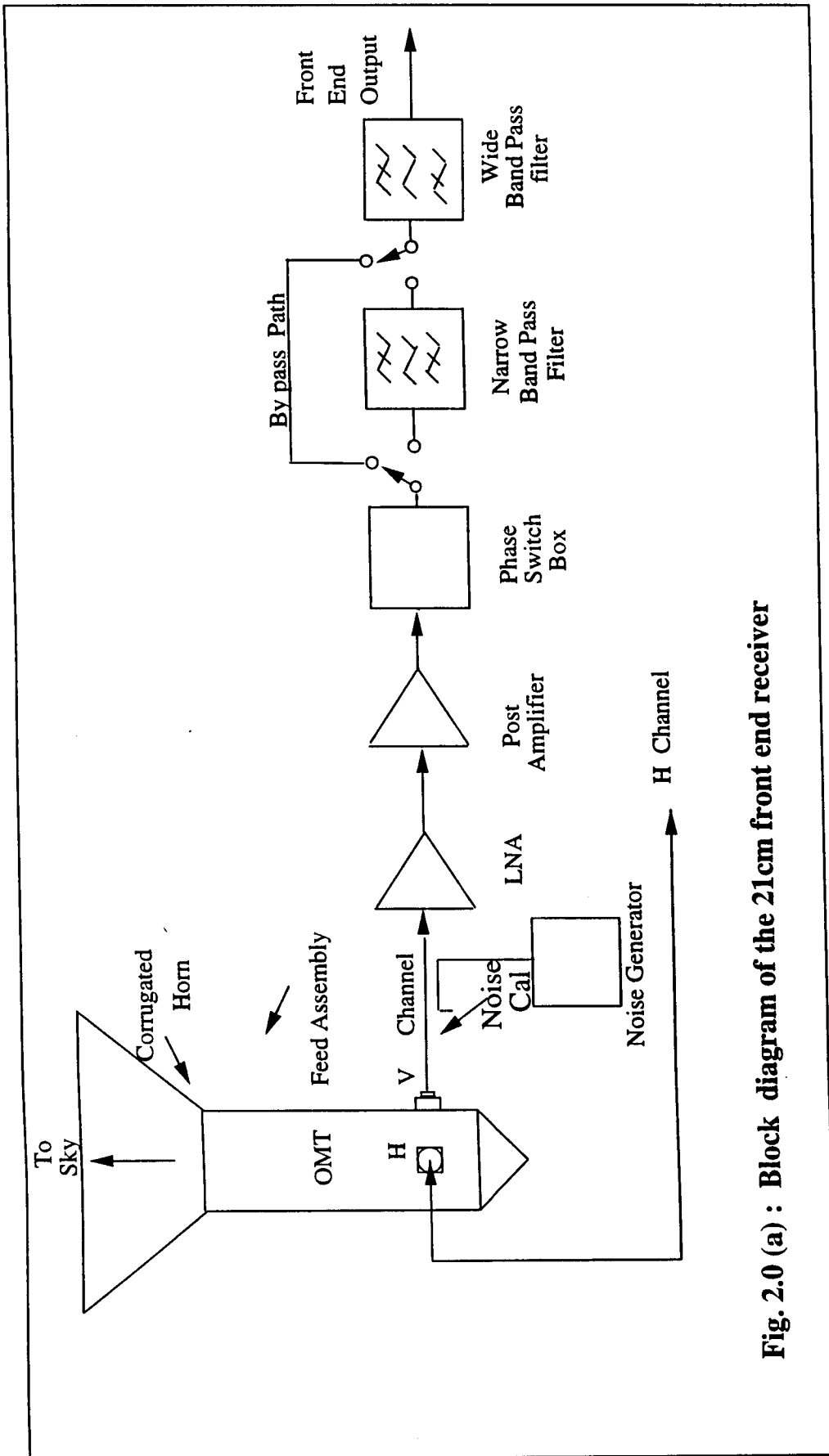
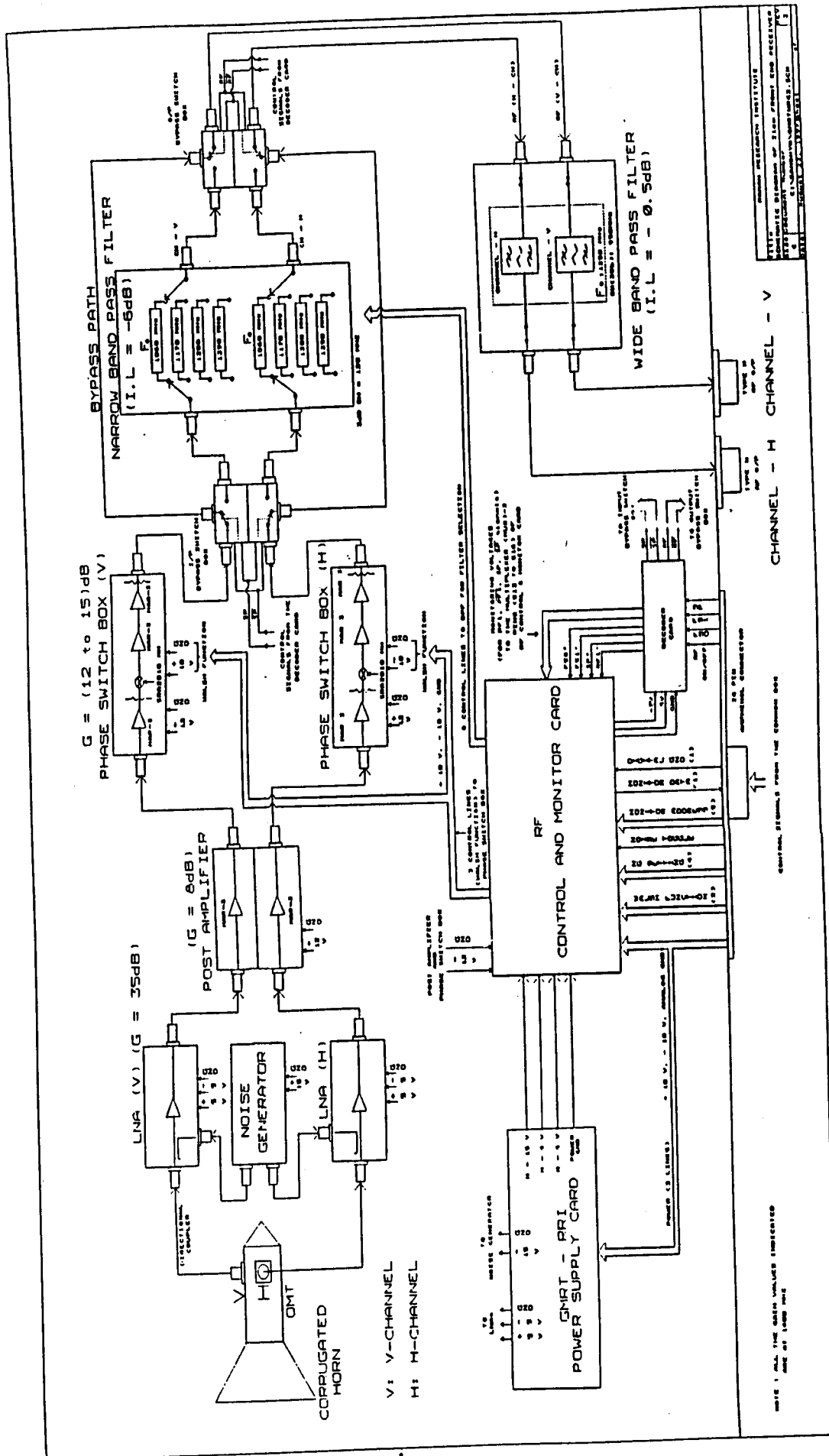


Fig. 2.0 (a) : Block diagram of the 21cm front end receiver



RESEARCH INSTITUTE
 3150
 100
 100
 100

Fig. 2.0(b) : SCHEMATIC DIAGRAM OF 21cm FRONT END RECEIVER

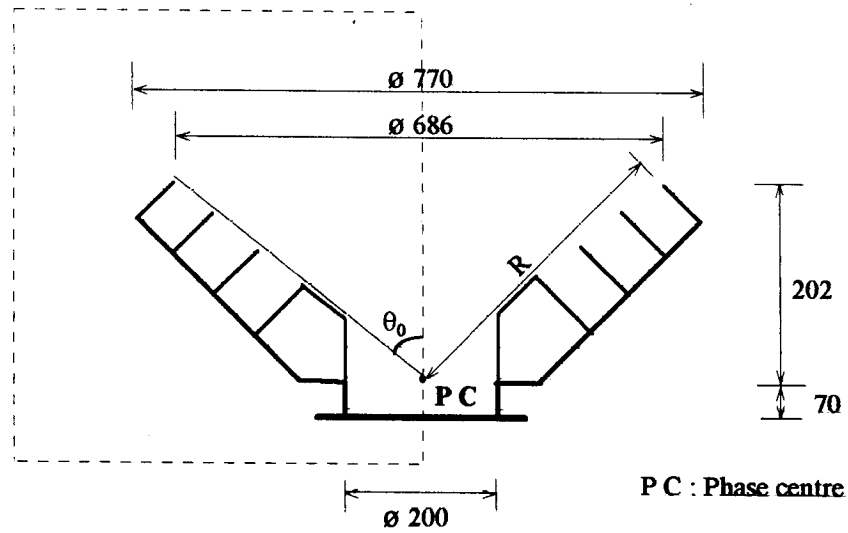
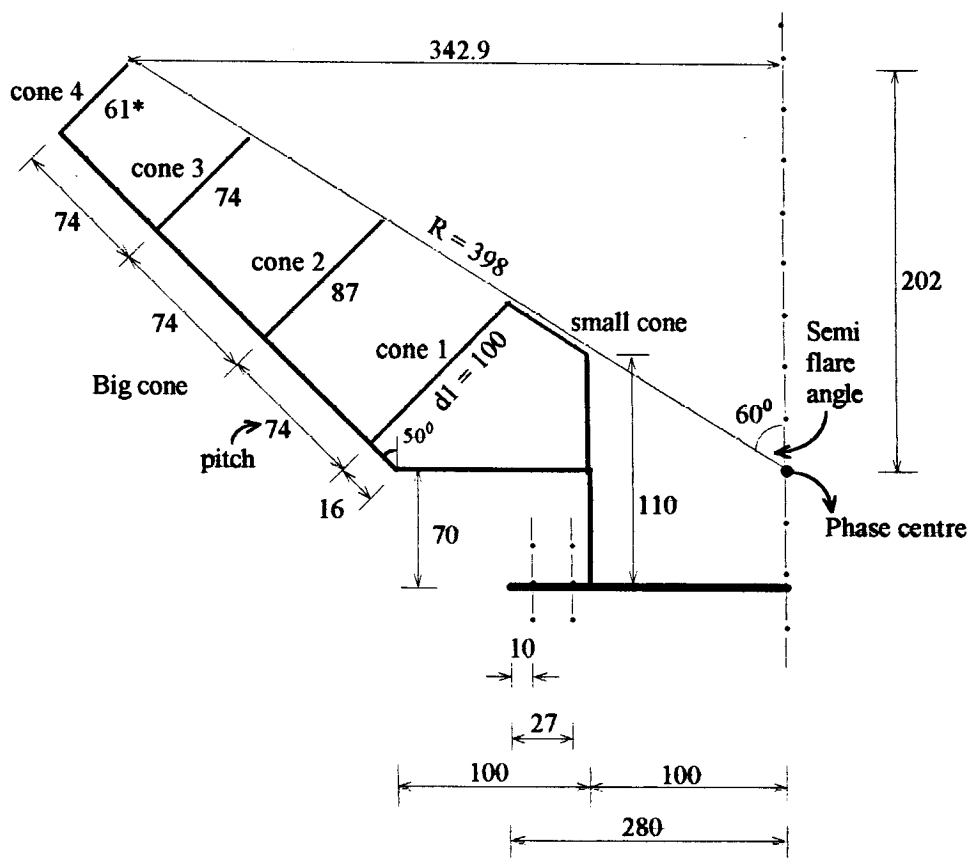


Fig. 2.1.1 a : Schematic diagram of Corrugated Horn of GMRT 21cm Front End Receiver



* Width of the metal vane
All dimensions are in mm

Fig. 2.1.1b : Expanded view of the dotted portion shown in fig. 2.1.1a

about 550 MHz. The main purpose of these filters is to reject the unwanted out-of-band noise from the rf signal. There are four narrow band pass filters in the frequency range 1.0 to 1.45 GHz; adjacent filters overlap at their 3 dB points. Any one of the four narrow band filters may be selected depending on the frequency of observation. A provision is made at the input of the bank of narrow band pass filters to bypass them so that a 550 MHz wide band rf signal may, if necessary, be obtained at the receiver output.

2.1. CORRUGATED HORN

The horn is designed to be a prime focus feed to illuminate the 45 m diameter parabolic reflectors of the GMRT antennae. This feed is designed to have nearly uniform illumination with a low spill-over and identical V and H plane radiation patterns. It should also possess very low side lobe and back lobe structures along with good cross polar properties. The phase centres of the horn in both E and H planes must be as close to each other over a wide range of frequencies. Design had to be carried out in such a way that the horn possesses all the above desired properties over the frequency band 1.0 to 1.45 GHz. The schematic diagram of the corrugated horn is shown in Fig. 2.1.1 .

While designing a corrugated prime focus horn feed, three parameters are to be determined. They are

- (i) Flare angle ($2\theta_o$),
- (ii) Distance R between the phase centre and the last corrugation, and
- (iii) The dimensions of corrugations.

2.1.1 FLARE ANGLE ($2\theta_o$)

The flare angle is not influenced by the absolute values of F and D , where F and D are respectively the focal length and aperture diameter of the dish, but by their ratio (F/D). The optimum value of F/D for a uniform aperture illumination and low spill over is found out to be equal to 0.4. For this value of F/D , the semi-flare-angle θ_o of the horn is obtained from the relation (Rudge et al, 1982)

$$\tan \frac{\theta_o}{2} = \frac{0.25}{(F/D)}. \quad (2.1)$$

For

$$\frac{F}{D} = 0.412, \quad \text{we get } \theta_o = 62.5^\circ. \quad (2.2)$$

Any horn with a semi-flare-angle greater than 30° is called a *wide flare angle horn*. The energy radiated by a wide flare angle horn is confined to an angular sector which is mainly determined by the horn flare angle rather than its aperture dimension. So the radiation pattern at any frequency is dependent only on the flare angle rather than the linear dimensions of the horn. As a consequence, identical radiation patterns exist at all frequencies. Therefore,

the beam width remains constant over a wide range of frequencies. In addition, the wide flare angle horn also has the phase centre at its throat for both the polarizations in contrast with non-corrugated horns where the phase centres for V and H are not only separated from each other but also from the throat of the horn.

2.1.2 DISTANCE BETWEEN THE PHASE CENTRE AND THE LAST CORRUGATION (R)

The distance (R) between the phase centre and the last corrugation is chosen in such a way that the deviation ($\Delta\lambda$) of the spherical wave front at the aperture of the horn from a plane wave is more than $\frac{\lambda}{2}$. This ensures independence of the radiation pattern from the frequency of operation. Another consequence is that at least over an octave frequency band width, the 15 dB beam width is approximately equal to the total flare angle (Ref. Fig. 2.1.2(a)). This maintains almost identical edge tapers for all the beams in the frequency range 1-1.45 GHz. Since the spherical wave at the aperture departs from a plane wave by more than $\frac{\lambda}{2}$, the shape of the radiation pattern mainly depends on the flare angle instead of the frequency of operation.

For the GMRT 21 cm horn (Ref. Fig. 2.1.1), the value of $\Delta\lambda$ is chosen to be 0.76λ . For this value of $\Delta\lambda$, the value of the product $kR\theta_o$ is found to be equal to 10.5 from the design chart (Thomas, 1978) shown in Fig. 2.1.2(b), where $k = \frac{2\pi}{\lambda}$ and θ_o is the semi flare angle in radians.

$$kR\theta_o = 10.5 \quad (2.3)$$

The design frequency is chosen to be 1250 MHz which is approximately the centre of the frequency band 1–1.45 GHz. The corresponding wavelength λ for this frequency is 24 cm. Substituting the above value of λ and flare angle $\theta_o = 1.047$ radians in the above relation we get

$$\frac{2\pi R\theta_o}{\lambda} = 10.5 \quad (2.4)$$

$$\text{and, therefore, } R = 36.76 \text{ cm.} \quad (2.5)$$

The variations in the dimensional values shown in the figures are due to the inaccuracies involved in the fabrication of the horn and OMT.

2.1.3 THE DIMENSIONS OF CORRUGATIONS

The spill-over in any dish antenna with a prime-focus feed system can be minimised by having an appropriately designed horn feed at the prime focus. The prime focus horn with large aperture will possess a narrow beam so that it does not see much of the ground when

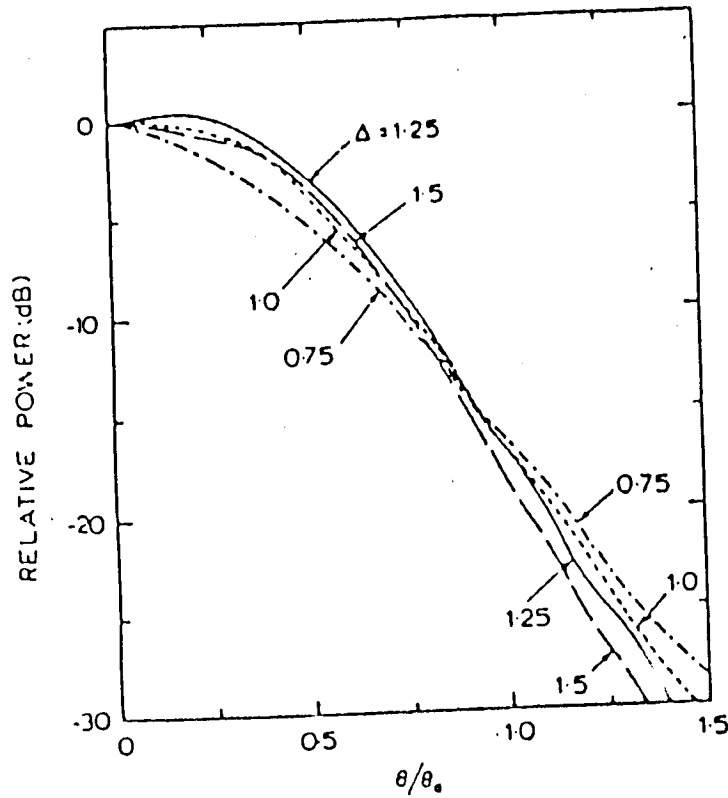


Fig. 2.1.2(a) : Normalised radiation patterns for wide-band corrugated horns with $\theta_0 < 70^\circ$

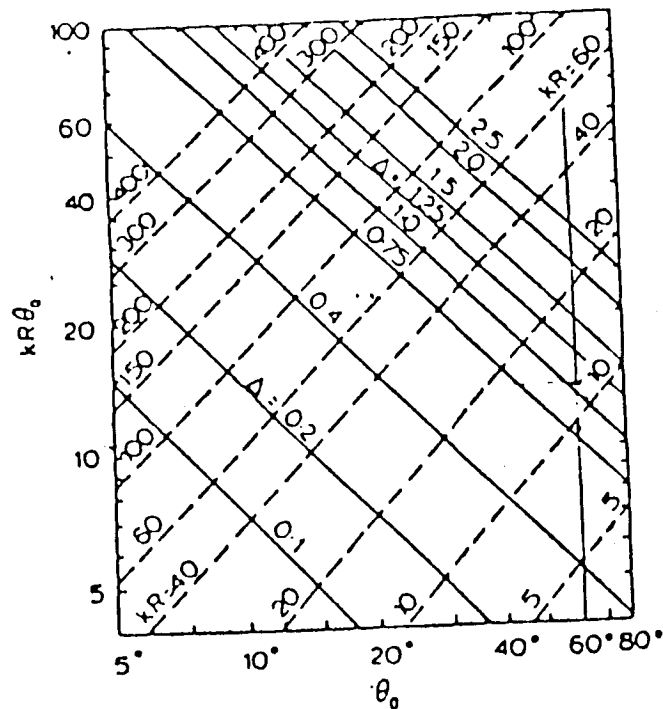


Fig. 2.1.2(b) : Relationships between horn parameters. Constant values of Δ are shown by full lines and constant normalized horn lengths by dashed lines. These are plotted as function of θ_0 (horn half angle) and $kR\theta_0$ (normalised spherical aperture).

used to illuminate the dish. This advantage may be obtained only in the H-plane pattern because the E-plane pattern suffers from high side lobes that are attributed to the excitation of the rim of the horn in that plane. The main reason for this is the non-existence of identical boundary conditions in both the planes. However, a metal surface with a number of closely spaced corrugations formed out of metal vanes is experimentally found to present an identical reactive boundary for both TE and TM waves. Therefore, if a horn possesses corrugations, it can have identical patterns in both E and H planes. Any horn having the same boundary conditions in both E and H planes is called a *scalar horn*. If the corrugations are cut deep enough so that the surface impedance becomes capacitive in nature, then the electromagnetic wave gets pulled off the surface as it cannot be supported by it. This results in a lower surface current and hence a lower ohmic loss in the horn.

The throat of the horn is designed such that a good impedance match exists between the OMT and the horn. This is accomplished by making the slot depth of the first corrugation equal to $\frac{\lambda}{2}$ (Love, 1976) at the highest frequency of operation. The successive slot depths should taper down to $\frac{\lambda}{4}$ at the center frequency. The thickness of the metal vanes forming corrugations is kept very small. The pitch (p) of the corrugations is chosen to be 30% smaller than $\frac{\lambda}{2}$.

For the GMRT horn shown in the Fig. 2.1.1, the first slot depth is given by

$$d1 = \frac{\lambda}{2} = \frac{21}{2} \text{ cm} = 10.5 \text{ cm.} \quad (2.6)$$

The pitch (p) is chosen to be 30% smaller than 10.5 cm and, therefore,

$$p = 7.35 \text{ cm.} \quad (2.7)$$

2.2 ORTHOMODE TRANSDUCER (OMT)

In radio astronomy, since the available signal strength is very small, one cannot afford to lose any amount of signal either in the form of ohmic loss or reflection loss. Reflection loss can be minimised by having a good return loss over the required bandwidth. Acceptable level of return loss would be about -15 dB in which case 3 % of the incoming power gets reflected and 97 % transmitted. An isolation of at least 30 dB is desired between V and H channels of the OMT whenever a dual polarization observation is carried out. In a wave guide, inappropriate design could excite unwanted higher order modes and these could result in an enhancement of the crosspolarization coupling. Therefore, the higher order modes should be strongly suppressed in order to get a good cross polar performance.

The bandwidth of a regular circular waveguide is about 30 % of the cutoff frequency and above this higher order modes start developing. By constructing ridges in the waveguide, the generation of higher order modes may be pushed to higher frequencies and thereby a wider

bandwidth may be achieved. The main disadvantage of having ridges is that it increases the ohmic loss in the OMT by several orders of magnitude as compared to a a ridge-free wave guide. A quadridged orthomode transducer (OMT) is a waveguide having four tapered fins or ridges in it. The two pairs of orthogonal ridges concentrate the field into a small gap at the centre of the waveguide. The field energy is extracted by a pair of coaxial probes. While designing a wave guide two important aspects have to be considered:

- (i) Smooth transition from circular waveguide to quadridge wave guide and
- (ii) Proper matching of the probes to the waveguide impedance over a wide bandwidth.

2.2.1 DESIGN OF OMT

IF λ_L is the wavelength corresponding to the lowest frequency of operation, then to achieve a reasonable value of return loss of about -15 dB over an octave bandwidth, the dimensions of the wave guide and the ridges have been experimentally determined to be as follows (James, 1992):

- $(\alpha_1/\lambda_L) = 0.75$ where α_1 is the diameter of OMT at the aperture,
- $(\alpha_2/\lambda_L) = 0.44$ where α_2 is the diameter of OMT near the probes,
- $(L_1/\lambda_L) > 4.00$ where L_1 is the length of the tapered section of the ridge,
- $(L_2/\lambda_L) = 0.015$ where L_2 is the small linear section from the centre pin towards the aperture plane,
- $(L_3/\lambda_L) = 0.040$ where L_3 is the distance between the centre pin and the backshort aperture plane,
- $(\Delta_1/\lambda_L) = 0.050$ where Δ_1 is the width of the ridge,
- $(\Delta_2/\lambda_L) = 0.010$ where Δ_2 is the diameter of the probe,
- $(\Delta_3/\lambda_L) = 0.005$ where Δ_3 is the gap between the orthogonal ridges at the centre of the OMT.

The lowest frequency of operation of the GMRT 21 cm front end receiver is 1000 MHz. The diameter of the orthomode transducer according to the above specifications becomes $0.75\lambda_L = 0.75 \times 30 = 22.5$ cm. Since 20 cm diameter alluminium tubes were available commercialy, waveguide diameter was fixed at 20 cm instead of 22.5 cm.

To ease the fabrication of waveguides, the following changes were made to the dimensions:

1. α_2 is made equal to α_1 .
2. Ridge tapering is made linear instead of sine square.
3. The length of the tapered section L_1 is fixed at 2.3 times the wavelength which is approximately 70 cm.
4. Near the probes, the ridges are not given any taper for about a length (L_2) of 83 mm.
5. The overall length of the OMT excluding the back short is maintained at 80 cm.
6. The back short is a cone having a height of 70 mm which is $\approx \frac{\lambda}{4}$ at the lowest frequency.

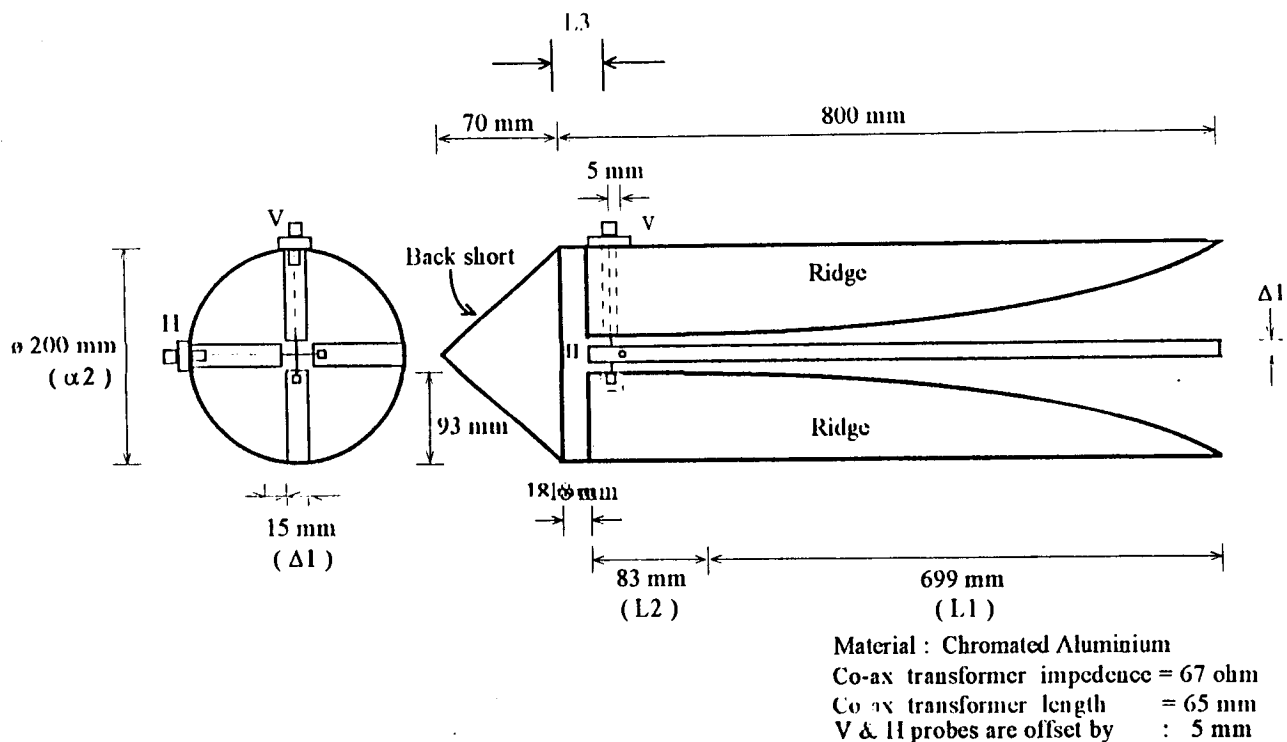


Fig. 2.2.1 : SCHEMATIC DIAGRAM OF QUADRIDGE ORTHOMODE TRANSDUCER OF GMRT 21CM FRONT END RECEIVER

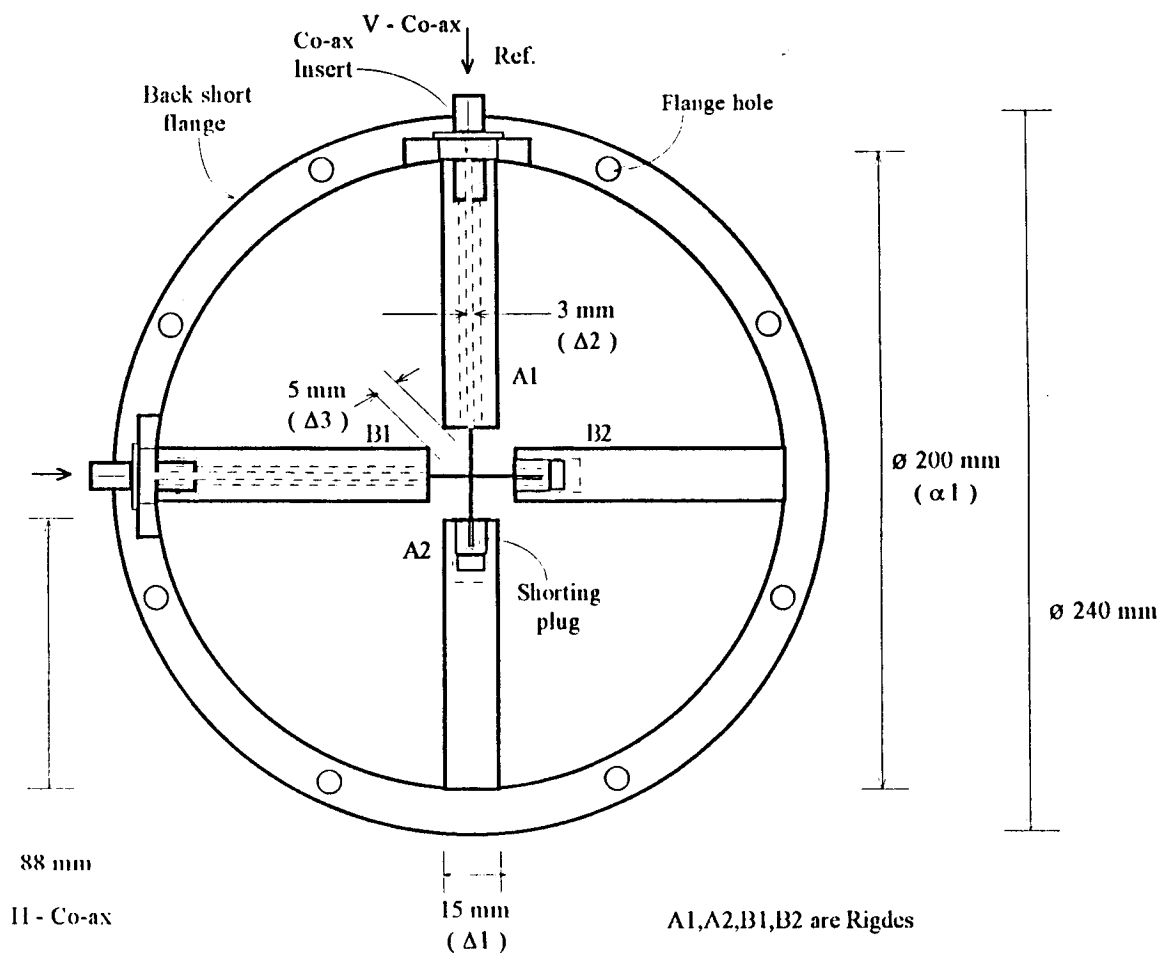


Fig 2.2.2 : FACE VIEW OF THE QUADRIDGE ORTHOMODE TRANSDUCER OF GMRT 21CM FRONT END RECEIVER.

7. The width of the ridge is kept at 15 mm which is 0.05 times λ_L .
8. The probe diameter of the OMT is kept at 0.007 times λ_L .
9. The gap between the orthogonal ridges near the probes is maintained at 5 mm.

Experimentally it has been found that for wide-band performance, the length of the OMT is a more important parameter as compared to the design of the ridge profile provided that the ridges vary in dimension smoothly from near the probe to the aperture. The schematic diagrams of various cross sections of the GMRT OMT are shown in Fig. 2.2.1 and Fig. 2.2.2.

2.2.2 PERFORMANCE CHARACTERISTICS OF HORN AND OMT

After designing and fabricating the horn and OMT, their performance was characterised by making measurements. The main characterization involved

- (i) Measurement of the radiation patterns of the (Horn+OMT) feed unit,
- (ii) VSWR measurement of the OMT, and
- (iii) Measurement of the insertion loss of the OMT.

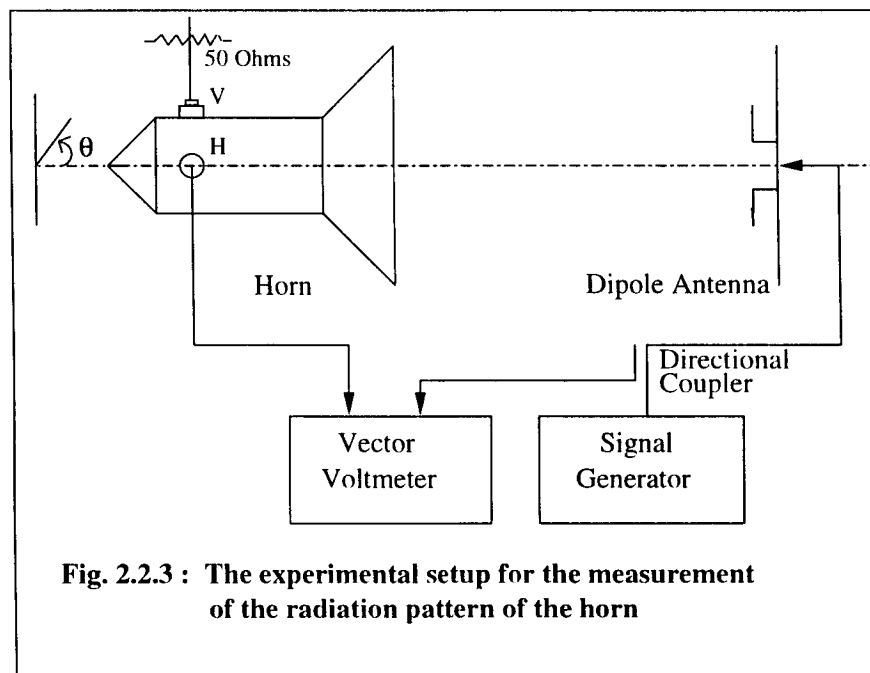


Fig. 2.2.3 : The experimental setup for the measurement of the radiation pattern of the horn

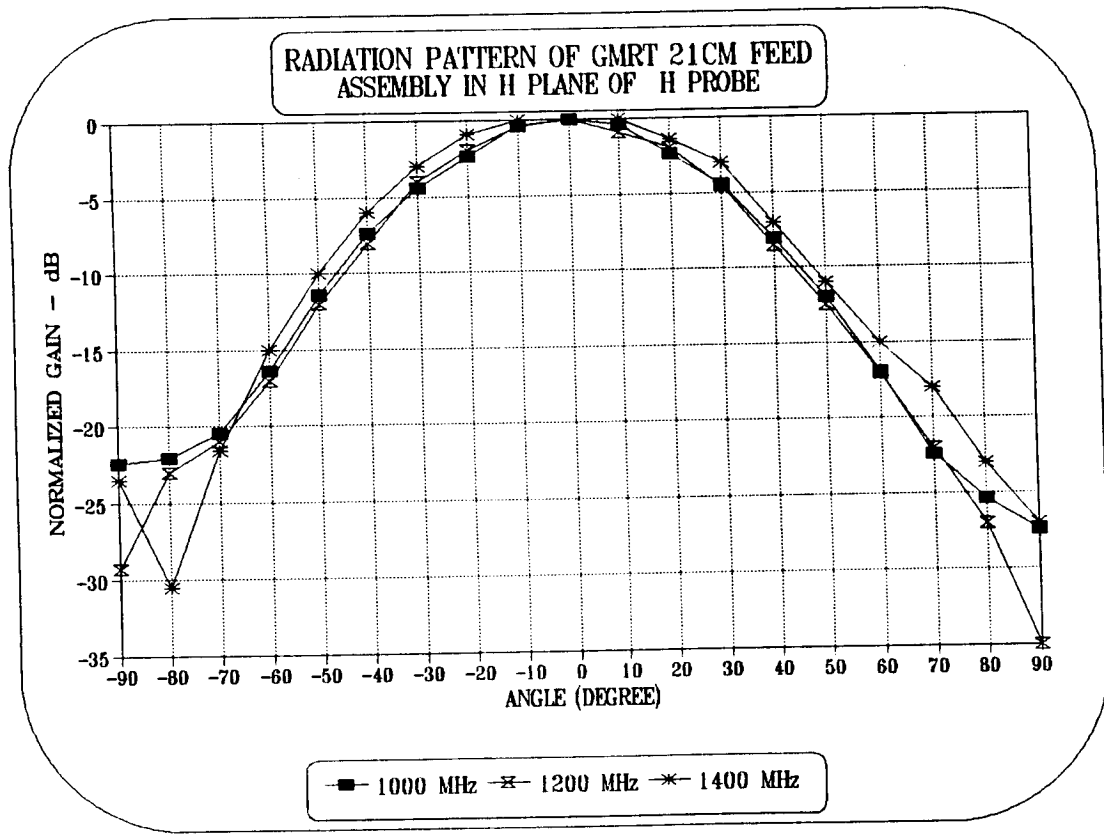
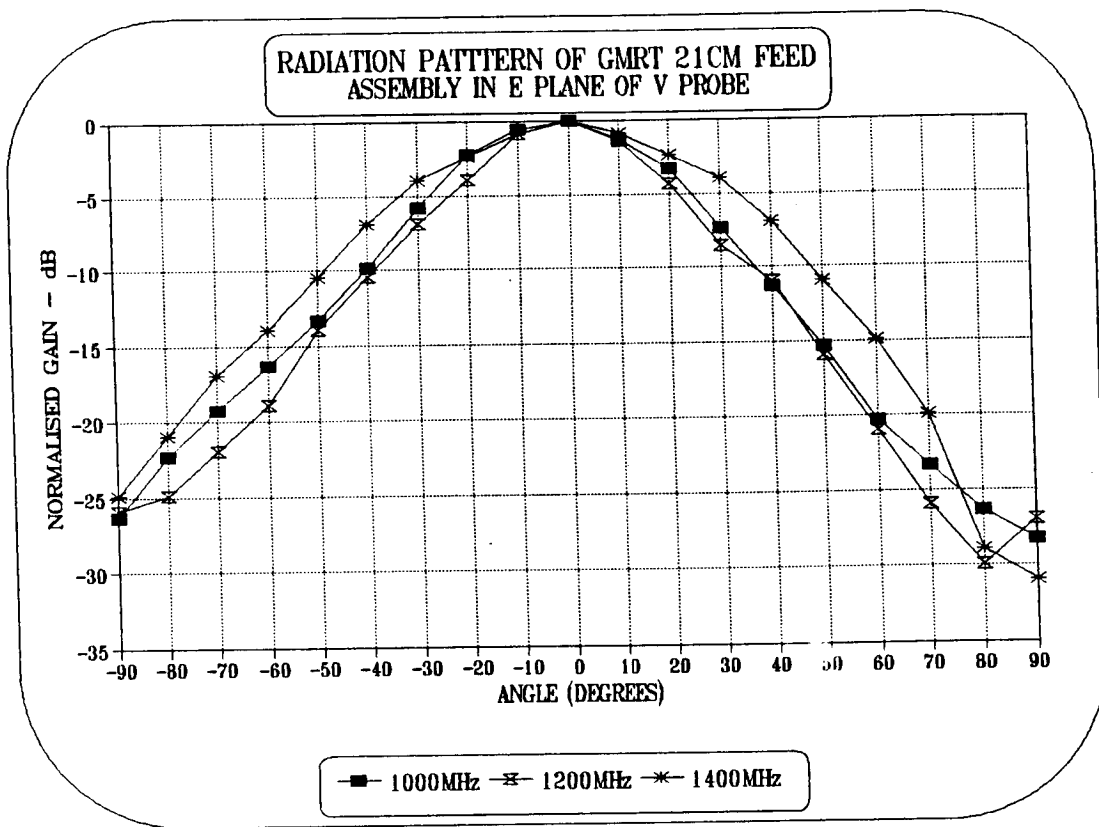
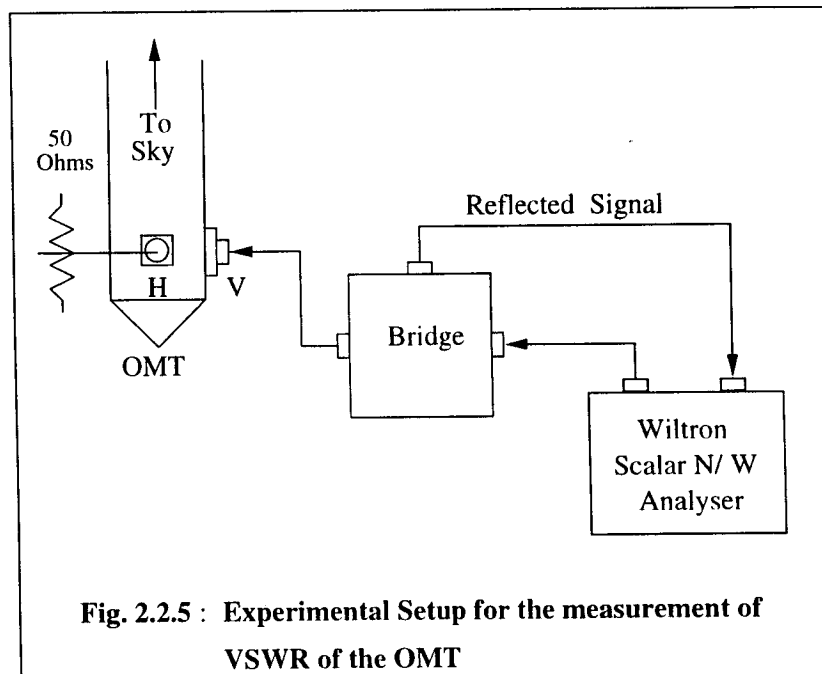


Fig. 2.2.4 : NORMALIZED PLOTS OF E & H PLANE RADIATION PATTERNS OF GMRT 21CM FEED ASSEMBLY

2.2.2.1 MEASUREMENT OF THE RADIATION PATTERN

Using the GMRT horn+OMT as a receiver and a dipole as the transmitter, the horn+OMT radiation patterns in both the E and H planes were measured. For the measurement of the radiation pattern in the E-Plane, the V-probe of the horn is kept parallel to the dipole with the unused H-port terminated in a good 50 ohm load. The relative power of the horn is measured using the a vector voltmeter. The experimental setup for conducting the radiation pattern measurement is as shown in Fig. 2.2.3. For various angular positions of the horn with respect to dipole, the relative power of the horn was measured. Care was taken to avoid obstacles like trees in the vicinity of the horn so that unwanted reflections from them are minimised. The normalised relative power measured is plotted against the angular displacement to get the radiation pattern. The above experiment is repeated at various frequencies to get the E-plane radiation pattern of the horn as a function of frequency. A similar experiment, as performed above, is conducted for the measurement of the radiation pattern in the H-plane. Fig. 2.2.4 shows the normalized plots of E and H plane radiation patterns of the horn at three different frequencies.



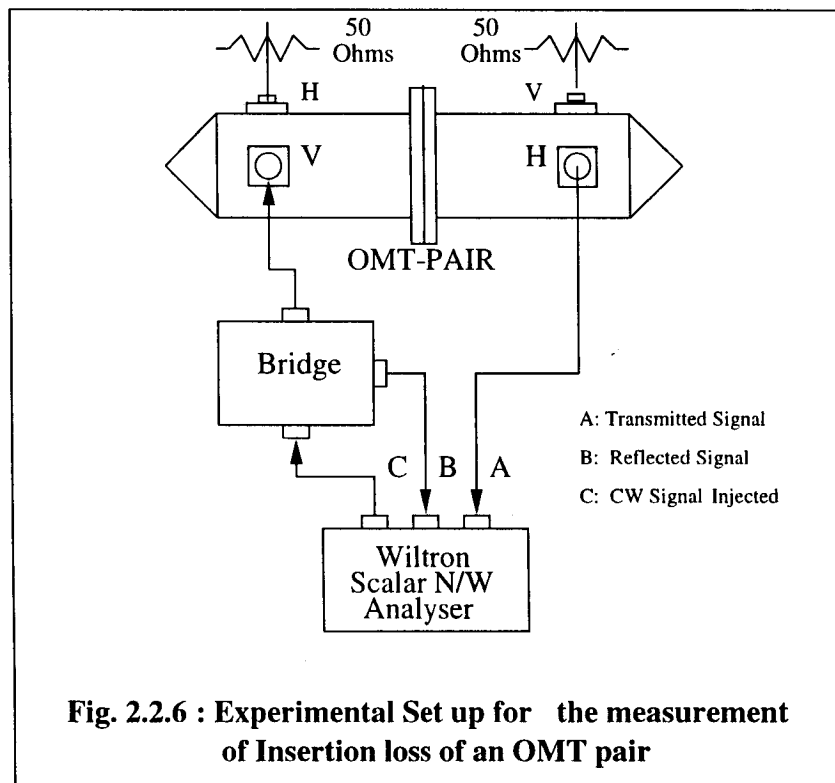
2.2.2.2 VSWR MEASUREMENT OF OMT

VSWR measurement for the OMT was performed to know the matching of the OMT to 50 ohms at the probe end and 377 ohms at the aperture. This experiment is performed using the scalar network analyser as shown in Fig. 2.2.5. A CW signal is injected into the OMT which is kept open to sky. A part of the injected signal gets transmitted and the rest gets

reflected. The amount of signal that gets reflected is mainly dependent on the impedance matching of the OMT at both the probe end and aperture end. The performance is measured by the instrument in terms of the *return loss* of the OMT; this is defined as the ratio of reflected power to the injected power. The return loss is measured at various frequencies to know the matching of the OMT over the desired band of interest. From the measured values of return loss, the VSWR is computed using the relation:

$$\text{Return Loss} = \log_{10} \frac{1}{\Gamma^2}, \text{ where} \quad (2.8)$$

$$\Gamma = \frac{\text{VSWR} - 1}{\text{VSWR} + 1}. \quad (2.9)$$



2.2.2.3 MEASUREMENT OF THE INSERTION LOSS OF THE OMT

It is important to know the ohmic loss of the OMT since it not only attenuates the astronomical signal but also worsens the system temperature by contributing its own thermal noise. Thermal noise produced by the OMT is proportional to the amount of attenuation that it offers for the transmission of any rf signal. The attenuation of the OMT is determined by measuring the insertion loss that a CW signal suffers when passed through it. The *insertion loss* is defined as the ratio of the transmitted signal to the incident signal. Fig. 2.2.6 shows the experimental setup for the measurement of insertion loss for a pair of OMTs connected

back to back. The insertion loss of a single OMT will be half of the total insertion loss of a pair of OMTs. This method of measuring the insertion loss should be correct provided the frequency is not near the frequencies at which there are resonances set up in the cavity. Also, the OMTs used here are cylindrical and so there will not be any discontinuity when a pair is connected back-to-back. Fig. 2.2.7 shows the plots of both insertion loss and return loss for a pair of OMTs. It should be noted that the loss of an OMT with ridges is about 0.15 dB per OMT as compared to 0.03 dB for a ridgeless waveguide (Theodore, 1989).

2.3. LOW NOISE AMPLIFIER (LNA)

The state of the art low noise amplifiers enable radio astronomers to detect weak astronomical sky signals whose power may be as low as $10^{-32} \text{ W m}^2 \text{ Hz}^{-1}$ on the surface of the Earth. The main specifications for an LNA would be (i) high gain with small gain variations over a large frequency bandwidth and (ii) a low inherent noise. The low noise amplifier designed for the GMRT 21cm front end receiver has a gain of about 35 dB and noise temperature of 25–30 K over the frequency band of about 500 MHz. The systematic procedure that was followed for the analysis and design of the low noise amplifier, based on S parameters of the transistor, is given below.

2.3.1 ANALYSIS

An amplifier can be considered as a two port network with an input being driven by a signal source V_s and the output terminated in a load impedance Z_L . The incident and reflected voltages at the amplifier input and output are represented by a_1, b_1, a_2 and b_2 respectively. An amplifier, in general, is characterised in terms of four S-parameters — S_{11} , S_{22} , S_{12} and S_{21} — when analysed at high frequencies. S_{11} and S_{22} represent the input and output voltage reflection coefficients, S_{21} and S_{12} represent the forward and the reverse transmission coefficients. Usually, the driving source and the load are associated with their own voltage reflection coefficients owing to their impedance mismatches. Therefore, for the analysis, the amplifier circuit is written in terms of its voltage reflection coefficients along with source and load voltage reflection coefficients as shown in Fig. 2.3.1 (Gonzalez, 1984).

2.3.2 TOTAL GAIN OF THE LNA

The net gain of an amplifier is decided by three different sections of the amplifier circuit (Ref. Fig. 2.3.2):

- (i) input matching section connecting the voltage driving source and the amplifier input,
- (ii) the transistor, and
- (iii) the output matching section connecting the amplifier output and the load.

In the input section, the voltage driving source impedance is matched to the amplifier input impedance and in the output section, the amplifier output impedance is matched to the load impedance.

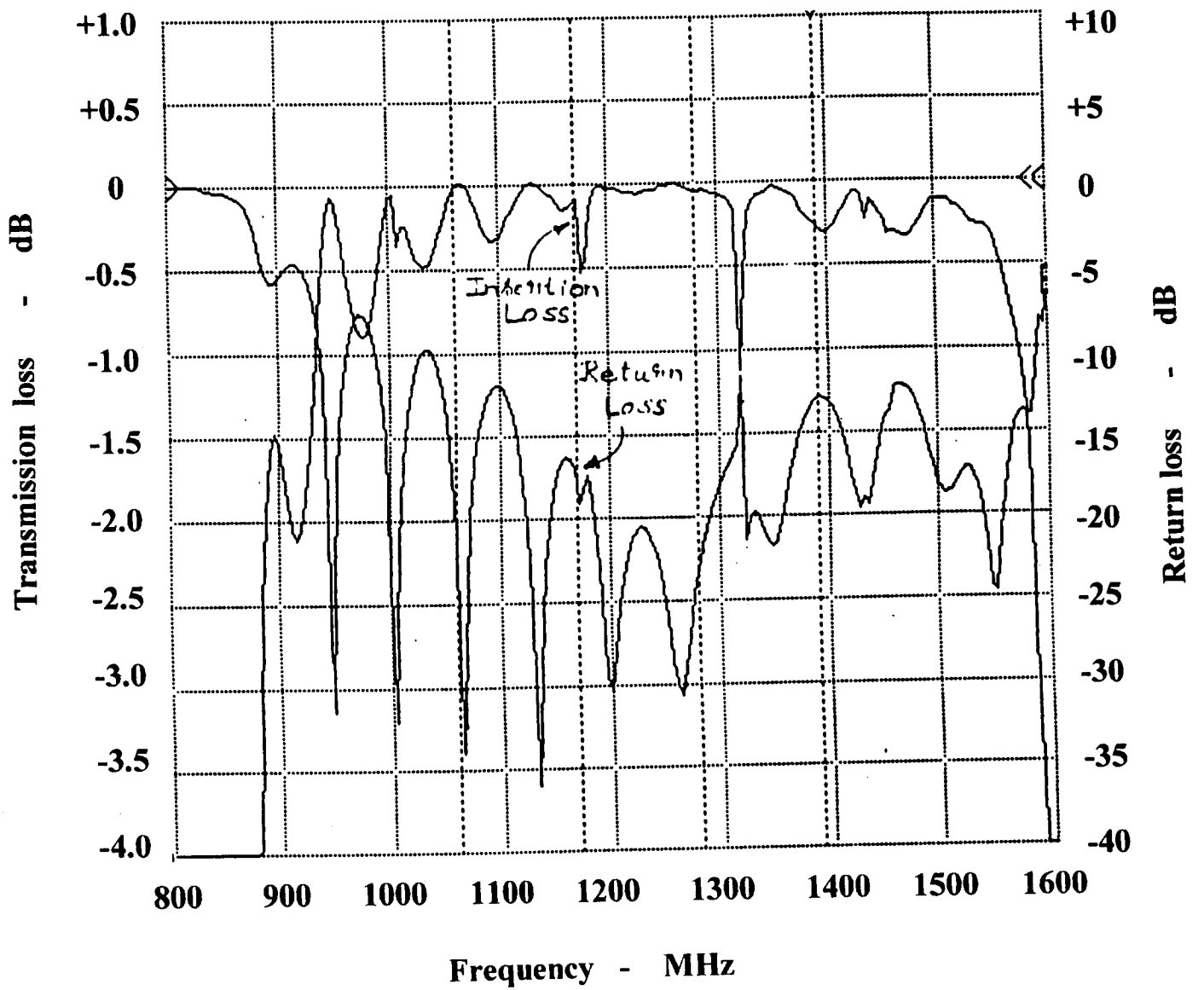
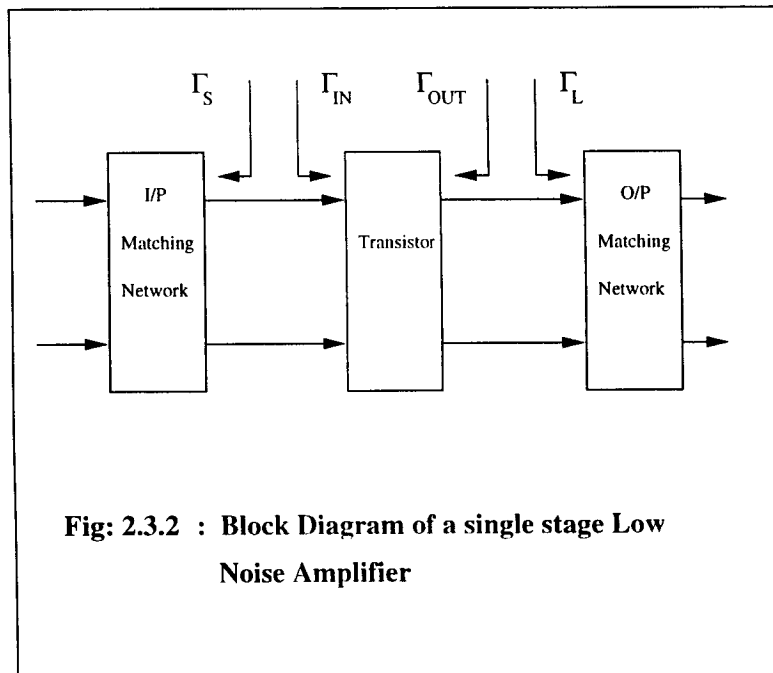
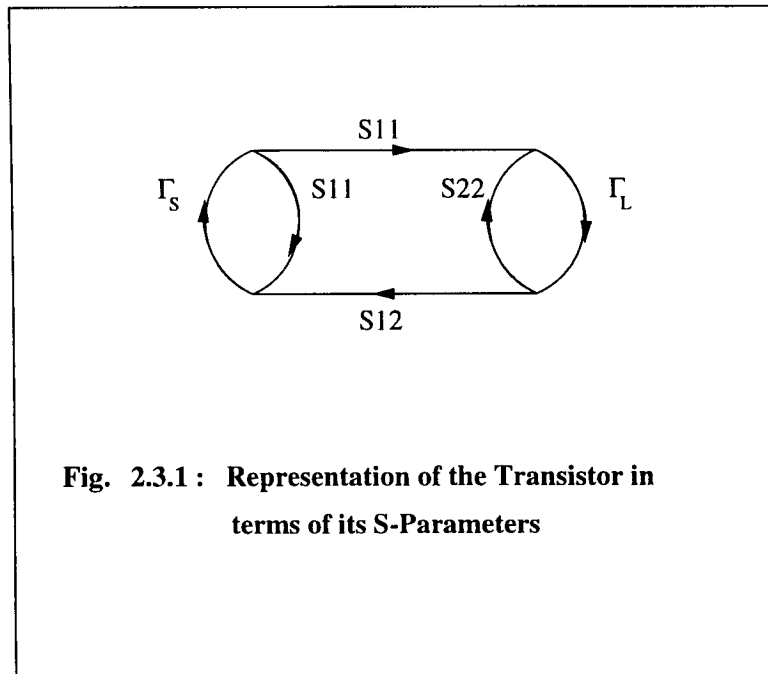


Fig. 2.2.7 : PLOTS OF TRANSMISSION LOSS AND RETURN LOSS CHARACTERISTICS OF A PAIR OF OMTs



Through rigorous analysis, it has been determined that for a unilateral network (*i.e.*, where $S_{12} = 0$) the gain contribution due to the input section is given by

$$G_1 = \frac{1 - |\Gamma_s|^2}{|1 - \Gamma_{IN}\Gamma_s|^2}, \quad (2.10)$$

and that owing to the output section is given by

$$G_2 = \frac{1 - |\Gamma_L|^2}{|1 - \Gamma_L S_{22}|^2}. \quad (2.11)$$

The gain of the transistor (G_0) alone is given by its $|S_{21}|^2$ parameter. Therefore, the net gain of the amplifier is given by

$$G = (G_1 G_0 G_2), \quad \text{or,}$$

$$G = \frac{1 - |\Gamma_s|^2}{|1 - \Gamma_{IN}\Gamma_s|^2} |S_{21}|^2 \frac{1 - |\Gamma_L|^2}{|1 - \Gamma_L S_{22}|^2}. \quad (2.12)$$

When the source and the load reflection coefficients are conjugately matched to the transistor input and output impedance, *i.e.*, when $\Gamma_s^* = \Gamma_{IN}$ and $\Gamma_L^* = S_{22}$, we get a maximum gain that is given by

$$G_{max} = \frac{1}{1 - |\Gamma_{IN}|^2} |S_{21}|^2 \frac{1}{1 - |S_{22}|^2}. \quad (2.13)$$

During the design of the amplifier, considerable attention needs to be given to the stability aspect of the circuit. In general, amplifiers are designed so as to be unconditionally stable for any value of load. For unconditional stability, the conditions to be satisfied are

$$|\Gamma_s| < 1, \quad (2.14)$$

$$|\Gamma_L| < 1, \quad (2.15)$$

$$|\Gamma_{IN}| = \left| S_{11} + \frac{S_{12}S_{21}\Gamma_L}{1 - S_{22}\Gamma_L} \right| < 1, \quad \text{and} \quad (2.16)$$

$$|\Gamma_{OUT}| = \left| S_{22} + \frac{S_{12}S_{21}\Gamma_s}{1 - S_{11}\Gamma_s} \right| < 1. \quad (2.17)$$

For conditional stability, the load and the source impedances are to be selected such that Γ_s and Γ_L take values less than unity. However, if the S parameters of the transistor can be modified such that the condition

$$K = \frac{1 - |S_{11}|^2 - |S_{22}|^2 + |\Delta|^2}{2 |S_{12}S_{21}|} > 1 \quad (2.18)$$

is satisfied, where $\Delta = |S_{11}S_{22} - S_{12}S_{21}| < 1$, then the amplifier will become unconditionally stable. The modification of the S parameters can be achieved by using a feed back technique described below.

2.3.3 NOISE FIGURE OF AN AMPLIFIER

The *amplifier noise power* is the power seen at the amplifier output when there is no input signal. This output power may be viewed as being composed of two components: (i) an amplified input noise power and (ii) a noise output power produced by the amplifier. The first component, the input noise power, may be modelled to be due to a noisy resistor R_N at the input of the amplifier. The resistor produces thermal noise and the maximum noise power per unit bandwidth available at the terminals of the resistor is given by $P = kT$ where T is the temperature of the resistor and k is the Boltzmann's constant. The second component, namely the noise produced by the amplifier, is dependent upon the transistor used and the input and output matching networks.

The *noise figure* (F) of an amplifier is defined as the ratio of total available noise power at the output of an amplifier to the available noise power at the output owing to the thermal noise source component at the input.

Let P_{No} represent the total noise power at the output of amplifier, P_{Ni} represent the thermal noise power available from the resistor R_N and G_A represent the amplifier gain. The Noise figure can then be expressed as

$$F = \frac{P_{No}}{P_{Ni}G_A}. \quad (2.19)$$

But G_A can be written as the ratio of P_{So} to P_{Si} , where P_{So} and P_{Si} are the available signal power at the output and input respectively. Substituting in equation 2.19 we get

$$F = \frac{P_{No}/P_{Ni}}{P_{So}/P_{Si}}. \quad (2.20)$$

The noise figure of an amplifier is primarily influenced by the source impedance. Therefore, in general, the noise figure of a two port amplifier can be written as

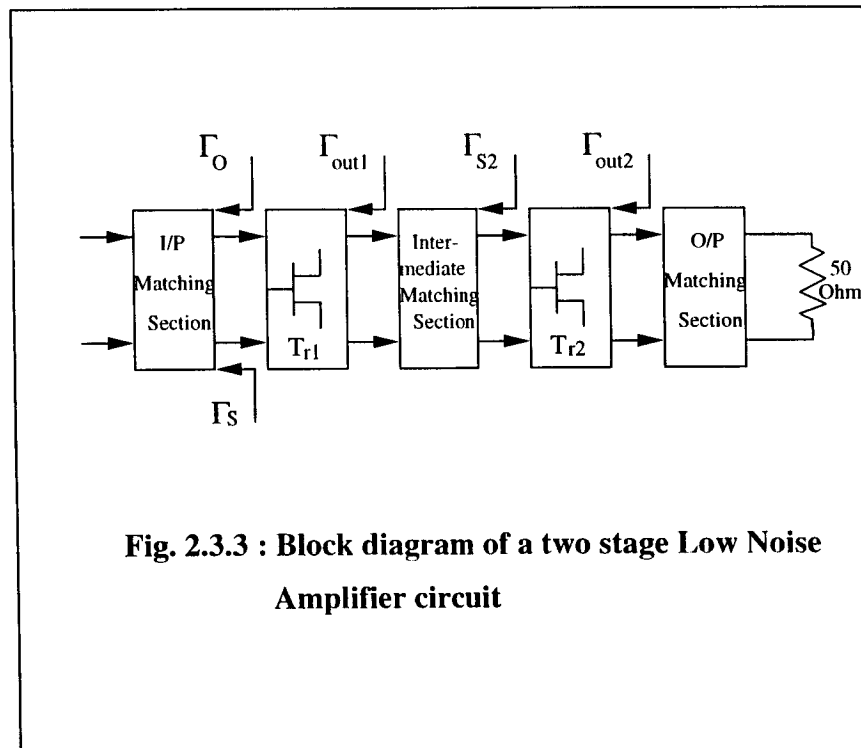
$$F = F_{min} + r_n |Y_s - Y_o|^2, \quad (2.21)$$

where F_{min} is the minimum noise figure that one can obtain from the amplifier under favourable conditions, r_n is the normalised noise resistance modelled for the noise temperature, Y_s is the source admittance and Y_o is the optimum source admittance which results in

a minimum noise figure. Expressing Y_s and Y_o in terms of the reflection coefficients Γ_s and Γ_o we get

$$F = F_{min} + \frac{4r_n |\Gamma_s - \Gamma_o|^2}{(1 - |\Gamma_s|^2) |1 + \Gamma_o|^2} \quad (2.22)$$

From the above equation it is obvious that for $\Gamma_s = \Gamma_o$ we get minimum noise figure. But according to the equation (2.13) maximum gain is obtained only for a unique value of $\Gamma_s \neq \Gamma_o$. This implies that both maximum gain and minimum noise figure cannot be obtained simultaneously. Therefore, a trade-off must be made between these two parameters.



2.3.4 USE OF FEEDBACK TECHNIQUE

Any deviation from the matched condition, *i.e.* $\Gamma_s = \Gamma_{in}^*$, not only results in a lower gain but also a poor return loss. This situation can be marginally improved by altering the S-parameter values of the transistor by means of negative feedback. The negative feedback may be viewed as introducing a noiseless resistance at the base of the transistor thereby changing the input impedance of the transistor. The amount of feedback is adjusted until the transistor input impedance becomes almost equal to the optimised impedance for the minimum noise figure. Once the two impedances are close, simultaneous matching of both

the noise and the gain may be achieved. However, there will be a reduction in the gain due to the feed back mechanism.

Taking into consideration the various aspects of low-noise-amplifier design discussed in the previous section, a proper circuit has been designed to meet the GMRT requirements. The procedure is outlined here. Consider a two stage low noise amplifier as shown in Fig. 2.3.3 where the reflection coefficients are as shown at various stages of the circuit. Before designing the amplifier, one requires knowledge of various parameters of the transistor like (i) S-parameters, (ii) minimum noise figure (F_{min}), (iii) Γ_o : optimum reflection coefficient for minimum noise and (iv) normalised noise resistance : r_n . The main steps involved in the design of the amplifier circuit are:

STEP 1

The source impedance of value 50 ohms is to be transformed to the required impedance Z_{b1} at the gate of the first stage transistor. Γ_o of this transistor requires a particular value of impedance to be present at the transistor input for a minimum noise requirement. Since both the gain and noise are to be considered equally, the S-parameters of the transistor are altered using a feedback in the source leg of the transistor. Feedback is provided through an inductor and its value is varied until $\Gamma_s \approx \Gamma_o$. Once the value of $\Gamma_s = \Gamma_{s1}$ is determined, the corresponding impedance Z_{b1} is calculated by using the relation

$$Z_{b1} = \frac{1 - \Gamma_{s1}}{1 + \Gamma_{s1}}. \quad (2.23)$$

One may use, *e.g.*, a $\frac{\lambda}{4}$ transformer to transform 50 ohms to Z_{b1} along with other lumped elements.

STEP 2

The output impedance Z_{o1} of the first transistor needs to be transformed to the required impedance Z_{b2} at the base of the second transistor. This impedance is again determined in the same manner as stated in Step 1 by applying feedback at the source leg. This transformation can be realised using lumped elements.

STEP 3

The output impedance of the second transistor is transformed to the load impedance, which is again 50 ohms, through the use of lumped capacitors and inductors.

STEP 4

The amplifier circuit must be properly biased for its class-A operation. From the recommended values of V_{DS} and I_D as given by the manufacturer, where V_{DS} is the voltage across the drain and source of the transistor and I_D is the drain current of the transistor, V_{GS} may

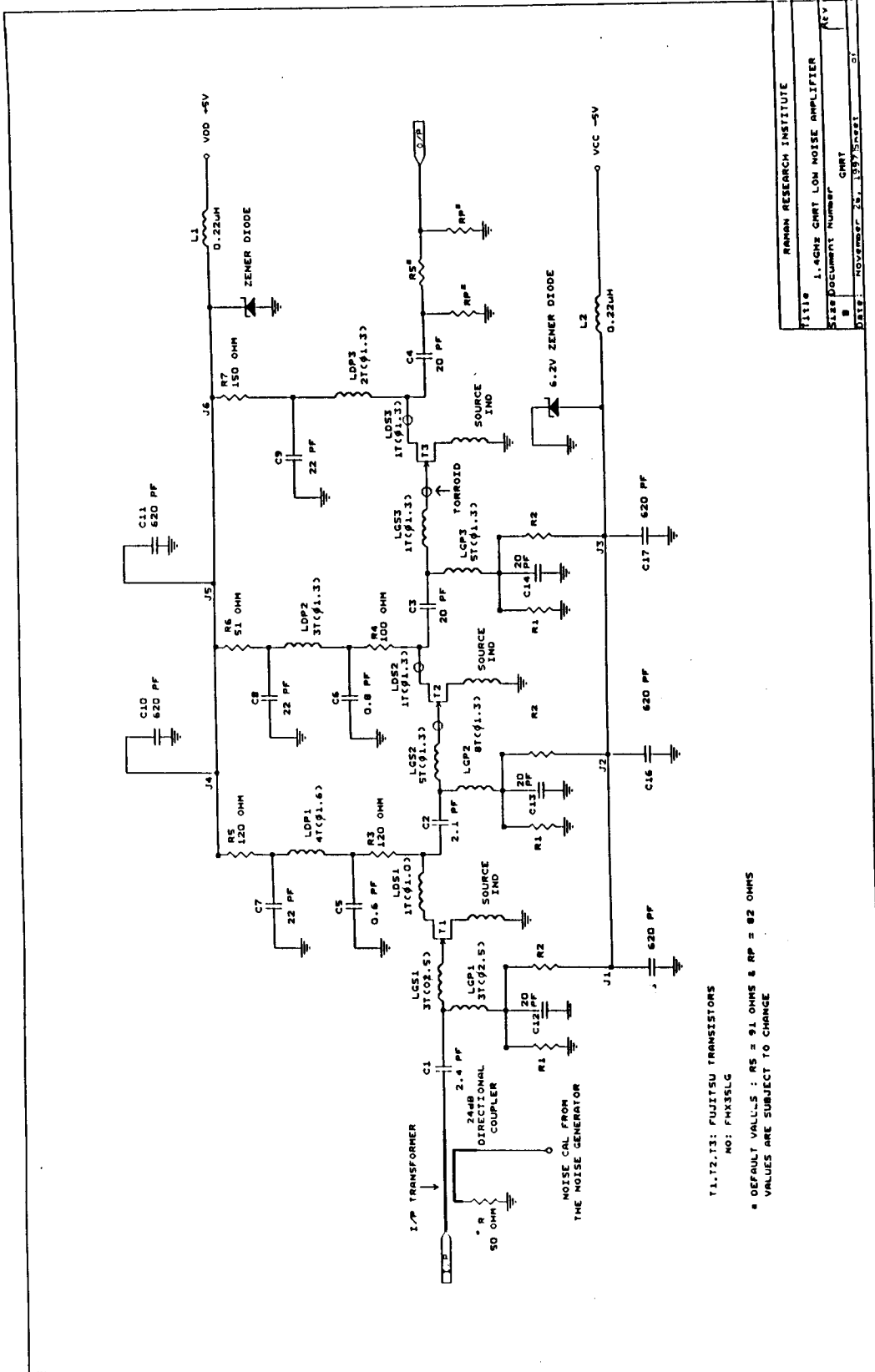


Fig 2.3.4: CIRCUIT DIAGRAM OF 1.4 GHz GMRT LOW NOISE AMPLIFIER

be separately determined by applying V_{DS} across the transistor and passing current I_D through it. From the value of V_{GS} , the source resistance R_s is calculated using the relation

$$R_s = \frac{V_{GS}}{I_D}. \quad (2.24)$$

From knowledge of V_{DS} , the voltage V_{R_s} across R_s and the supply voltage V_{cc} , the drain resistance R_D can be calculated using the relation

$$R_D = \frac{(V_{cc} - V_{DS} - V_{R_s})}{I_D}. \quad (2.25)$$

The low noise amplifier for the GMRT 21 cm front end receiver has been designed following the various rules mentioned above and is shown in Fig. 2.3.4.

At the input of the LNA, a directional coupler exists using which a calibration signal is injected into the system. The directional coupler is a four port device which is characterised in terms of its coupling factor and directivity. Coupling factor is defined as the ratio of incident power to the coupled power. So if P_A and P_D are the incident power and coupled power of the directional coupler as shown in Fig. 2.3.5, then

$$\text{Coupling factor(dB)} = \frac{P_A}{P_D}. \quad (2.26)$$

Similarly, the directivity is defined as

$$\text{Directivity} = \frac{P_D}{P_C}, \quad (2.27)$$

where P_C is the available at the isolated port. In the GMRT LNA, the coupling factor is ≈ 24 dB and the directivity is ≈ 10 dB over the frequency range 1–1.45 GHz.

2.3.5 MEASUREMENT OF THE PERFORMANCE CHARACTERISTICS OF THE LNA

The important parameters of the LNA that are to be characterised are:

- (i) Gain of the amplifier,
- (ii) Input return loss of the amplifier, and
- (iii) Noise figure of the amplifier.

2.3.5.1 MEASUREMENT OF THE GAIN AND RETURN LOSS OF THE LNA

Fig 2.3.6 shows the experimental setup for the measurement of gain and input return loss of the amplifier. A swept CW signal is fed to a pair of directional couplers from the

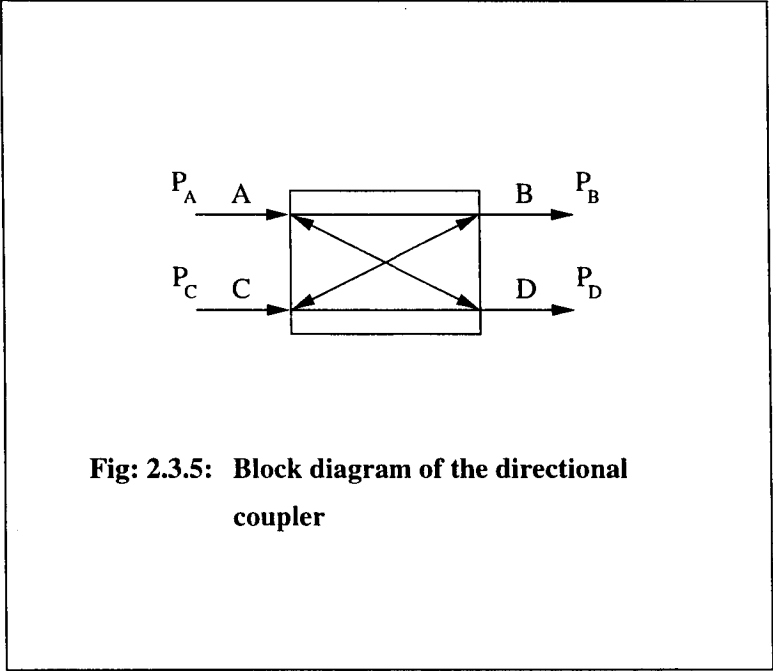


Fig: 2.3.5: Block diagram of the directional coupler

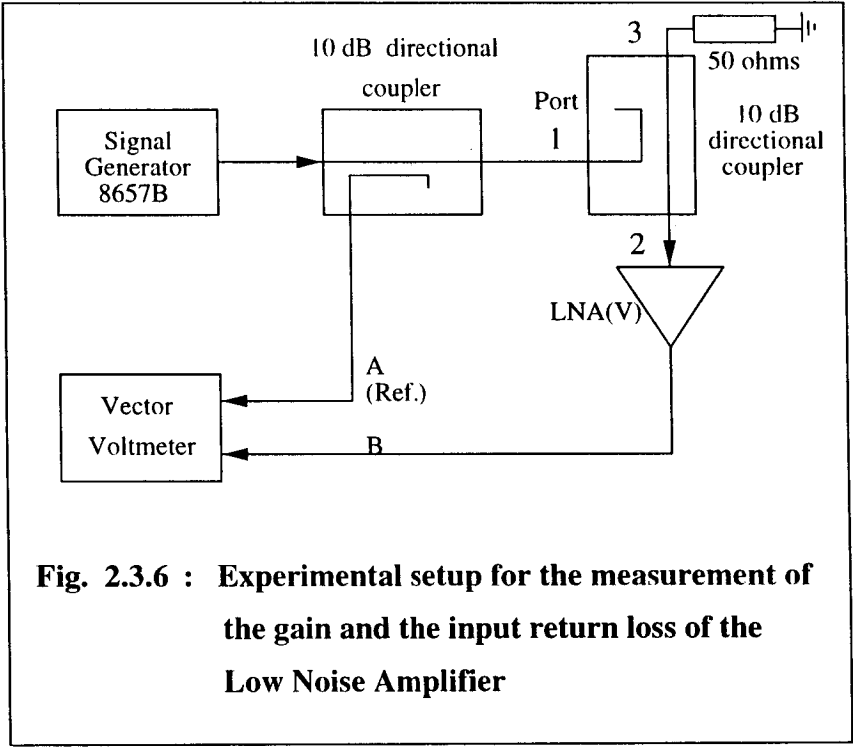


Fig. 2.3.6 : Experimental setup for the measurement of the gain and the input return loss of the Low Noise Amplifier

FREQ MHZ	GAIN (dB)	NOISE TEMPERATURE (K)	PHASE (DEG)	NOISE COUPLING (dB)	INPUT RET LOSS (dB)
1000	35.06	23.00	12.17	-27.22	-11.61
1050	34.07	24.00	-22.55	-26.29	-10.00
1100	34.10	25.00	-46.30	-26.00	-7.54
1150	35.43	24.00	-75.30	-26.48	-6.41
1200	35.88	23.00	-114.65	-25.76	-6.61
1250	34.94	23.00	-146.12	-23.72	-7.32
1300	35.19	23.00	188.08	-23.81	-7.75
1350	36.31	26.00	152.61	-25.81	-7.34
1400	35.23	28.00	107.69	-25.88	-5.43
1450	32.39	33.00	76.69	-24.04	-4.55
1500	30.73	37.00	55.95	-22.83	-4.05

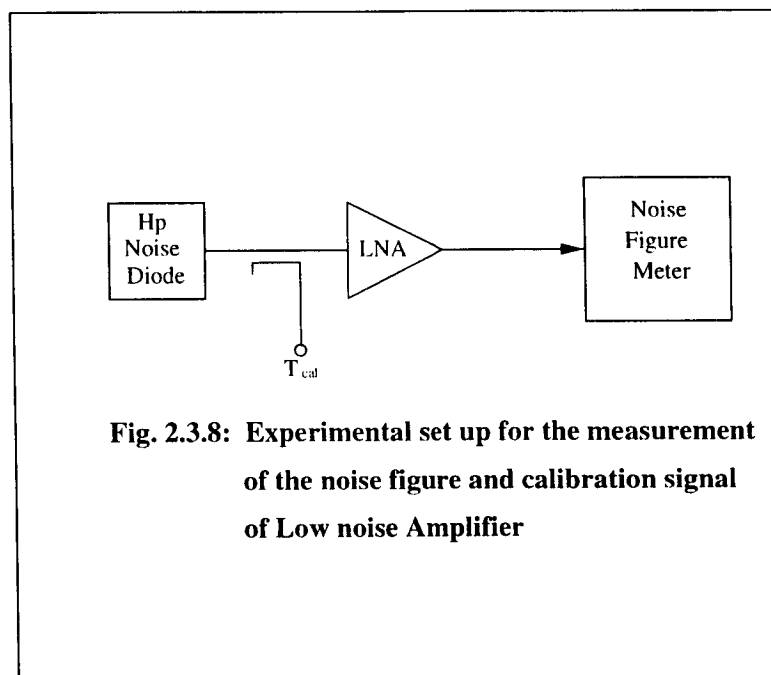
Table 2.1 : TYPICAL CHARACTERISTICS OF A LOW NOISE AMPLIFIER

signal generator 8657B. The first directional coupler provides a reference signal at its coupled port and this is connected as one input to the vector voltmeter.

The second directional coupler provides a signal at its main port and this is fed to the amplifier input, the amplifier output is connected as the second input to the vector voltmeter. Under these conditions, the gain and phase of the amplifier are measured by differencing the readings of the voltmeter with a calibration reading obtained with the amplifier bypassed. For the return loss measurement, the reflected signal from the amplifier that appears at port 3 of the second directional coupler is fed to the Vector Voltmeter; for this measurement the LNA output is terminated in a 50 ohm load. This set up is calibrated by connecting the port 2 of the second directional coupler, which went to the LNA input for the return loss measurement, with an open or short load. The results obtained for one of the LNAs is tabulated in Table 2.1.

2.3.5.2 MEASUREMENT OF THE NOISE FIGURE OF THE LNA AND THE STRENGTH OF THE CALIBRATION SIGNAL

The noise figure, which is a figure of merit for the LNA, indicates the quantum of amplifier-generated noise signal which gets added on to the input rf signal. Usually, the amplifier noise is measured by comparing it with a calibrated noise source. Using this principle, the receiver temperature of the LNA was measured with the help of an HP noise source. The HP noise source, which injects noise at periodic intervals of time, was connected to the LNA input as shown in Fig. 2.3.8. The LNA output is connected to the Noise figure meter which



separately measures the noise power with the noise source ON and OFF. It calculates the noise temperature of the amplifier using the Y-factor method and this is described below. In the analysis given below all the noise powers are represented in terms of their equivalent temperatures using the relationship $P = kTB$ as before.

Let T_H represent the noise temperature injected when the noise diode is ON, T_C represent the noise temperature injected when the noise diode is OFF, T_R represent the receiver temperature of the LNA, V_1 represent the voltage at the detector output in the Noise figure meter for the input power $(T_H + T_R)$, and V_2 represent the voltage at the detector output in the Noise figure meter for the input power $(T_C + T_R)$.

Then

$$V_1 \propto (T_H + T_R), \quad \text{and}, \quad (2.28)$$

$$V_2 \propto (T_C + T_R). \quad (2.29)$$

From the above two equations we get

$$\frac{(V_1 - V_2)}{V_2} = \frac{(T_H - T_R)}{T_C + T_R}. \quad (2.30)$$

Solving for T_R and representing $\frac{V_1}{V_2}$ by the symbol Y , we get

$$T_R = \frac{T_H - T_C}{Y - 1} - T_C. \quad (2.31)$$

In a similar way, the calibration signal which is injected into the LNA is also measured using this technique.

2.4 POST AMPLIFIER

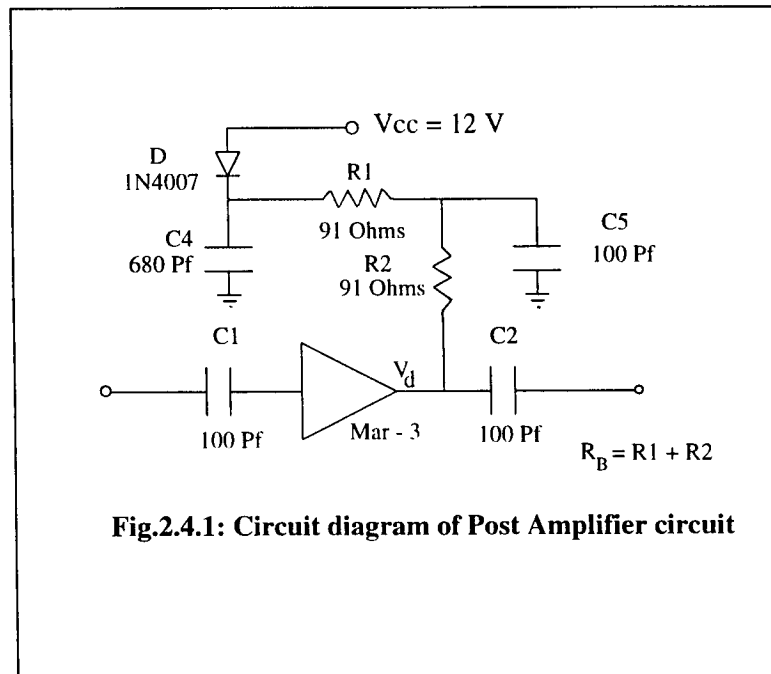
The rf signal is first amplified in the LNA and is subsequently further amplified in the post amplifier. The amplifier used is a commercially available module from Mini-Circuits. From among the various amplifiers available, MAR-3 was selected because its frequency response has a low droop over the band of interest, it has a moderate gain of 8 to 10 dB and is cost effective. The designer is expected to put input and output dc decoupling capacitors and a proper biasing resistor to pass the specified current through the device.

2.4.1 DESIGN OF THE POST AMPLIFIER

The schematic diagram of the amplifier circuit, as designed for the GMRT front end, is shown in Fig. 2.4.1.

The recommended voltage V_d at the collector end of the transistor inside the amplifier is 4.5 V for a device current (I_d) of 35 mA. The power supply voltage is selected to be 12 V and the biasing resistor is calculated using the relation

$$R_B = \frac{(V_{cc} - V_d)}{I_d}. \quad (2.32)$$



Both the ends of the biasing resistor are grounded so that any rf signal leaking into the biasing circuit is bypassed to the ground. The input and output coupling capacitors are designed in such a way that they pass only frequencies above a certain value. The values of these coupling capacitors are fixed at 100 pF. Similarly, the bypass capacitors are fixed at 680 pF. The gain and phase of this amplifier are measured using a vector voltmeter with the same experimental setup as used for measurements of the LNA. The results obtained are presented in Table 2.2.

2.5 PHASE SWITCH BOX

The rf signal is phase modulated in a phase switch box that follows the LNA and post amplifier and is phase demodulated down the signal path post sampling. Phases of 0° or 180° are added to the signal phase in the phase switch module and the switching is controlled by a Walsh function waveform which is unique to each of the two individual channels of any front end receiver. Because the Walsh functions form an orthogonal set, the phase modulation/demodulation result in the cancellation (in the integrator that follows the corre-

Freq. MHz	Input R.Loss-dB	Gain (dB)		Amplitude Balance-dB	Transmission Phase-deg		Phase Diff.(d0)	Isolation bet. two channels (w.r.t I/P)
		CH-V	CH-H		CH-V(01)	CH-H(02)		
1000	-20.87	8.70	8.60	0.10	-8.58	-12.10	3.52	-50.37
1050	-21.47	8.55	8.47	0.08	-17.95	-20.94	2.99	-47.76
1100	-22.22	8.52	8.38	0.14	-25.72	-30.44	4.72	-41.51
1150	-23.06	8.64	8.57	0.07	-35.16	-39.28	4.12	-53.25
1200	-23.59	8.63	8.56	0.07	-46.46	-50.26	3.80	-58.60
1250	-23.94	8.48	8.37	0.11	-55.81	-59.91	4.10	-57.74
1300	-24.06	8.38	8.14	0.24	-65.44	-69.54	4.10	-55.91
1350	-24.51	8.15	7.98	0.17	285.20	281.10	4.10	-57.37
1400	-25.50	8.13	7.93	0.20	276.20	272.60	3.60	-56.20
1450	-26.42	8.03	7.91	0.12	266.50	263.20	3.30	-54.71
1500	-29.05	8.04	7.94	0.10	257.63	253.71	3.92	-55.33

Table 2.2: TYPICAL CHARACTERISTICS OF A POST AMPLIFIER

lator) of any common mode interference that may get added to the antenna signals in the electronics path following the phase switch module.

The phase modulation involves addition of 180° and 0° to the rf signal in synchronism with a control digital waveform that is a Walsh function. The phase modulation is performed using a commercially available mixer in which the IF port is used to control the phase of the rf signal by appropriately supplying a dc bias. A positive dc bias at the IF port will add 180° phase to the rf signal and a negative bias will add 0° phase to the rf signal. A current of 10 mA is passed through the bridge rectifier inside the mixer to put the diodes into saturation whenever they are made to conduct. The mixer is chosen in such a way that the variation in the amplitude of the signal is minimum whenever the phase of the rf signal is changed from 180° to 0° or vice versa. This avoids amplitude modulation of the signal along with phase modulation. Besides being modulated, the rf signal is also amplified in the phase switch module by a pair of MAR-3 amplifiers. The circuit diagram of the phase switch box is shown in Fig. 2.5.1.

2.5.1 DESIGN OF PHASE SWITCH BOX

The design of the amplifier in the phase switch box is done following the same procedure as for the post amplifier. For the mixer, a biasing resistor (R_9) is to be designed to pass the required current through the diodes inside the mixer.

The control Walsh functions are of ± 10 V voltage waveforms which will be applied to the mixer. If V_f represents the total voltage drop across the two diodes in the bridge rectifier inside the mixer, the biasing resistor is computed using the relation

$$R_9 = \frac{(10 - V_f)}{10 \cdot 10^{-3}}. \quad (2.33)$$

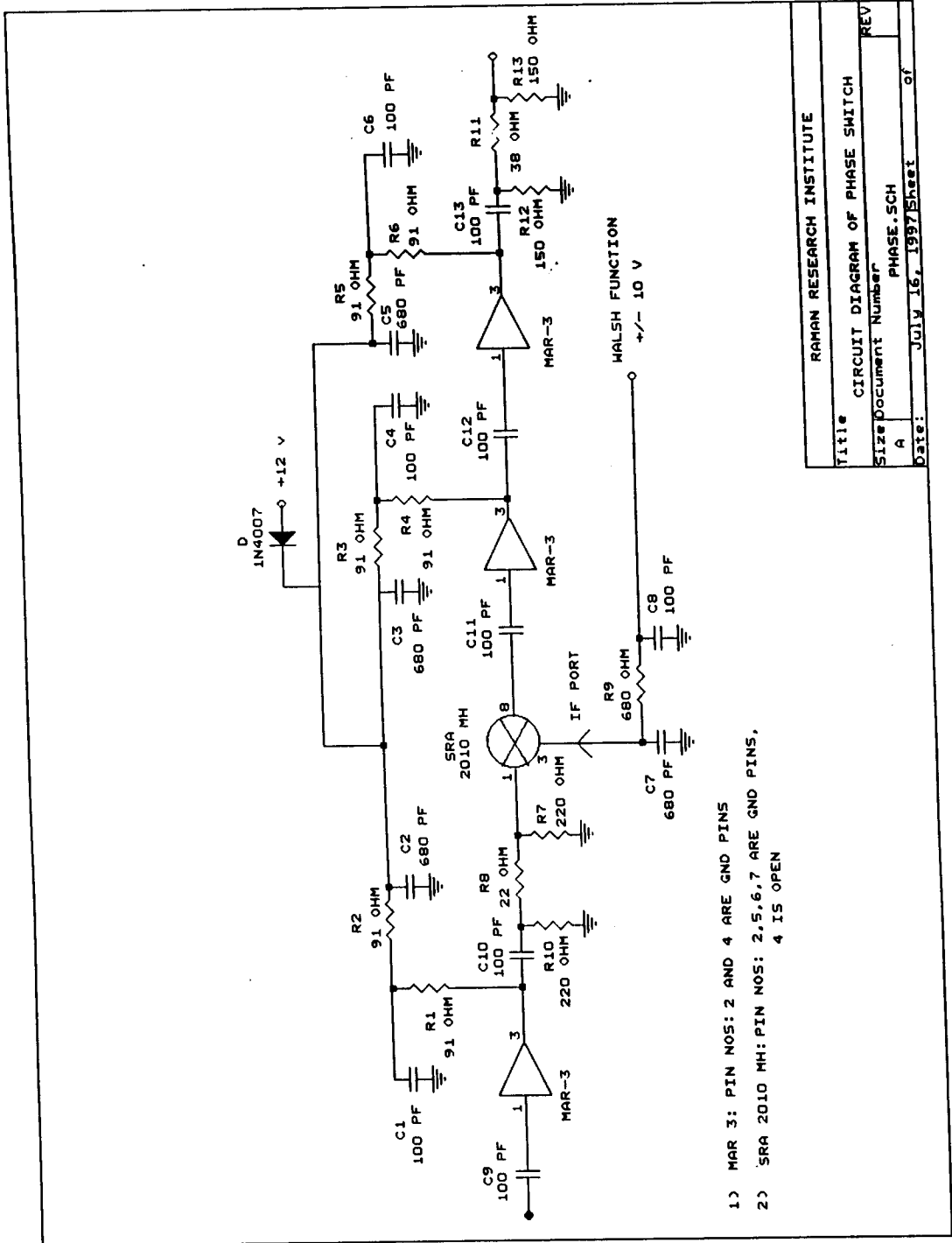
The two ends of the biasing resistor are grounded using 680 pF capacitors.

2.5.2 PERFORMANCE CHARACTERISTICS OF THE PHASE SWITCH

The phase switch module is characterised for its gain and phase response both when the Walsh function value is +10 V and -10 V. The gain and phase differences are also computed from the measurements. Walsh function control voltages were set statically to +10 V and -10 V and the characteristics obtained are given in Table 2.3.

2.6 NARROW BAND PASS FILTERS

The rf signal at the output of the phase switch box is wide band in nature. To frequency limit the signal to the desired band, it is next passed through a narrow band pass filter having 3 dB bandwidth of 120 MHz and 30 dB bandwidth of 200 MHz. There are four narrow band



- 1) MAR 3: PIN NOS: 2 AND 4 ARE GND PINS
- 2) SRA 2010 MH: PIN NOS: 2,5,6,7 ARE GND PINS,
4 IS OPEN

RAMAN RESEARCH INSTITUTE	
Title	CIRCUIT DIAGRAM OF PHASE SWITCH
Size	Document Number
A	PHASE.SCH
Date:	JULY 16, 1997
Sheet	of

Fig. 2.5.1 : CIRCUIT DIAGRAM OF PHASE SWITCH BOX

Freq. MHz	Input Return Loss(dB)	Output Return Loss(dB)	Gain dB		Gain Diff. (dG)	Phase-deg		Phase Diff. (dO)
			Walsh= 10 V(G1)	Walsh= -10 V(G2)		Walsh= 10 V(O1)	Walsh= -10 V(O2)	
1000	-27.33	-26.20	14.78	14.71	-0.07	153.21	-27.19	-180.40
1050	-26.32	-26.56	14.49	14.43	-0.06	124.84	304.60	179.76
1100	-25.76	-26.99	14.32	14.25	-0.07	-263.30	-83.93	179.37
1150	-25.62	-27.68	14.14	14.05	-0.09	68.46	-112.34	-180.80
1200	-25.73	-28.25	13.83	13.75	-0.08	39.15	218.75	179.60
1250	-25.82	-28.79	13.56	13.45	-0.11	10.50	189.67	179.17
1300	-25.82	-29.22	13.13	13.01	-0.12	-19.14	-199.31	-180.17
1350	-25.80	-29.62	12.73	12.64	-0.09	-47.99	131.84	179.83
1400	-25.50	-30.00	12.20	12.10	-0.10	-76.30	103.27	179.57
1450	-25.21	-30.41	11.75	11.66	-0.09	-103.94	-284.00	-180.06
1500	-24.93	-30.90	11.33	11.23	-0.10	-130.95	49.06	180.01

Table 2.3 : TYPICAL CHARACTERISTICS OF A PHASE SWITCH BOX

pass filters in the frequency range 1–1.45 GHz, they are centered at 1.06 GHz, 1.17 GHz, 1.28 GHz and 1.39 GHz. Depending on the frequency of observation, the rf signal can be routed through any of these filters with the help of rf switches.

Considerations that were taken into account in the design of the filter bank were, *e.g.*, ease of mass production, that the characteristics should not vary considerably from one filter bank to another, and the available space in the front end receiver box that is to be accommodated at the prime focus of the GMRT dish antennas. If all the resonators in a half wave parallel coupled line filter are bent in the form of a U-shape, then the filter is called a hairpin-line filter. On the other hand, if all the resonators except the input and output half wave parallel coupled lines are bent, then the filter is called a hybrid hairpin-line filter because it involves both hairpin structure as well as parallel coupled lines. A hybrid hairpin-line configuration was chosen to realise the narrow bandpass filter banks. An additional advantage of this choice is that the geometry of the filters are well suited for fabrication on a substrate that does not require connections to ground.

2.6.1 DESIGN OF THE NARROW BANDPASS FILTERS

The specifications for the narrow bandpass filters are

- (i) Center frequencies at 1.06, 1.17, 1.28 and 1.39 GHz,
- (ii) 3 dB bandwidth of 120 MHz,
- (iii) 30 dB bandwidth of 200 MHz, and
- (iv) Good return loss over the 3 dB bandwidth.

For the above specifications, design was carried out using the design procedure given by Edward & Frankel (1972) and Matthaei, Young & Jones (1964). All the four filters are realised on a common substrate. The planar structure of the filter is shown in Fig. 2.6.1. At the input and output of the filter, rf switches are provided to select one of the filters.

2.6.2 PERFORMANCE CHARACTERISTICS OF THE NARROW BANDPASS FILTERS

After designing the filter, it is realised on a microstrip base. The circuit is characterised for its various parameters like bandwidth, return loss, pass band ripple etc. The characterization is made using a vector network analyser which has got the capability of measuring both magnitude as well as the phase of the signal. The results obtained in the form of plots are shown in Fig. 2.6.2.

2.7 WIDE BANDPASS FILTERS

A wide bandpass filter follows the narrow bandpass filter in the signal path. The 3 dB bandwidth of the wide band filter is about 550 MHz. The main purpose of this filter is to increase the rejection for out of band noise and spurious signals above and in addition to what the narrow band pass filter provides. The filter is realised in the suspended strip form

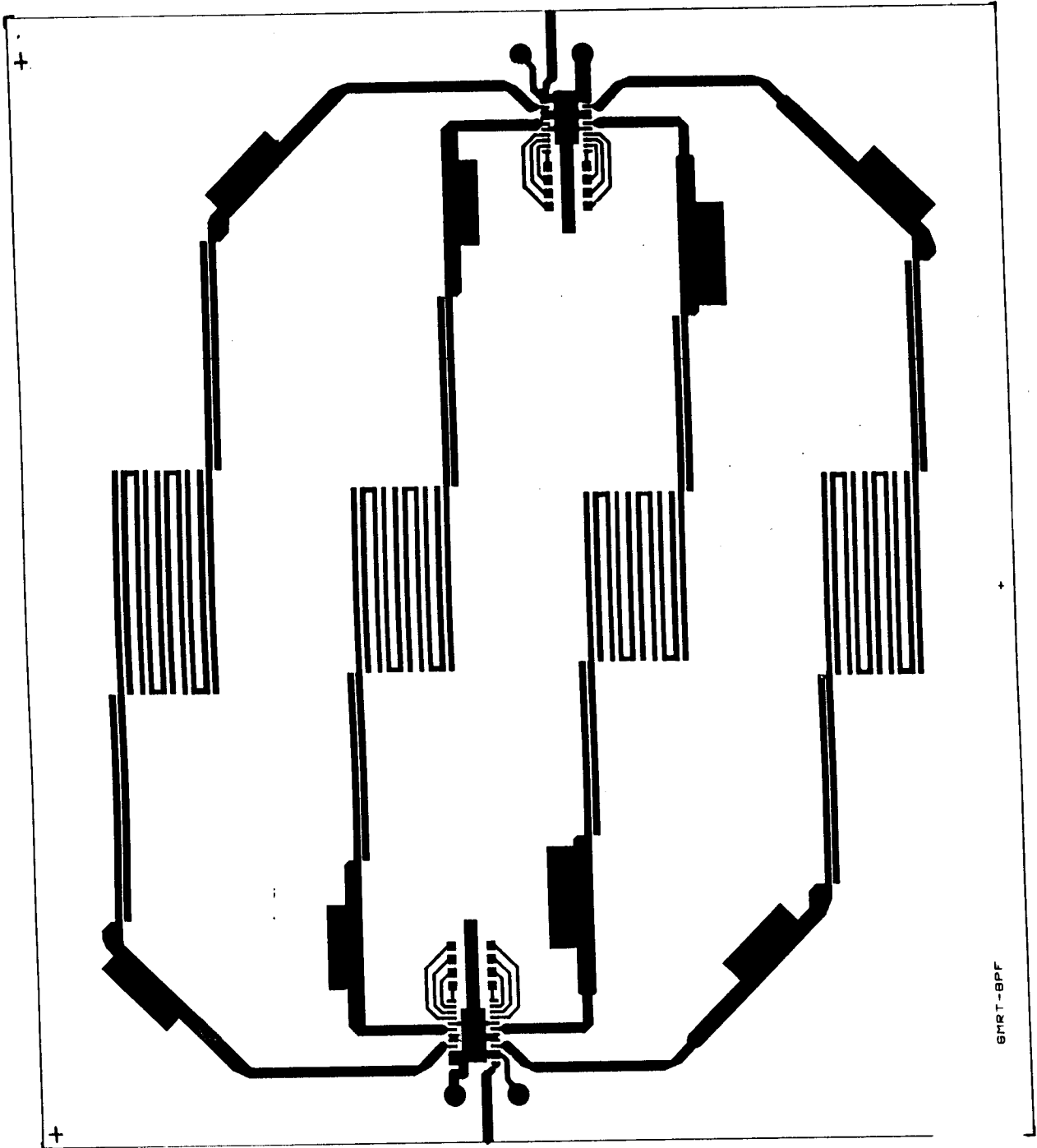


Fig. 2.6.1 : PLANAR STRUCTURE OF A NARROW BAND PASS FILTER

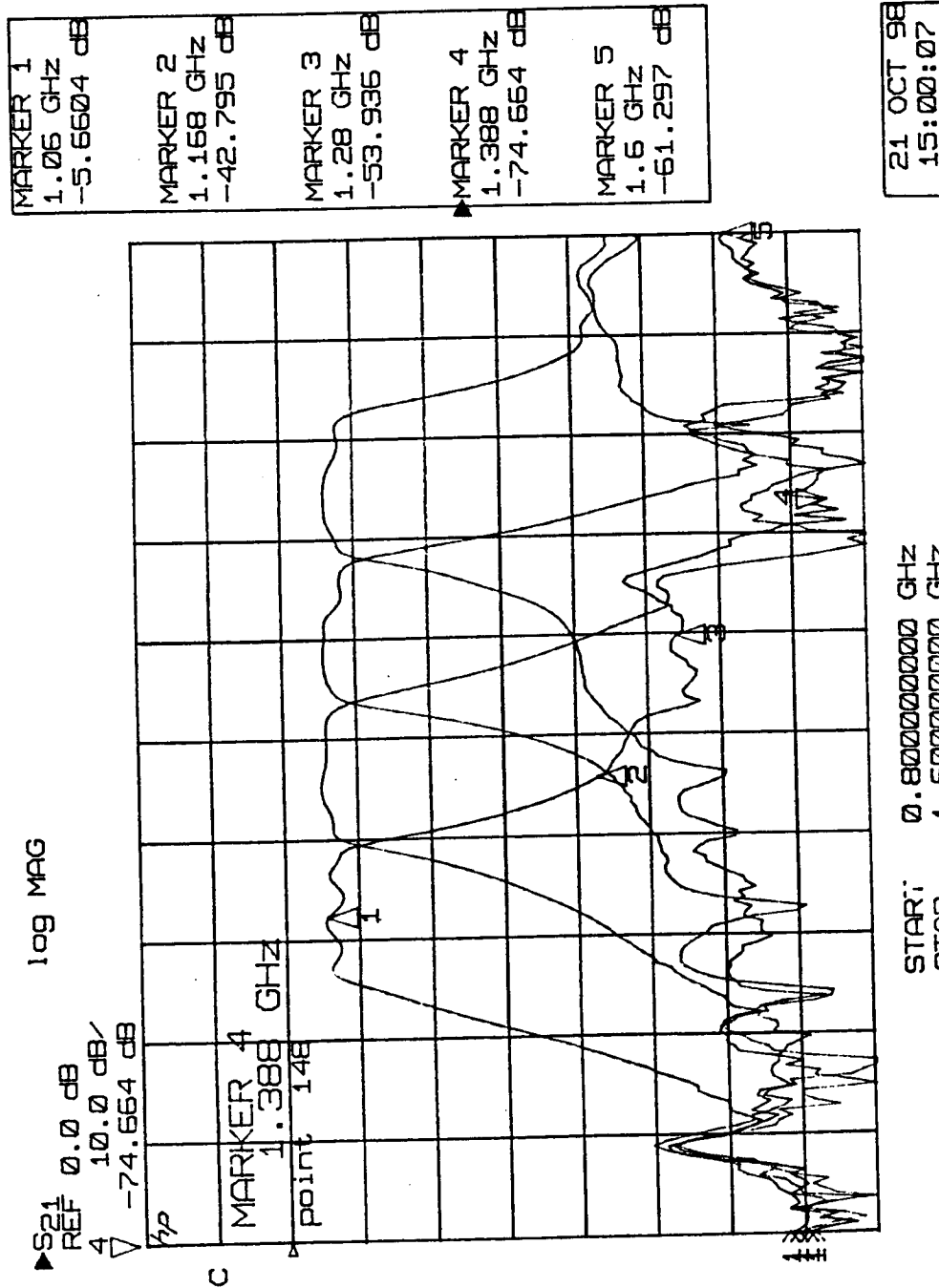


Fig. 2.6.2 : INSERTION LOSS CHARACTERISTICS OF NARROW BAND PASS FILTER

following the design procedure given by Matthaei, Young & Jones (1964). The planar structure of the filter is shown in Fig. 2.7.1. The filter has been characterised using a vector network analyser for its bandwidth, return loss and phase response. The results obtained are shown in the form of plots in Fig. 2.7.2.

2.8 NOISE GENERATOR

The GMRT receivers have automatic gain control (AGC) circuits in the IF signal path in order to maintain the signal power levels at fairly constant values, this is particularly important because the signals are transmitted from the antennas to the central station as analogue signals via optic fibres. In order to calibrate the correlated signals at the end of the signal path, it is necessary to constantly measure/monitor the overall system gain. Equivalently, the detected signals at the end of the receiver chain have to be calibrated and referred to as equivalent power at the input of the LNA. For this purpose, one injects and adds to the signal a stable amount of noise (T_{cal}) at the input of the LNA; this is synchronously detected at the receiver output and is used to calibrate the output signal. This calibrates out variations in the output owing to gain variations in the receiver.

As discussed at the beginning of this chapter, the amount of noise injected during an astronomical observation depends on the source being observed. There are four different levels of noise which may be injected from 10 to 500 K. Fig. 2.8.1 shows the schematic diagram of the noise generator module. The noise source output is selectively passed through a pair of attenuators to get four different possible noise levels. The attenuators are selected by using four rf switches. A CAL-OFF state, in which the noise injection is disabled, may also be achieved by toggling the middle two rf switches (NS_3 and NS_1) when any one of the four CAL-ON states are selected. The noise coming from the noise source is passed through a two way divider so that the same noise CAL is available in both the polarisation channels. The noise is injected into the system through a 24 dB directional coupler at the LNA input.

2.8.1 DESIGN OF THE NOISE GENERATOR MODULE

The noise source used in the noise generator module is a commercially available unit from Noise-Com. Its ENR (excess noise ratio) value is 36 dB. The power divider used to split the noise signal is a commercially available device from Mini-Circuits. The SP2T rf switches used to route the rf signal through attenuators are of absorptive type and sourced from Anzac. One advantage with the absorptive type switch is that whenever one of its ports is not used, then that port will be terminated in 50 Ohms. This ensures that the rf circuits on either side of the switch are always connected to 50 Ohms. This avoids reflections of rf signals due to impedance mismatch. A constant current source is used to drive the noise source to enable it to produce a constant noise output. The constant current source is built using a LM334 device. The noise CAL power at the output of the directional coupler inside the LNA is measured at various frequencies using a Noise figure meter. Table 2.4 shows typical values of the calibration signal (T_{cal}) at various frequencies for both the V and H channels.

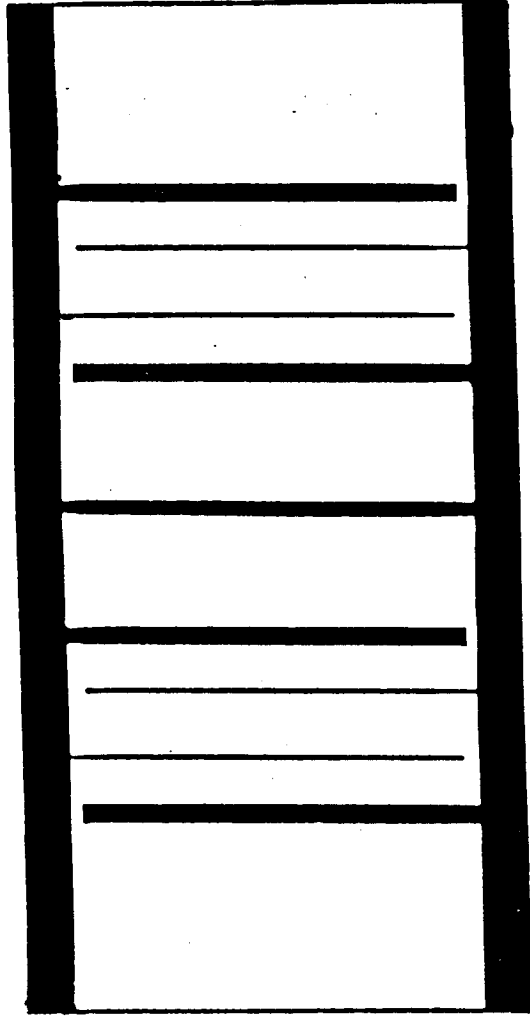


Fig. 2.7.1 : PLANAR STRUCTURE OF A WIDE BAND PASS FILTER

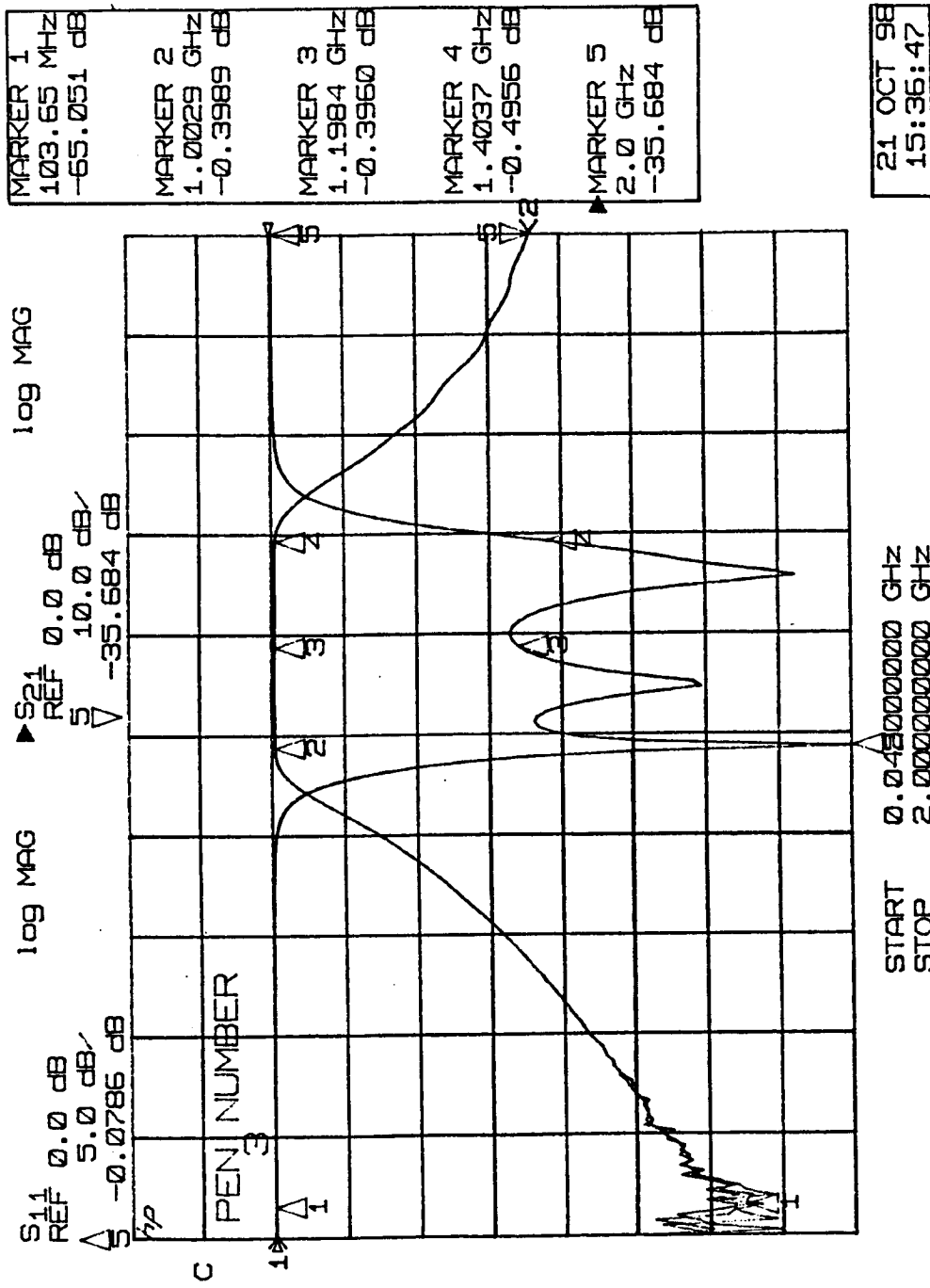


Fig. 2.7.2 : INSERTION LOSS AND RETURN LOSS CHARACTERISTICS OF WIDE BAND PASS FILTER

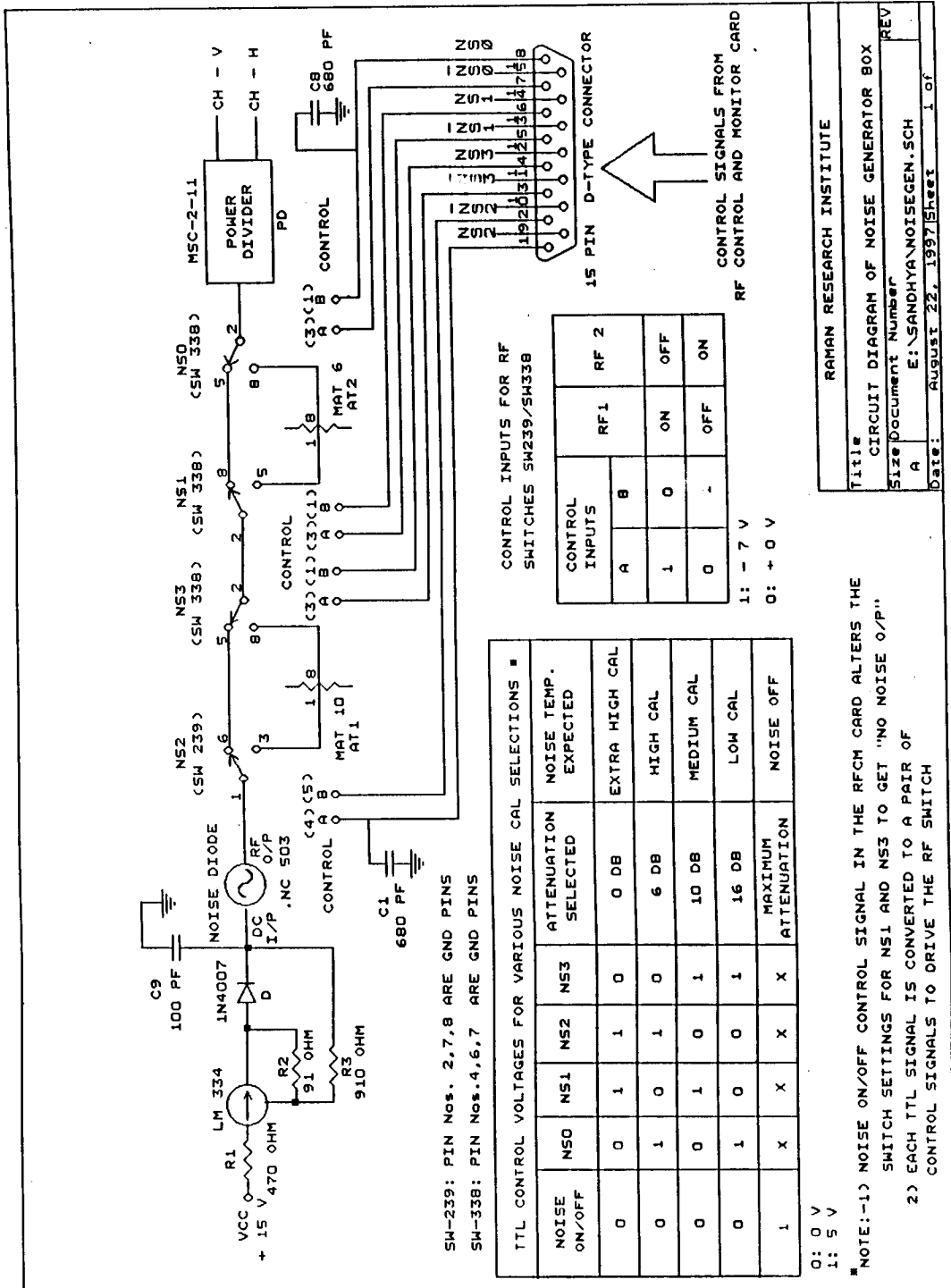


Fig. 2.8.1 : CIRCUIT DIAGRAM OF A NOISE GENERATOR BOX

Freq MHz	Noise CAL injected at the LNA input									
	Extra		Hi Cal (K)		High Cal (K)		Medium Cal (K)		Low Cal (K)	
	CHI	CH2	CHI	CH2	CHI	CH2	CHI	CH2	CHI	CH2
1000	607	620	218	224	80	81	18	18	18	18
1100	927	949	207	208	73	75	16	16	16	14
1200	1198	1214	193	197	73	70	18	18	18	16
1300	777	795	193	200	67	70	16	16	16	15
1400	561	578	207	213	66	67	18	18	18	14
1500	640	677	168	176	63	64	14	14	14	15

Table 2.4 : TYPICAL CHARACTERISTICS OF A NOISE GENERATOR BOX

2.9 POWER SUPPLY FOR THE 21 CM FRONT END RECEIVER

A separate power supply card has been designed to provide regulated voltages (*e.g.*, ± 5 V, 15 V) from an input unregulated voltage of ± 18 V. 78XX series voltage regulators are used for the purpose of regulation. The regulators have various capacitors at their input and output to reduce the ripple. They have, at their outputs, bleeders which are resistances drawing a constant current from the regulators. This helps in maintaining the regulation when the load current is very small. Another voltage of +12 V is obtained from an 'RFCM card', described below, which also provides various control signals to the receiver.

2.10 RF MONITOR AND CONTROL CARD

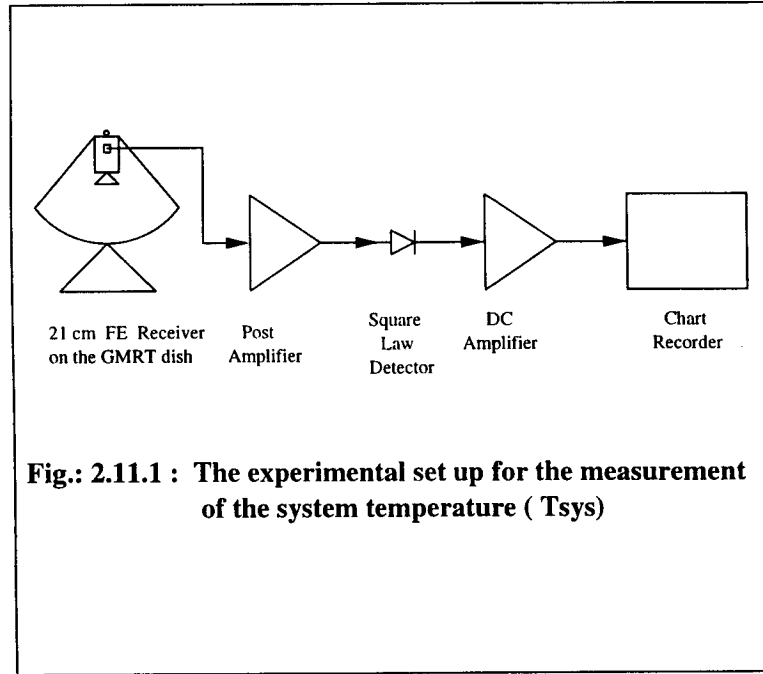
The RFCM card provides various control signals required for the control of the noise generator and narrow bandpass filters. In addition, it also provides a pair of Walsh function waveforms used for the phase modulation of the rf signal. It has two multiplexers of 16 inputs each, using which 32 different voltages can be monitored. This card accepts TTL inputs and gives out various control signals whose voltages can have either 0 V or -7 V, except for the Walsh switching signal.

2.11 MEASUREMENT OF SYSTEM TEMPERATURE

A low system temperature is one of the qualities that a receiver should possess for making sensitive observations in a short span of time and effectively using the aperture area of the antenna. It is defined as the sum of the antenna temperature obtained with the sky background present in its field of view and the receiver temperature. Therefore, for the measurement of the system temperature, the antenna should be pointed towards a region of the sky devoid of strong sources. The experimental setup for the measurement of T_{sys} is as shown in the Fig. 2.11.1. The rf signal from the 21cm front end output is amplified to the desired level by using a pair of post amplifiers and fed to a square law detector which produces a dc output signal proportional to the input rf power. The dc signal obtained is amplified using a dc amplifier and fed to a chart recorder. During the process of measurement, the CAL is switched ON and OFF manually to get a calibrated step which can be used to estimate the value of system temperature. Before starting the measurement, the chart recorder zero is marked to get the reference position with respect to which the deflections of the chart recorder would be measured. This may be achieved by shorting the input terminals of the recorder.

Let l_2 be the total amount of deflection obtained on the chart recorder when the receiver is connected to it (with CAL off) and l_1 be the total amount of deflection obtained on the chart recorder when the receiver, with CAL signal injected into it, is connected. Then

$$l_1 \propto (T_R + T_a + T_{CAL}), \quad (2.34)$$



$$l_2 \propto (T_R + T_a). \quad (2.35)$$

Manipulating the above equations we get

$$\frac{(l_1 - l_2)}{l_2} = \frac{T_{CAL}}{T_{sys}}, \quad \text{and} \quad (2.36)$$

$$T_{sys} = T_{CAL} \frac{l_2}{\Delta l}, \quad (2.37)$$

where $\Delta l = (l_1 - l_2)$.

The measurement of T_{sys} on GMRT dish is made several times at several frequencies by repeating the experiment as described above. The results obtained are shown in the Table 2.5.

Frequency MHz	System Temperature K	Dish Efficiency %
1060	53	38
1170	54	33
1280	63	35
1390	71	33

Table 2.5: System temperature and dish efficiencies of GMRT at various frequencies of the 21 cm FE receiver

2.12 MEASUREMENT OF THE APERTURE EFFICIENCY

Aperture efficiency of any antenna simply indicates what fractional part of the physical area of its aperture is effectively being utilised for collecting the sky radiation. By definition, it is the ratio of the effective area (A_e) to the physical area (A_{phy}) of the antenna. For the measurement of the aperture efficiency, the antenna beam is slewed across an unresolved celestial source with known flux density to get the deflection due to the source. The CAL signal is injected into the system before and after slewing across the source. The deflections obtained due to both CAL as well as the unresolved source in the sky are noted and from these T_a^{sky} is determined using the knowledge of the CAL injected. Then the value of T_a^{sky} is substituted in the relation (Ref. Eq. 1.21)

$$0.5SA_e = kT_a^{sky} \quad (2.38)$$

from which the effective area A_e is calculated. S in the above equation represents the flux density of the source being observed. The aperture efficiency is then found out by using the relation

$$\eta = \frac{A_e}{A_{phy}}. \quad (2.39)$$

The measured aperture efficiencies of the GMRT dish at various frequencies are listed in the Table 2.5.

2.13 POLARISATION IN THE 21 CM FRONT END RECEIVER

The polarisation state of any radiation may be analysed either with the help of linear basis components or a pair of circular components. Correspondingly, the feeds in the receiver system may be made either linearly polarised or circularly polarised. The choice is made depending on the type of observation being made. Even though the polarization properties of any wave may be determined completely either by circular or linear components, each one possesses its own advantages and disadvantages owing to the method adopted in analysing the data obtained and the way the measurement errors propagate to the required quantities.

Usually, if the percentage of circular polarization of an electromagnetic wave is to be determined accurately, linearly polarized feeds are preferred; whereas for linear polarization measurements circularly polarized feeds are preferred. If the IF signals are to be circularly polarized, the polarizer which is necessary to convert the linear components provided by linear OMTs in the feeds to circular components is placed immediately after the feed and before the LNAs so that the linear components get converted to circular before getting affected by any amplitude and phase mismatch between the two LNAs. The system temperature degradation due to the polarizer is minimised by cooling the polarizer. But the GMRT 21 cm front end receiver is uncooled and therefore the polarizer is placed after the LNA so that the system temperature is not degraded. This necessitates the rf signals in both the linear channels of the receiver at the input of the polarizer to be highly phase and amplitude matched over the entire frequency band. This may be very difficult to be implemented practically because the LNAs are easily tunable to have identical phase and gain only over a small range of frequencies. At other frequencies, phase and gain mismatches do exist and it may be difficult to study the polarization properties under this condition due to the unacceptably large leakage of one stokes parameter into the other. It may be also difficult to maintain the gain and phase stability between the LNAs over a long time because of variations in the ambient temperature.

GMRT 21 cm receiver is a 450 MHz wide band system and hence if the choice were made to have circularly polarized IFs, a major portion of the frequency band may not be useful for polarization studies. Therefore, it was decided to have linearly polarised IFs for the GMRT 21 cm system.

REFERENCES

- Bruce, M.T., 1978 , Antenna Design Notes, IEEE Trans. Antennas Prop., AP-26, p.367.
- Edward, G.C., Frankel, S., 1972, Hairpin-Line and Hybrid Hairpin line Half-wave parallel coupled Line filters, IEEE Trans. Microwave Theory Tech., MTT-20 , p.719. George, L.M., Leo, Y., Jones, E.M.T., 1964, Microwave Filters, Impedance Matching Networks and coupling structures, McGraw - Hill Book Company, New York.
- Guillermo, G., 1984, Microwave Transistor Amplifiers - Analysis and Design, Prentice Hall, In., Englewood cliffs, New Jersey.
- James, G.L., 1992, Journal of Electrical and Electronics Engineering , Australia - IE Aust. & IREE Aust.,12, p.137.
- Love, A.W., 1976, Electromagnetic Horn Antennas, IEEE Press, New York.
- Rudge, A.W., Milne, K., Olver, A.D., Knight, P., 1982, The Handbook of Antenna Design - IEE Electromagnetic Waves Series 15, p.338.
- Theodore, M., 1989, Microwave Transmission Design Data, Unisys, Inc.

CHAPTER 3

MEASUREMENT OF COSMIC MICROWAVE BACKGROUND TEMPERATURE USING THE GMRT 21 CM FRONT END RECEIVER

3.1 INTRODUCTION

Cosmology is the wholistic study of the properties and evolution of the universe and all of its constituents including galaxies and their distribution structures. Several models have been put forward to explain the details of the evolutionary process among which the Hot Big Bang theory is gaining substantial support from observations. According to this theory, when the density of matter was extremely high in the past, explosive expansion took place and the contents of the universe were thrown in all possible directions. Thus the universe was formed expanding with time. In the early stages of the explosion, when both the temperature and density were extremely high, the energetic photons combined together to produce particle and anti-particle pairs like electron-positron pairs and the pairs in turn annihilated to produce photons. The matter particles and radiation content of the universe were in thermodynamic equilibrium in which the abundances of particle species and the properties of the radiation were completely determined by the temperature of the universe. In this very early phase of the universe different particle species were relativistic and were present in roughly similar number densities with the radiation energy density dominating over the matter energy density.

As the universe expanded, the temperature decreased, the energies of the photons consequently decreased and pair creation of the more massive particles was no longer possible. These particles and their antiparticles continued to annihilate reducing their number density. For example, by the time the temperature of the universe had reduced to about 10^{10} K (when the universe was 1 sec old), only light particles (leptons) like electrons, positrons, neutrinos and anti-neutrinos were relativistic with number densities similar to that of the photons, whereas the more massive baryons — protons and neutrons — were non-relativistic and had number densities about a factor 10^{-10} of the photon number density. It may be noted that the residual numbers of these heavy baryons were determined by small fractional asymmetries in the number densities of bosons and their anti-particles which decay to produce protons and neutrons. Bosons annihilate slower than their anti-particles resulting in the asymmetry in their number density (Partridge, 1995).

As time progressed, the free neutrons were slowly decaying into the more stable protons. Simultaneously, the neutrons and protons combined together to give rise to deuterons (deuterium nuclei). Pairs of deuterons formed ^3He and these in turn produced ^4He after combining with other deuterons. The reactions also produced traces of ^7Be , ^7Li and ^6Li . The formation of these light element nuclei is critically dependent on the formation of deuterons. The deuteron nuclei are easily destroyed at early times when the temperatures were above

about 10^9 K, whereas at much later times the neutron abundance would be depleted owing to their decay and, therefore, there would not be sufficient neutrons that could form a significant amount of deuterons. As a consequence, the relative abundances of the light elements is fairly well determined by the baryon densities at the time when the universe was approximately 10^9 K. This formation of light elements continued until the neutrons were exhausted and all baryonic matter was in the form of nuclei of light elements like hydrogen, helium, beryllium and lithium. The hot big bang theory predicts that these light elements were formed primarily in the early universe and not in the stars we see today.

Observations of the nearby universe have yielded the values for the relative light elemental abundances: these have been used to calculate the baryonic matter density at the time when the temperature of the universe was about 10^9 K. Observations also tell us the present day baryonic density of the universe. Because the density of matter and the temperature of the radiation content of the universe decrease with cosmological expansion factor a ($a=1$ today) according to the relationships:

$$n_b = n_{b_0} a^{-3} \quad \text{and} \quad (3.1)$$

$$T_\gamma = T_{\gamma_0} a^{-1}, \quad (3.2)$$

the big bang hypothesis predicts about 3 K as the present day temperature of the radiation content of the Universe.

This thermal radiation which is left over from the hot and dense phase of the early universe is predicted to be present throughout the universe today. The 3 K radiation is called the *Cosmic Microwave Background Radiation* (CMB) and was predicted to have a blackbody Planck form. This is expected to have survived the expansion of the universe and its temperature has been falling off. The existence of the CMR was experimentally verified by Penzias and Wilson in 1965; this discovery is possibly the most important reason for the acceptance of the big bang cosmological model. Since then, several experimental groups around the world have made measurements of the CMB at different observing frequencies and have found that the spectrum of the radiation is very close to a Planck blackbody form.

One may ask the question as to why the Universe exists in the manner it is at present, why is the density of matter not greater or lesser than the observed value etc (Steven Weinberg). The answer for these questions lies in the ratio (n_ν/n_b) which decides the nature of the universe at earlier epochs. n_ν is the number density of photons of microwave background radiation and n_b is the number density of baryons. n_b can be estimated with fair accuracy by measuring the masses of stars, galaxies and other celestial objects in the Universe. But the determination of n_ν requires an accurate measurement of the background temperature T_{CMB} . Therefore, measurements of T_{CMB} improve the accuracy in our knowledge of the ratio (n_ν/n_b) ; this leads to a better understanding of light-element nucleosynthesis in the Early Universe.

3.2 DISTORTIONS IN THE COSMIC MICROWAVE BACKGROUND RADIATION SPECTRUM

To attain thermodynamic equilibrium between matter and radiation, there must be interactions between matter and radiation which can produce and absorb radiation and lead to an equilibrium condition in which the occupancies of energy states, by particles and photons, is completely specified by a common single temperature. The radiation spectrum thus obtained will have an energy density corresponding to the blackbody Planck form:

$$I(\nu) = \frac{8\pi h\nu^3}{c^2(\exp(\frac{h\nu}{kT}) - 1)}. \quad (3.3)$$

Some matter-radiation interactions that exchange energy are

- (i) Thermal Bremsstrahlung,
- (ii) Compton scattering, and
- (iii) Radiative Compton Scattering.

Thermal bremsstrahlung produces radiation whenever a free electron (e) is deflected by a positively charged particle (p) ($e + p \leftrightarrow e + p + \nu$). In Compton scattering, the electrons scatter the photons changing only their energy ($e + \nu \leftrightarrow e + \nu$), and the scattering interactions between photons and electrons allow only the photon energies to change but do not absorb or emit photons, *i.e.* the photon numbers are conserved. But in radiative Compton scattering, an additional photon is released when electron and photon interact with each other. If thermal bremsstrahlung or radiative Compton interactions were effective, any arbitrary spectrum would relax to the Planckian form as given in equation 3.3. It may be noted that for a radiation to relax to this form, it is necessary that the interactions between the radiation and matter allow both the photon numbers and energies to change. These interactions effectively occur only at a very high temperature and density at epochs when the temperature is of the order of 10^7 K and above. If these interactions become ineffective and only the Compton scattering interaction is effective, then the energy interchange between matter and the radiation gives rise to a non-Planckian Bose-Einstein spectrum for the radiation which is given by

$$I(\nu) = \frac{8\pi h\nu^3}{c^2(\exp(\frac{h\nu}{kT} + \mu) - 1)}, \quad (3.4)$$

where μ represents the amount of deviation of the Bose-Einstein spectrum from Planckian form. As the universe expanded and cooled, there was a time between when the temperature was in the range about 10^7 – 10^5 K when, indeed, Compton scattering was the only effective interaction, and if the radiation spectrum was distorted during this time from the Planck form, the spectral shape would be expected to have relaxed to a Bose-Einstein form.

As observed today, the spectrum would be expected to show an increasing deviation from the Planck spectrum at lower observing frequencies. However, the spectrum would

again be relaxed to Planck form at very low frequencies because the free-free interactions become increasingly effective at long wavelengths; therefore, the deviation is expected to be a maximum at an observing frequency of about 1 GHz today. Observations of the CMB brightness temperature at frequencies close to 1 GHz, therefore, will be a constraint on the models describing the processes occurring in the early universe at times when the temperatures were in the range 10^7 – 10^5 K.

When the radiation temperature dropped below about 10^5 K, none of the above interactions were effective in relaxing the spectrum back to either the Planck or Bose-Einstein form. If any energetic process caused a distortion of the radiation background, the radiation spectrum would have continued to remain distorted to the present day.

It has been observed that the CMB radiation is indeed thermal in nature and closely follows the Planckian spectrum. The measurement errors in the determinations of the CMB temperature increase with increasing wavelength, the 1-standard deviation ($1-\sigma$) errors are today about 0.3 K at 1.5 GHz and increase to 1 K at 1 GHz. In this chapter, an experiment is described which makes a measurement of CMB temperature over 100 MHz centered at 1.28 GHz.

3.3 MODIFICATIONS TO THE 21 CM FRONT END RECEIVER

The 21 cm front end receiver that was designed for GMRT and described in the previous chapter has been modified to meet the various requirements for absolute temperature measurements of the background sky; this is shown in Fig. 3.3.1. The corrugated horn is replaced by a corrugated plate in the feed assembly; this has been done mainly to reduce the sidelobe levels and minimise the ohmic loss in the feed. The corrugations are designed at the centre frequency of the 1 to 1.5 GHz band. The depth of the corrugations is kept at $\lambda/4$ and the spacing between the corrugations is maintained at 1.5λ at the centre frequency. The radio waves thus collected are guided through the orthomode transducer at the end of which it is picked up in the form of a co-axial signal. Only a single polarization signal has been used for this background measurement. The co-axial signal is fed to the low noise amplifier through a circulator. Port 1 of the circulator is connected to the V channel and port 3 is connected to the H channel of the OMT. The port 2 is connected to the LNA input. The circulator is a three terminal device used to avoid multiple reflections in the feed assembly. The multiple reflections, if allowed, may cause the LNA noise temperature contribution to be significantly dependent on the input matching and, consequently, the LNA temperature as measured under test conditions may be different from the LNA temperature when the LNA input is connected to the feed-OMT assembly. The reasons for using the circulator in this configuration are discussed in section 3.5. The RF signal, after getting amplified by the LNA, is phase modulated in the phase switch box. Then it is passed through both narrow band and wide band pass filters to get band limited to 120 MHz. The front end output is connected to the spectrum analyser through a commercial Miteq amplifier. The noise figure of the spectrum analyser is so high that in the absence of the Miteq amplifier, the spectrum analyser's noise contribution degrades the signal-to-noise by contributing significantly to the

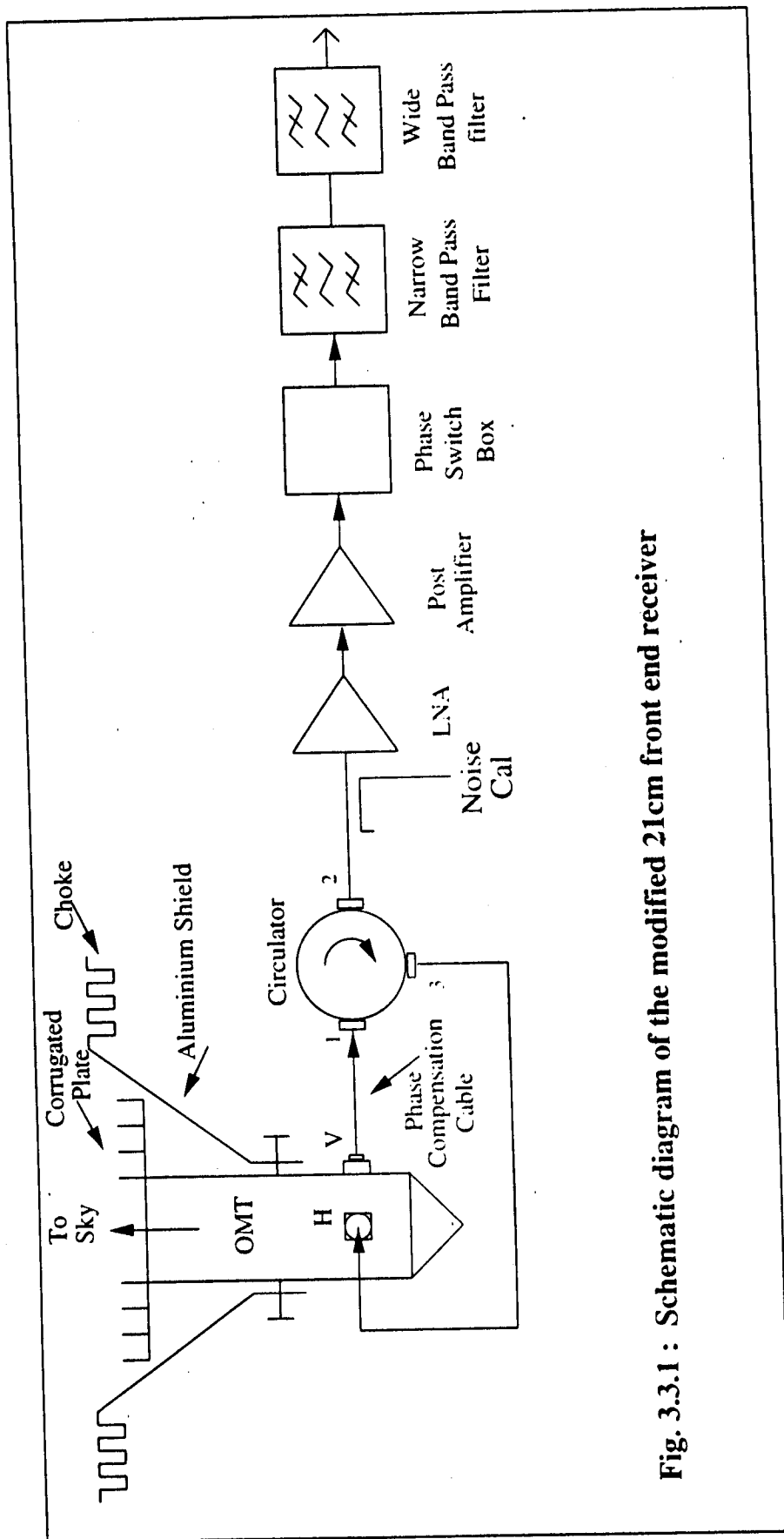


Fig. 3.3.1 : Schematic diagram of the modified 21cm front end receiver

system temperature. The power spectrum is measured by reading the trace of the spectrum analyser using a GPIB interface and its analysis is done in a PC. The receiver is covered all around by an aluminium sheet to minimise the ground radiation leakage into the front end receiver. With this shield the ground contribution could be reduced to as low as 0.3 K. The experimental procedure for measuring the ground contribution is discussed in Section 3.12.

Cosmic microwave background temperature (T_{CMB}) has been measured using the above receiver at 1280 MHz over a bandwidth of 100 MHz. The sky signal measured at the corrugated plate will be due to various sources like the cosmic microwave background, emission from our Milky Way Galaxy, atmosphere and ground contribution through sidelobes of the feed assembly; therefore, the sky temperature will be the sum of the Galactic temperature (T_{Gal}), atmospheric temperature (T_{atm}), ground temperature (T_{gnd}) and cosmic microwave background temperature (T_{CMB}). For an accurate determination of T_{CMB} , it is required to know the values of T_{Gal} , T_{atm} , and T_{gnd} so that these may be subtracted from the measurement of power at the corrugated plate. In addition, various system parameters like the receiver temperature (T_R), the reflection coefficient (Γ) and absorption coefficient (α) of the feed assembly (corrugated plate-OMT) are also to be determined. If T_a'' represents the sky signal incident on the corrugated plate, then the net (sky + noise) signal at the output terminal of the OMT is given by (Ref. Eq. 1.19)

$$T_a = T_a''(1 - \Gamma^2)(1 - \alpha) + \alpha T_{amb}, \quad (3.5)$$

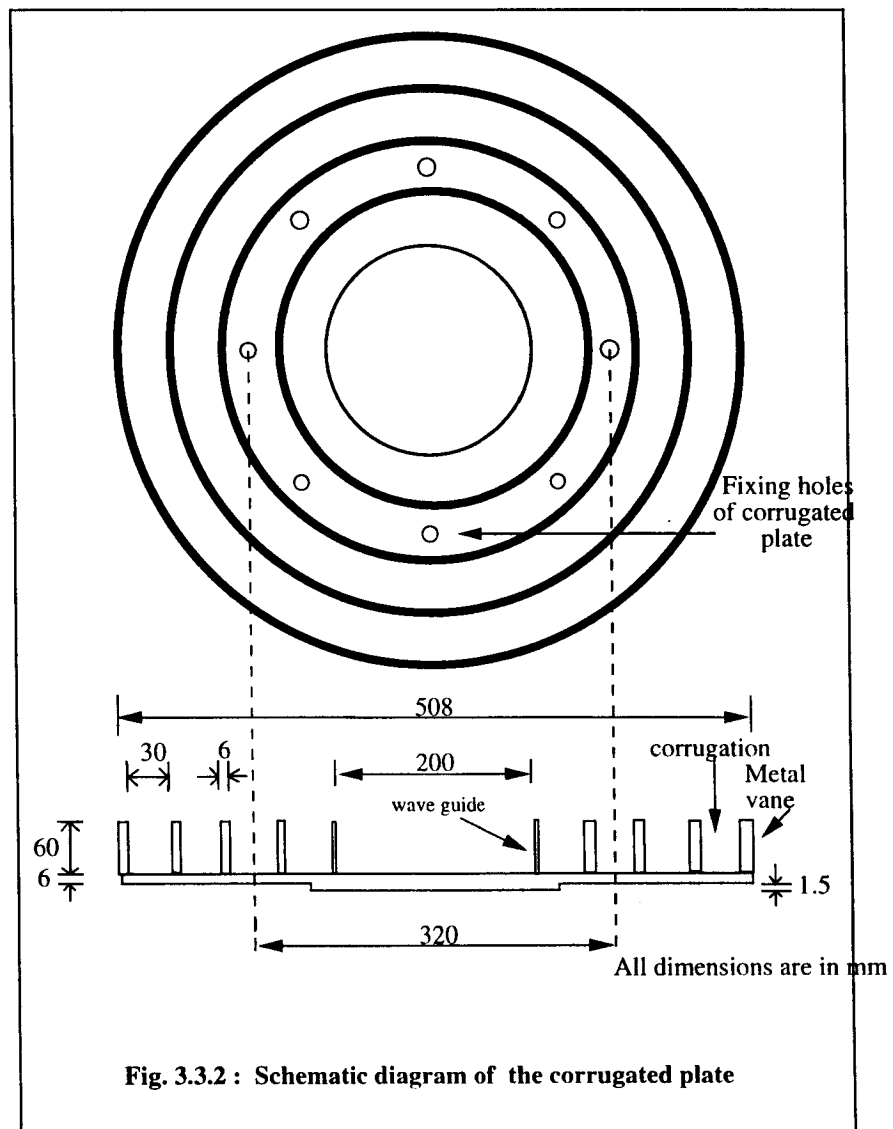
and the system temperature T_{sys} as referred to the input of the circulator (port 1) is given by

$$T_{sys} = T_a''(1 - \Gamma^2)(1 - \alpha) + \alpha T_{amb} + T_R \quad (3.6)$$

where $T_a'' = T_{Gal} + T_{atm} + T_{gnd} + T_{CMB}$. In the above equation 3.6, the first term represents the net sky signal present at the input of the circulator, the second term represents the thermal noise contribution from the horn assembly and the third term is the receiver temperature as referred to the circulator input. The measurement of the various parameters in the above equations are necessary for an estimation of the absolute value of T_{CMB} from a measurement of the net noise temperature at the input of the circulator.

A photographic view of the receiver for the CMB measurement is shown below. The entire electronics of the system is put inside a (40 cm x 60cm x 100cm) rectangular box. At the one end of it, extends out a corrugated plate connected to the OMT which is housed inside the box. The entire receiver box is covered on all the four sides by four identical aluminium sheets which act as a shield to prevent ground radiation from entering into the system. The receiver output is connected to the spectrum analyser mounted on the trolley with the help of an rf cable. The trace data obtained in the spectrum analyser is recorded in the computer.

with the corrugated plate is shown in Fig. 3.3.3. It is clear from the figure that the radiation patterns in both V and H planes are symmetrical and have a -3 dB beam width of $\approx 60^\circ$. This radiation pattern is symmetrical and uniform when compared to the radiation pattern of the OMT alone which possesses slightly less 3 dB beam width and more sidelobe level.



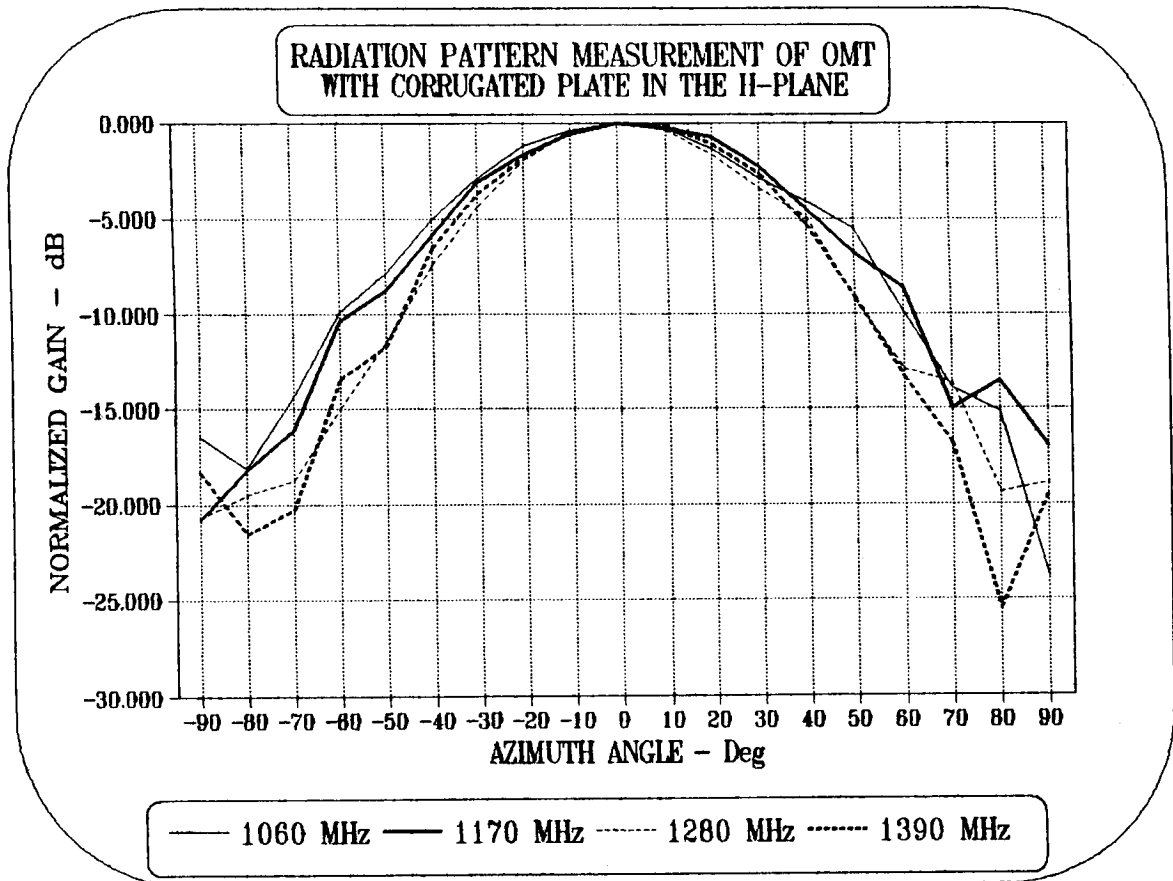
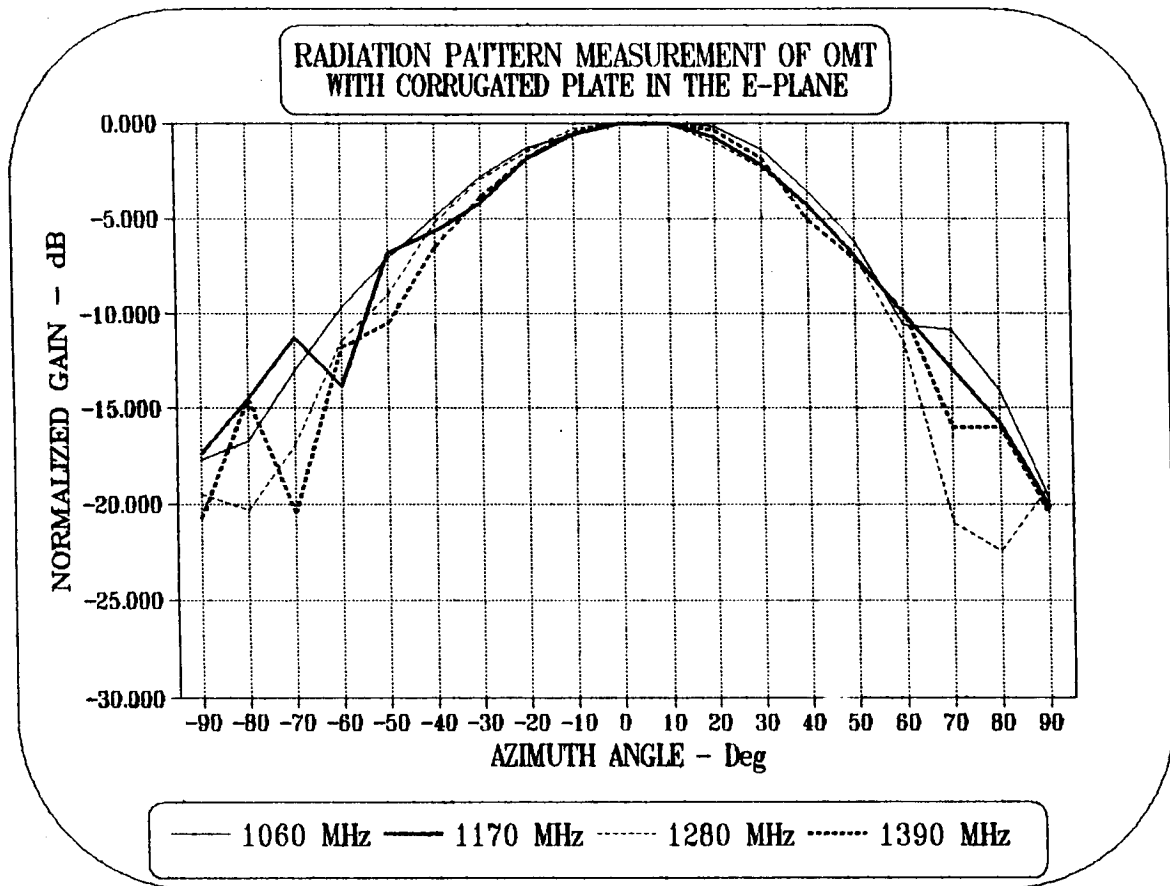
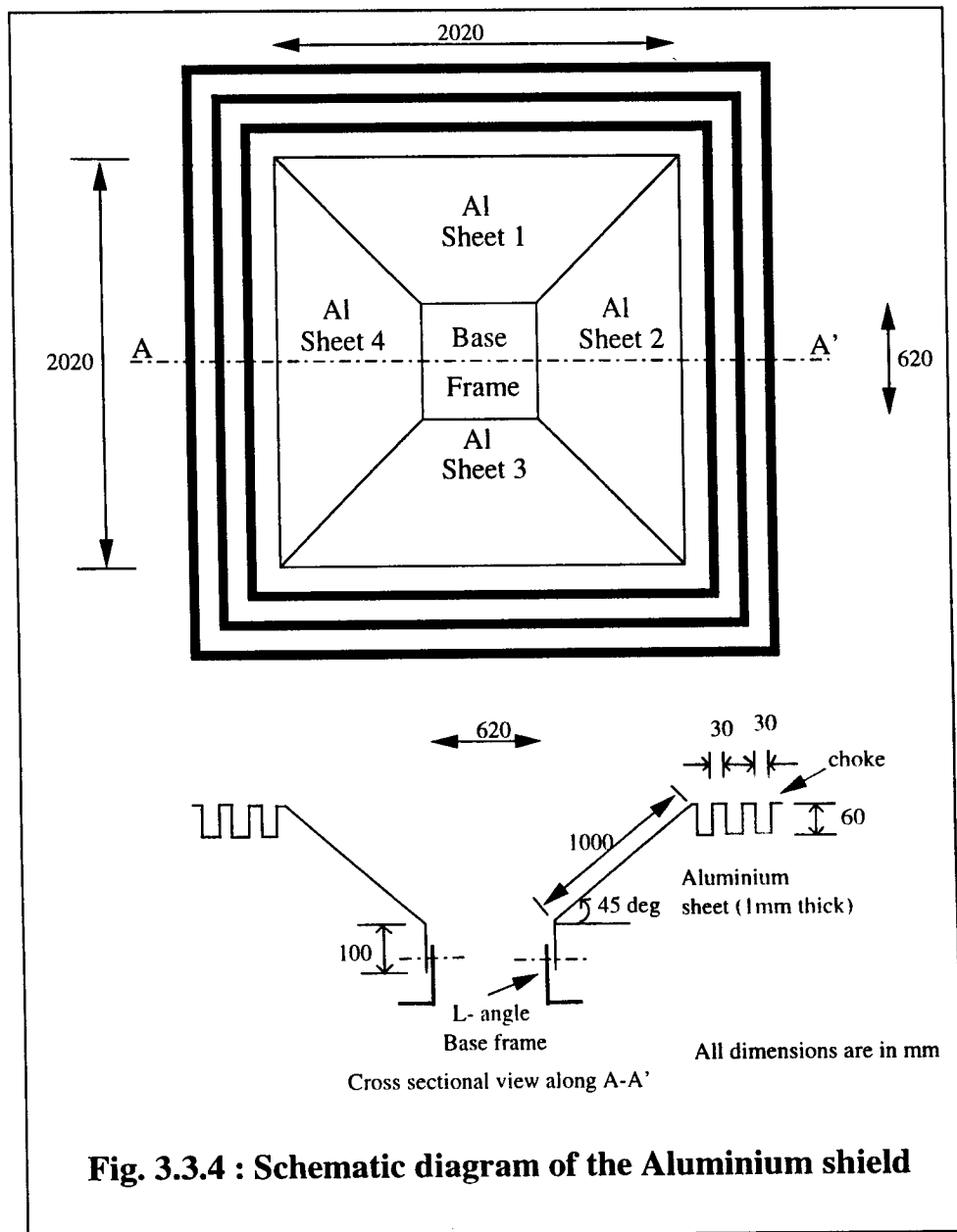


Fig. 3.3.3 : RADIATION PATTERN MEASUREMENTS OF OMT WITH CORRUGATED PLATE IN BOTH E & H PLANES

3.3.1.2 DESIGN OF THE ALUMINIUM SHIELD

An aluminium sheet is used as a shield to reduce the ground contribution to the system temperature of the 21 cm receiver. The shield is made of four discrete parts of similar dimensions, each having a vertical straight section of about 10 cm in height and then is bent at 45 deg. to the vertical axis over a length of 1m. At the end of it is attached a choke formed out of thin aluminium sheet. The main purpose of it is to reduce the ground noise entering into the system through edge diffraction. The dimensions of the choke are shown in Fig. 3.3.4. The shield is fixed to an aluminium square base frame made out of 1.5-inch angles. It may be fixed to the receiver at any height from ground level.



3.4 CALIBRATION OF A PLATINUM RESISTANCE THERMOMETER

The receiver system may be viewed as a thermometer that is specifically built to measure the sky temperature. The absolute precision of the measurement depends on the calibration and this has been done using liquid baths. The temperatures of the baths have been measured using platinum resistance thermometers whose primary calibration is described in this subsection.

The primary thermometer used for the calibration in the range 0-100° C was chosen to be a mercury thermometer. It was found that this thermometer reading was 0.1 ± 0.1 ° C when placed in a water bath with ice and 96.9 ± 0.1 ° C when placed in boiling water; these values are consistent with the expected freezing and boiling temperatures of water corresponding to the atmospheric pressure in the laboratory at Bangalore.

The sensor used for the measurement of temperature is made up of platinum material (Pt-100) whose resistance varies fairly linearly with temperature in the regime of interest to this experiment. The sensor is driven by a constant current source. Under this condition, the sensor changes its terminal voltage for any change in the ambient temperature by varying its resistance. The thermometer is calibrated by dipping it in a temperature controlled chiller (Ultra Temp. 2000) and measuring the voltage across it. A precision mercury thermometer was also placed in the bath in close proximity to the platinum resistor; this was deemed a better measure of the bath temperature as compared to the thermometer of the chiller unit because the internal sensor of the chiller was located at a distance from the platinum resistance. Indeed, it was found that the readings of the mercury thermometer deviated from the inbuilt thermometer of the chiller at temperatures within a few tens of degrees of the freezing and boiling points of the bath liquid (water).

From a plot of the measured voltage across the platinum resistance versus the temperature of the bath as measured by the mercury thermometer, a calibration relationship was determined for the platinum resistance. Fig. 3.4.1 shows the calibration measurements in the range 0–100° C for the sensor used for the temperature calibration. The sensor was also calibrated at liquid nitrogen temperatures by placing it in a liquid nitrogen bath whose temperature was measured using (a) a calibrated cryogenic thermometer in the Indian Space Research Organization (ISRO) at Bangalore and (b) a Pt-1k commercial calibrated sensor from Rosemount Corporation. Because the slope of the resistance versus temperature relation was known for the platinum sensor separately at liquid nitrogen temperatures and in the 0-100° C range, the calibration was used only to derive the normalizations at these two temperature regimes. The experimental setup for the calibration of the temperature sensor is as shown in Fig. 3.4.2. The relations obtained from the calibration measurements for the determination of temperature using the measured voltages are

$$V = 195.531799 + 0.757149(T + 273.15), \text{ and} \quad (3.7)$$

$$V = 0.83T - 25.88, \quad (3.8)$$

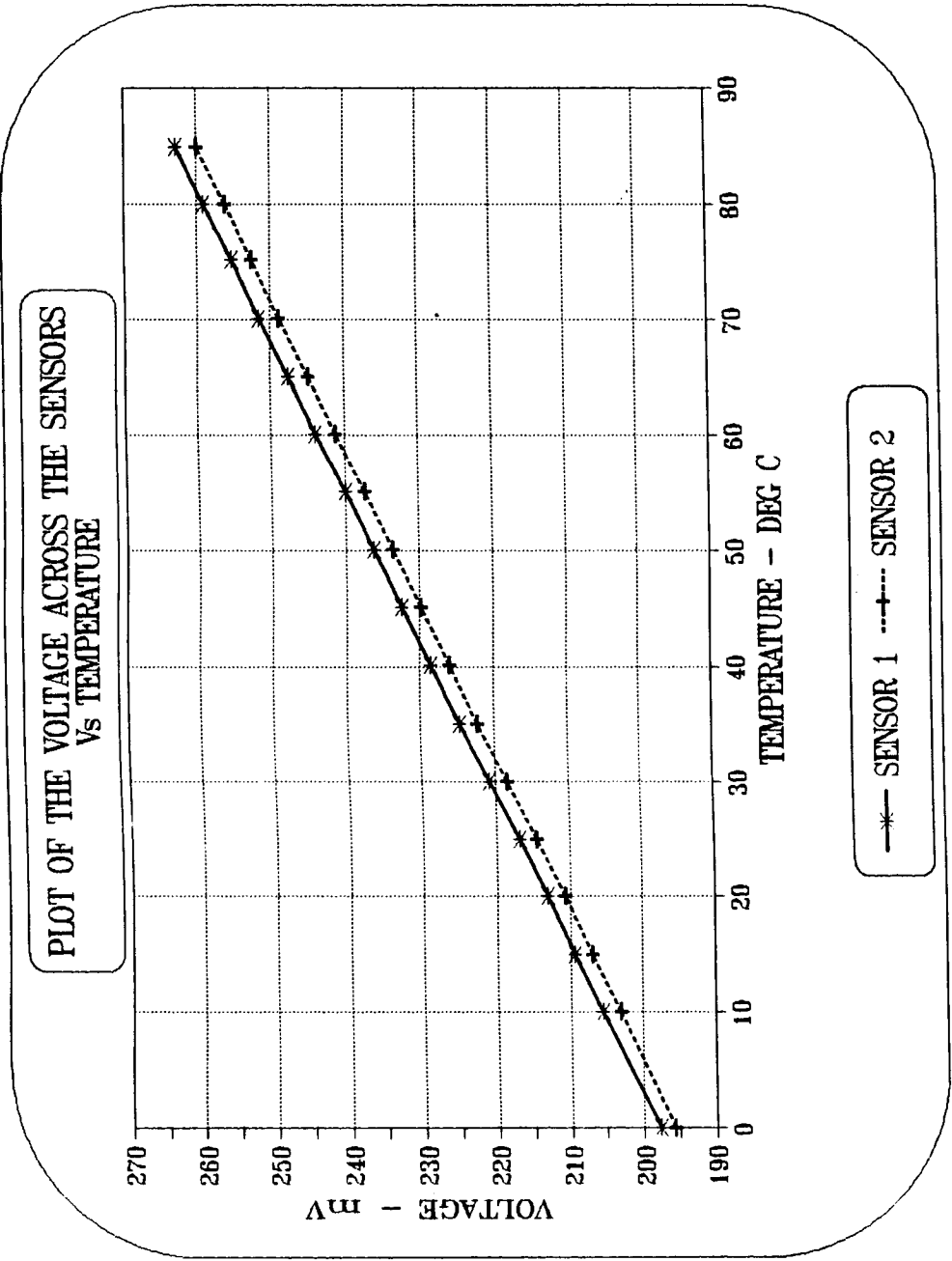


Fig. 3.4.1 : CALIBRATION CURVES OF THE SENSORS USED FOR THE TEMPERATURE MEASUREMENT

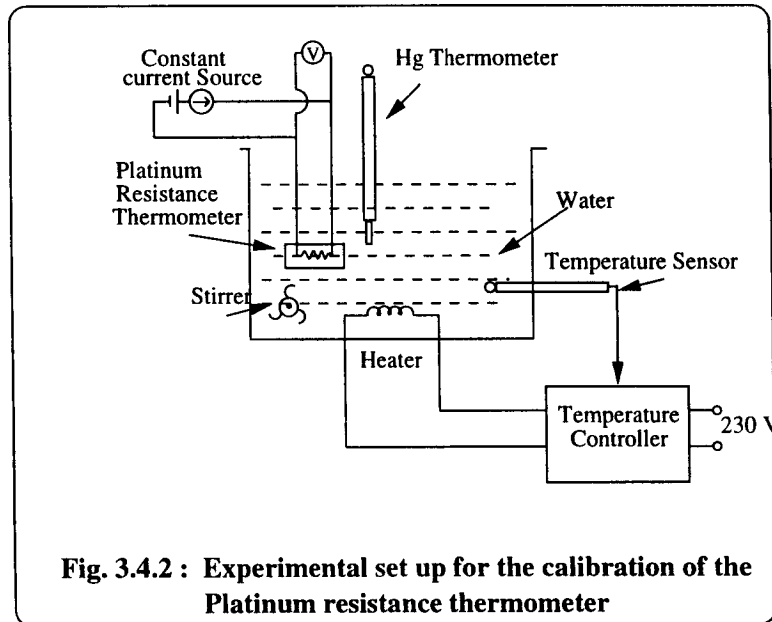
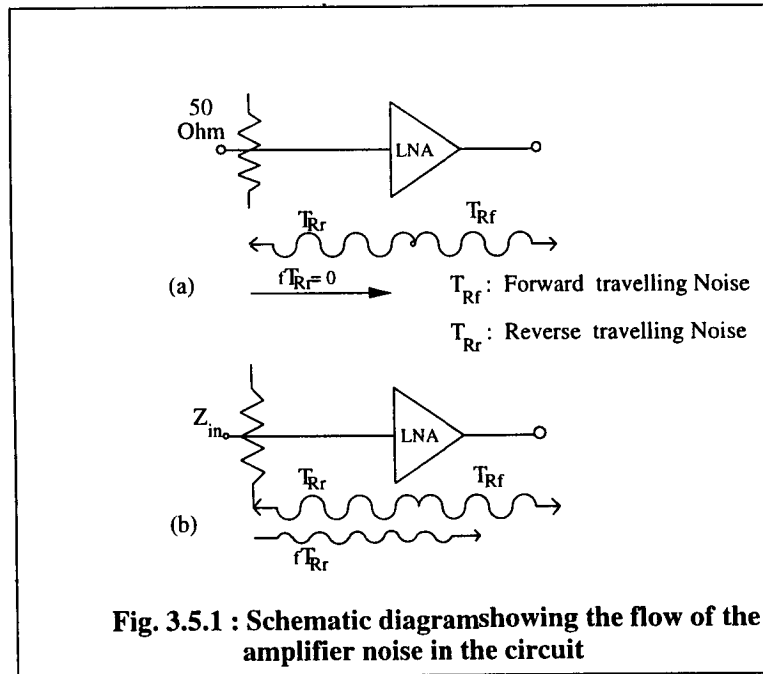


Fig. 3.4.2 : Experimental set up for the calibration of the Platinum resistance thermometer

where T is the temperature of the sensor in Kelvin and V is the voltage measured across the sensor when its temperature is T K. The equation 3.7 is used while measuring the temperature in the range $0-100^{\circ}\text{C}$ and equation 3.8 is used for the temperature range $-50-100\text{K}$. The calibrated platinum resistance thermometer is estimated to give the temperature of liquid nitrogen baths to within 0.2K and the temperature of water in the range $0-100^{\circ}\text{C}$ to within 0.1K .

3.5 INTRODUCTION OF A CIRCULATOR BETWEEN THE OMT AND LNA

The receiver temperature, which is the noise produced within the LNA, may be expected to propagate both towards the LNA output and towards the LNA input. If the noise power travelling towards the input is terminated in a good $50\ \Omega$ load, then the receiver temperature T_R , measured at the output of the LNA, will be due only to the noise travelling towards the output T_{Rf} (Ref. Fig. 3.5.1(a)). On the other hand, if the noise travelling towards the input of the amplifier T_{Rr} does not get fully absorbed in the load because of an impedance mismatch, a part of the power, fT_{Rr} will be reflected back to the LNA and will coherently combine with the noise component that was initially propagating towards the output. Consequently, under conditions where there is an impedance mismatch at the LNA input, the noise temperature T_R' will be equal to $T_R + \Delta T_R$, where ΔT_R is the change in the LNA noise temperature due to the reflected noise power at the input (Ref. Fig. 3.5.1(b)). The value of ΔT_R depends on the amount of impedance mismatch at the LNA input and the delay in the reflected noise signal when it combines with the forwardly propagating noise.



The receiver temperature T_R of the amplifier will be nearly T_{Rf} when a standard noise source of a Noise Figure Meter is used while determining the LNA T_R because the noise source is a good 50 ohm device and the LNA input matching network is designed for a 50 Ω input impedance. But when the corrugated plate-OMT combination is connected to the LNA for the sky observation, the actual receiver temperature would be different because the feed assembly is not well matched to 50 Ω . Therefore, under these conditions it would be erroneous to consider T_R as the receiver temperature. This problem may be overcome by either

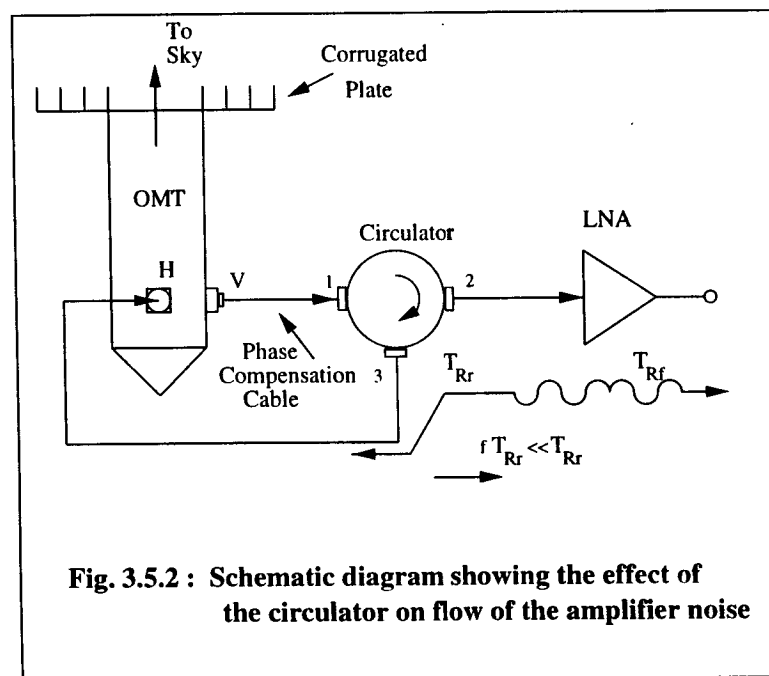
(i) properly estimating ΔT_R by measuring the amount of mismatch and the delay of the reflected noise, or

(ii) by minimizing the absolute value of ΔT_R .

(iii) by introducing a long lossless rf line at the LNA input which will introduce a large delay equal to or greater than the inverse bandwidth for the reflected signal. This will make the reflected noise add incoherently with the forward noise minimising the value of ΔT_R .

A circulator is commonly used to minimize the magnitude of ΔT_R . A circulator is a three terminal passive device having a characteristic feature of offering least amount of attenuation for the flow of rf signal in the direction from port 1 to port 2 as shown in the Fig. 3.5.2, and maximum attenuation in the reverse direction. The V-channel output from the OMT, which represents the sky signal T_a that is to be measured, is connected to port 1 of the circulator; this signal appears at port 2 with a small attenuation and the port 2 is connected to the input of the LNA. The H-channel of the OMT is connected to port 3 of the circulator. The LNA noise power that travels towards the LNA input enters port 2; this power is transmitted to port 3 and most of it is radiated towards the sky via the H port of the OMT which is

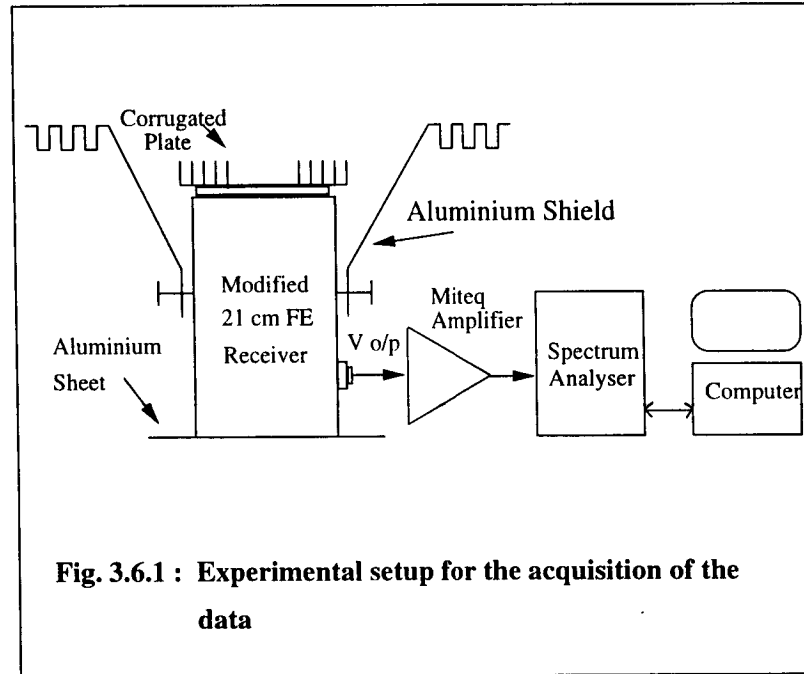
connected to the port 3. The LNA noise that is reflected at the H-channel port of the OMT owing to the impedance mismatch, as well as sky power that enters the feed assembly with a polarization appropriate to the H port, propagate into the circulator via its port 3. With a small attenuation, these appear at port 1, a major portion of it gets radiated towards the sky through the V-channel of the OMT; an approximately -20 dB down component gets reflected and propagates into the port 1 of the circulator and emerges from port 2. This will combine with the direct noise coming from the port 3 towards port 2 coherently. The effect of this coherent addition may be reduced by adjusting the phase of one of the signals so that they cancel at port 2. This can be done by introducing a semi-rigid cable of appropriate length between the OMT V-channel and circulator port 1. This cable is shown in the Fig. 3.3.1 as the phase compensation cable. Because the introduction of the circulator in the signal path along with the phase compensation cable minimizes the reflection of LNA noise emerging from the LNA input and also cancels the noise travelling from port 3 to port 2 entering port 3 of the circulator, the noise temperature ΔT_R also gets reduced quite significantly. Signals entering port 3 have been measured to appear at port 2 attenuated by at least 25 dB because of the cancellation.



3.6 THE DATA ACQUISITION SYSTEM

The experimental setup for the measurement of the cosmic microwave background temperature is as shown in Fig. 3.6.1. The sky radiation collected by the corrugated plate-OMT is amplified and band limited in the 21 cm front end receiver. The V-channel of the receiver output is connected to the spectrum analyser to measure the power received. Using a PC,

data is acquired from the spectrum analyser after setting the various instrument parameters. The noise CAL is periodically switched ON and OFF during the acquisition for calibrating the receiver; the CAL remains ON for about a second and OFF for a second. The appropriate CAL power level and filter selections are manually set.



While acquiring the data, the spectrum analyser is set to cover a 100 MHz span around 1280 MHz center frequency at 1 MHz resolution bandwidth. The video averaging function is disabled. The spectrum analyser is interfaced to a PC with an industry-standard general purpose interface board (GPIB) and measurement of the power spectrum is made by acquiring the trace as displayed by the spectrum analyser into the PC. During each readout, 401 points of the frequency spectrum are read from the spectrum analyser. In about a second, 120x2 traces are read (120 with CAL in ON state and 120 with CAL OFF) and the average power in those traces are calculated separately for the CAL ON and CAL OFF states over a 100 MHz band. Spectra may be obtained with a fractional accuracy of about 0.15% if data is acquired over a period of one hour.

3.7 MEASUREMENT OF THE RECEIVER TEMPERATURE (T_R) AND CALIBRATION-SIGNAL TEMPERATURE (T_{cal})

Receiver temperature T_R is the noise contribution due to the low noise amplifier, and the calibration-signal temperature T_{cal} is the power in the calibration signal which is injected into the system for the purpose of calibration. The measurements of T_R and T_{cal} are made by comparing their noise powers with those from resistor terminations placed in standard

temperature baths containing separately liquid nitrogen T_{N_2} and ambient temperature water T_{amb} . The experimental setup for the measurement is shown in Fig. 3.7.1. A circulator is used at the input of the LNA to isolate the LNA from reflections in the corrugated plate-OMT assembly while observing the sky. For the calibration of T_R and T_{cal} , Port 1 and port 3 of the circulator are terminated in 50Ω loads and port 2 is connected to the LNA input. The termination at port 3 is kept immersed in liquid nitrogen, while the termination at port 1 is separately immersed in liquid nitrogen and then ambient temperature water for the process of calibration. The calibrated platinum resistance thermometer is used to measure the temperature of the 50Ω load at port 1. The calibration signal (T_{cal}) is injected in alternate seconds of time into the LNA module from the noise generator box and this calibration signal is coupled into the signal path through a directional coupler. The front end output is connected to the spectrum analyser to measure the powers separately with the cal signal ON and OFF. When the termination load at port 1 of the circulator is immersed in water, let P_1 and P_2 be the receiver output powers when the CAL is ON and OFF respectively. Similarly, when the termination load is immersed in liquid nitrogen, let P_3 and P_4 be the receiver output power when the CAL is ON and OFF respectively. Then,

$$P_1 \propto (T_R + T_{amb} + T_{cal}), \quad (3.9)$$

$$P_2 \propto (T_R + T_{amb}), \quad (3.10)$$

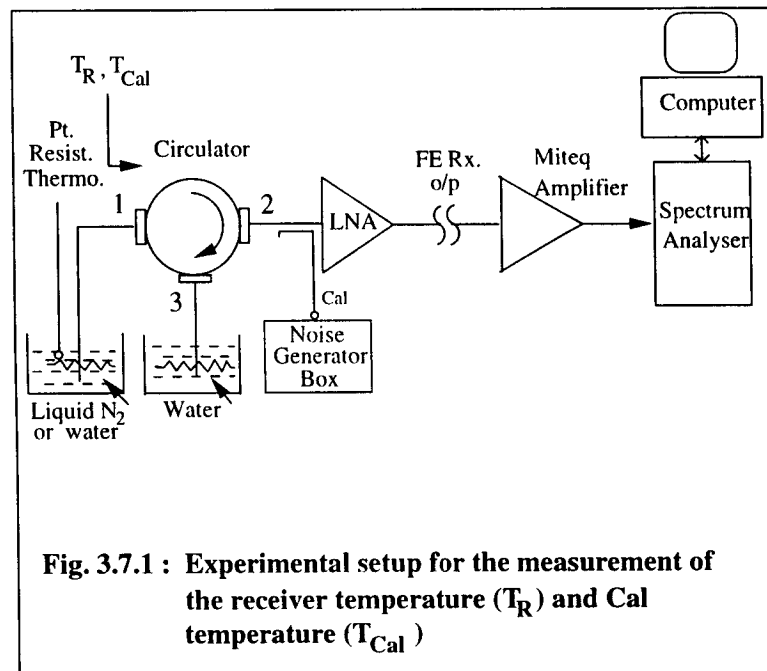


Fig. 3.7.1 : Experimental setup for the measurement of the receiver temperature (T_R) and Cal temperature (T_{Cal})

$$P_3 \propto (T_R + T_{N2} + T_{cal}) \quad \text{and} \quad (3.11)$$

$$P_4 \propto (T_R + T_{N2}). \quad (3.12)$$

Simplifying the above equations,

$$\frac{(P_1 - P_2)}{P_2} = \frac{T_{cal}}{T_R + T_{amb}} \quad \text{and} \quad (3.13)$$

$$\frac{(P_3 - P_4)}{P_4} = \frac{T_{cal}}{T_R + T_{N2}}. \quad (3.14)$$

Let x and y represent the LHS of equations 3.13 and 3.14 respectively. These are quantities which are obtained from the total power measurements and are independent of the gain of the system and are, therefore, not sensitive to temporal drifts in the system amplifier gains. Substituting these observables in the above equations,

$$T_{cal} = x(T_R + T_{amb}) \quad \text{and} \quad (3.15)$$

$$T_{cal} = y(T_R + T_{N2}). \quad (3.16)$$

Equating these two equations,

$$x(T_R + T_{amb}) = y(T_R + T_{N2}), \quad \text{or}$$

$$T_R = \frac{(xT_{amb} - yT_{N2})}{(y - x)}. \quad (3.17)$$

Having estimated the value of T_R , T_{cal} may be calculated using equation 3.15. The measurements were made adopting the acquisition procedure outlined in section 3.6. The $1-\sigma$ errors in the T_R and T_{cal} estimates owing to measurement noise (corresponding to the finite bandwidth and averaging time of the measurement) are 0.38 K and 0.20 K respectively. The errors due to the uncertainty in the temperatures of the liquid nitrogen and ambient temperature water baths are 0.34 K for T_R and 0.08 K for T_{CAL} . The measured values of T_R and T_{cal} are

$$T_R = 52.12 \pm 0.51 \text{ K} \quad \text{and} \quad (3.18)$$

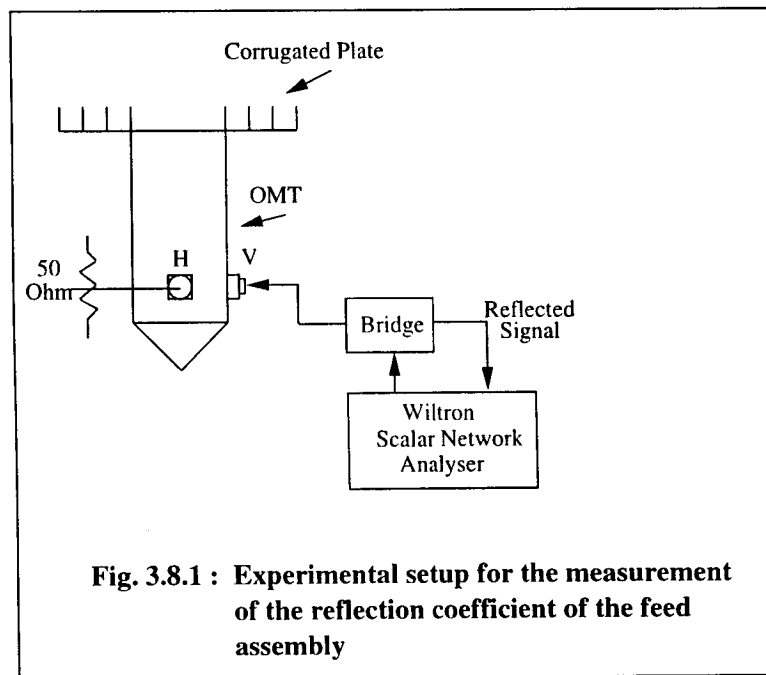
$$T_{CAL} = 70.166 \pm 0.215 \text{ K}, \quad (3.19)$$

where the uncertainties quoted represent $1-\sigma$ errors.

3.8 MEASUREMENT OF THE REFLECTION COEFFICIENT (Γ) OF THE FEED ASSEMBLY

Due to any impedance mismatch between the antenna and the sky, only some portion of the incident signal gets absorbed and the rest gets reflected. The amount of signal that gets reflected is determined by the voltage reflection coefficient (Γ) of the feed assembly. Fig. 3.8.1 shows the experimental setup for the determination of the reflection coefficient of the feed: because the feed system is passive and hence reciprocal, the system may be operated as a radiator in order to measure the reflection coefficient. The setup consists of a scalar network analyser connected to the V-channel of the feed assembly. A CW signal with a frequency that sweeps through the range of interest is injected into the V-channel connector of the OMT and the reflected signal is fed back to the analyser for comparison. The return loss of the feed assembly over the relevant range of frequencies is shown in the form of a plot in Fig. 3.8.2. From the return loss measurements the reflection coefficient Γ is determined using the relation

$$\text{Return Loss} = 10 \log_{10} \left(\frac{1}{\Gamma^2} \right). \quad (3.20)$$



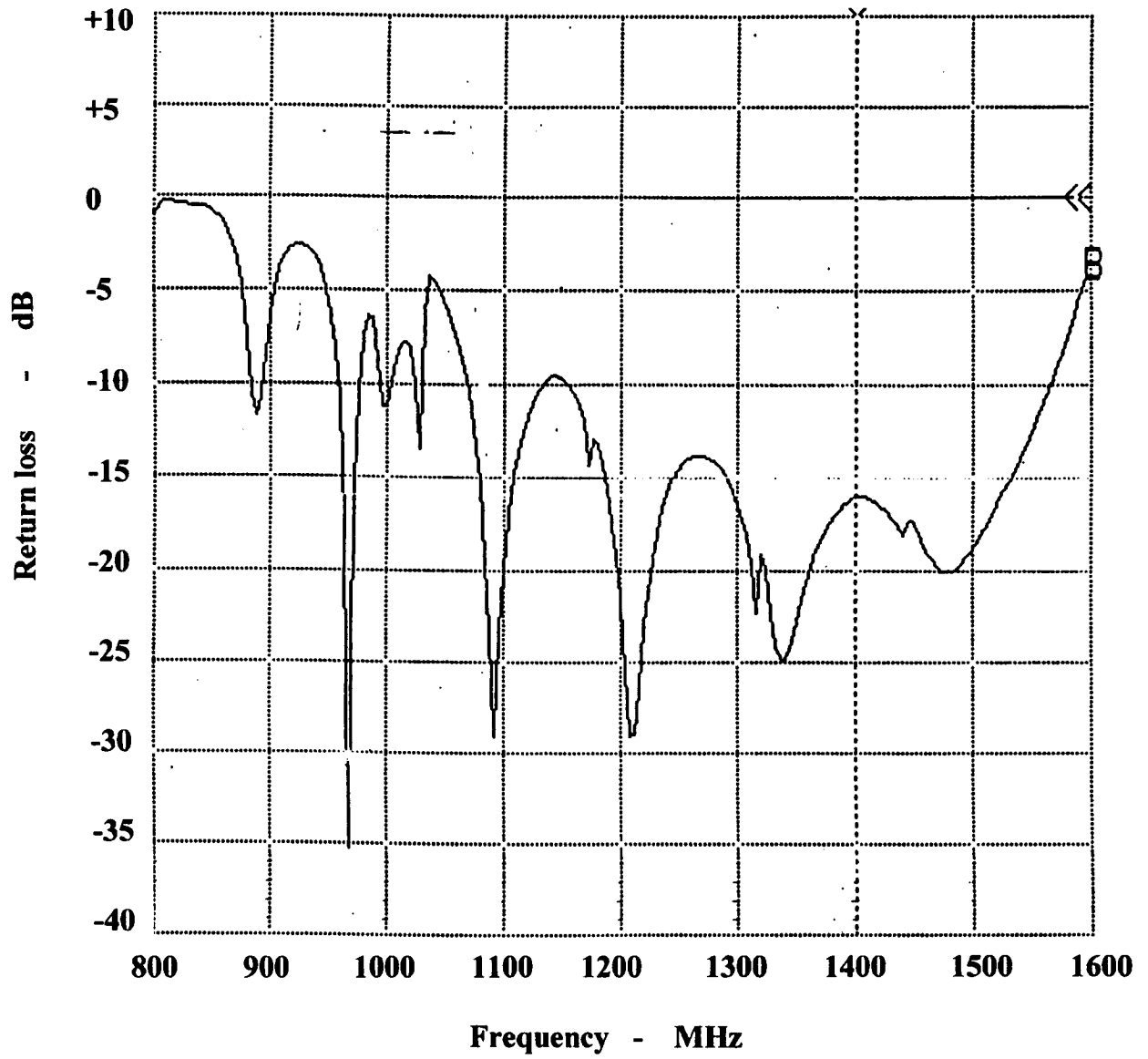


Fig. 3.8.2 : RETURN LOSS CHARACTERISTICS OF THE MODIFIED FEED ASSEMBLY

The reflection coefficient of the feed assembly, as computed from the return loss measurements, is

$$\Gamma = 0.1265 \pm 0.01 . \quad (3.21)$$

The uncertainty in this estimate has been assumed to be the measurement accuracy of the scalar network analyser.

3.9 MEASUREMENT OF THE ABSORPTION COEFFICIENT OF THE FEED ASSEMBLY

The absorption coefficient of the feed assembly is the sum of the absorption coefficients of the corrugated plate and the OMT. When the feed assembly is used as a transmitter, the corrugated plate confines the radiation on-axis and reduces the distant sidelobes by at least 10 dB. Conversely, as a receiving system, the plate ensures that the received power arrives off the surface of the plate thus avoiding ohmic losses in the corrugated plate. Therefore, it has been assumed that the ohmic loss in the corrugated plate is negligible and that the absorption coefficient of the feed assembly is solely due to the ohmic loss in the OMT.

The experimental setup for the measurement of the absorption coefficient of an OMT pair, along with a pair of phase compensation cables, is as shown in Fig. 3.9.1. The absorption coefficient of the OMT+phase compensation cable is determined by combining it with another OMT back-to-back and measuring the ohmic loss in the combined system. The apertures of the two OMTs are bolted together, the H-channel ports are terminated in 50Ω loads and the V-channel ports are connected to identical-length phase compensation cables. The procedure described in section 3.7 for the measurement of the receiver temperature T_R is repeated with the back-to-back OMT+phase compensation cables introduced inbetween the port 1 of the circulator and the load termination that was separately placed in liquid nitrogen and ambient water baths. With these measurements, the absorption coefficient (α) is determined as follows:

Let T_R be the receiver temperature before the introduction of the OMT pair,

T_R' be the receiver temperature after the introduction of the OMT pair,

α_p be the absorption coefficient of the OMT pair along with the two phase compensation cables,

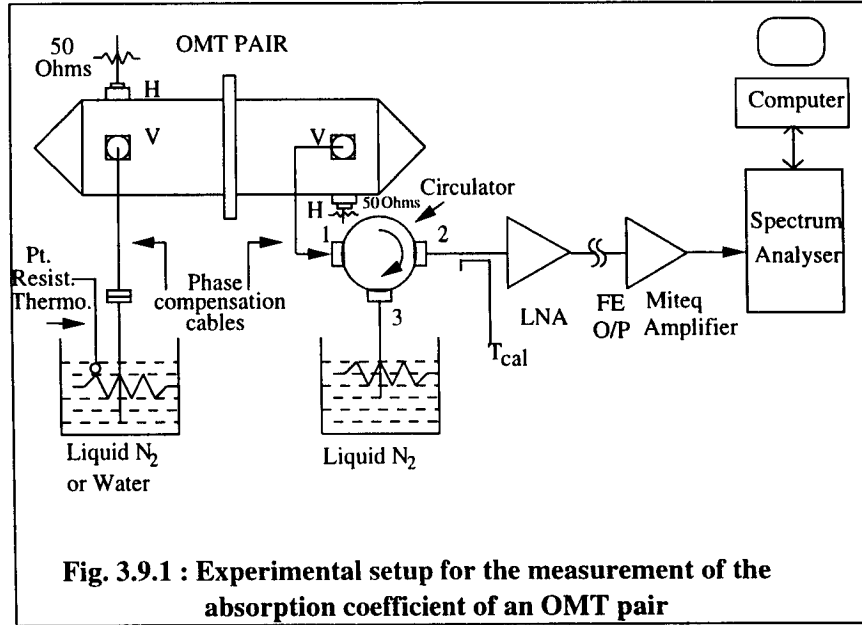
P_1 be the output power of the receiver with the CAL OFF when the input termination is immersed in liquid nitrogen,

P_2 be the output power of the receiver with the CAL ON when the input termination is immersed in liquid nitrogen,

G be the total gain of the system,

T_L be the small leakage signal at port 2 due to the load at port 3 of the circulator, and

Γ_o be the voltage reflection coefficient of the OMT pair.



Because the OMTs are identical in electrical characteristics, each OMT may be considered to have a voltage reflection coefficient of $\Gamma_o/2$ at its input port. In the back-to-back connected OMT pair, we may assume that the impedance discontinuity is primarily at the ports and that there is continuity at the mouths of the OMTs where they are joined together. It may also be noted that the reflection coefficient attributed to each OMT in the back-to-back connected pair, $\Gamma_o/2$, may be different from the reflection coefficient of an OMT with the mouth open to sky (this was measured in the preceding section). The power output of the receiver, after the introduction of the back-to-back OMT pair, may be written as

$$P_1 = G \left[[T_N(1 - \alpha_p)(1 - \frac{\Gamma_o^2}{4}) + \alpha_p T_{amb}](1 - \frac{\Gamma_o^2}{4}) + T_R + T_L \right]. \quad (3.22)$$

and

$$P_2 = G \left[[T_N(1 - \alpha_p)(1 - \frac{\Gamma_o^2}{4}) + \alpha_p T_{amb}](1 - \frac{\Gamma_o^2}{4}) + T_R + T_L + T_{CAL} \right]. \quad (3.23)$$

Equation (3.22) may be rewritten in the form

$$P_1 = G(1 - \alpha_p)\left(1 - \frac{\Gamma_o^2}{4}\right)^2 \left[T_N + \frac{\alpha_p T_{amb}}{(1 - \alpha_p)\left(1 - \frac{\Gamma_o^2}{4}\right)} + \frac{T_R + T_L}{(1 - \alpha_p)\left(1 - \frac{\Gamma_o^2}{4}\right)^2} \right]. \quad (3.24)$$

From this equation it follows that the new receiver temperature T_R' is equal to

$$T_R' = \left[\frac{\alpha_p T_{amb}}{(1 - \alpha_p)\left(1 - \frac{\Gamma_o^2}{4}\right)} + \frac{T_R + T_L}{(1 - \alpha_p)\left(1 - \frac{\Gamma_o^2}{4}\right)^2} \right]. \quad (3.25)$$

In a similar way, the new cal temperature T_{CAL}' is

$$T_{CAL}' = \left[\frac{T_{CAL}}{\left(1 - \alpha_p\right)\left(1 - \frac{\Gamma_o^2}{4}\right)^2} \right] \quad (3.26)$$

from equation (3.23). Substituting the value of α_p obtained in terms of T_{CAL} , T_{CAL}' and Γ_o from equation (3.26), in the equation (3.25), the value of Γ_o is calculated to be 0.1824. The value of $\alpha_p/2$ was then obtained using equation (3.26). $\alpha_p/2$ gives the absorption coefficient of a single OMT along with a phase compensation cable.

The measurements yielded the value of T_R' to be 80.3 ± 1.4 K when the ambient temperature was 31.2 °C. The absorption coefficient was determined to be

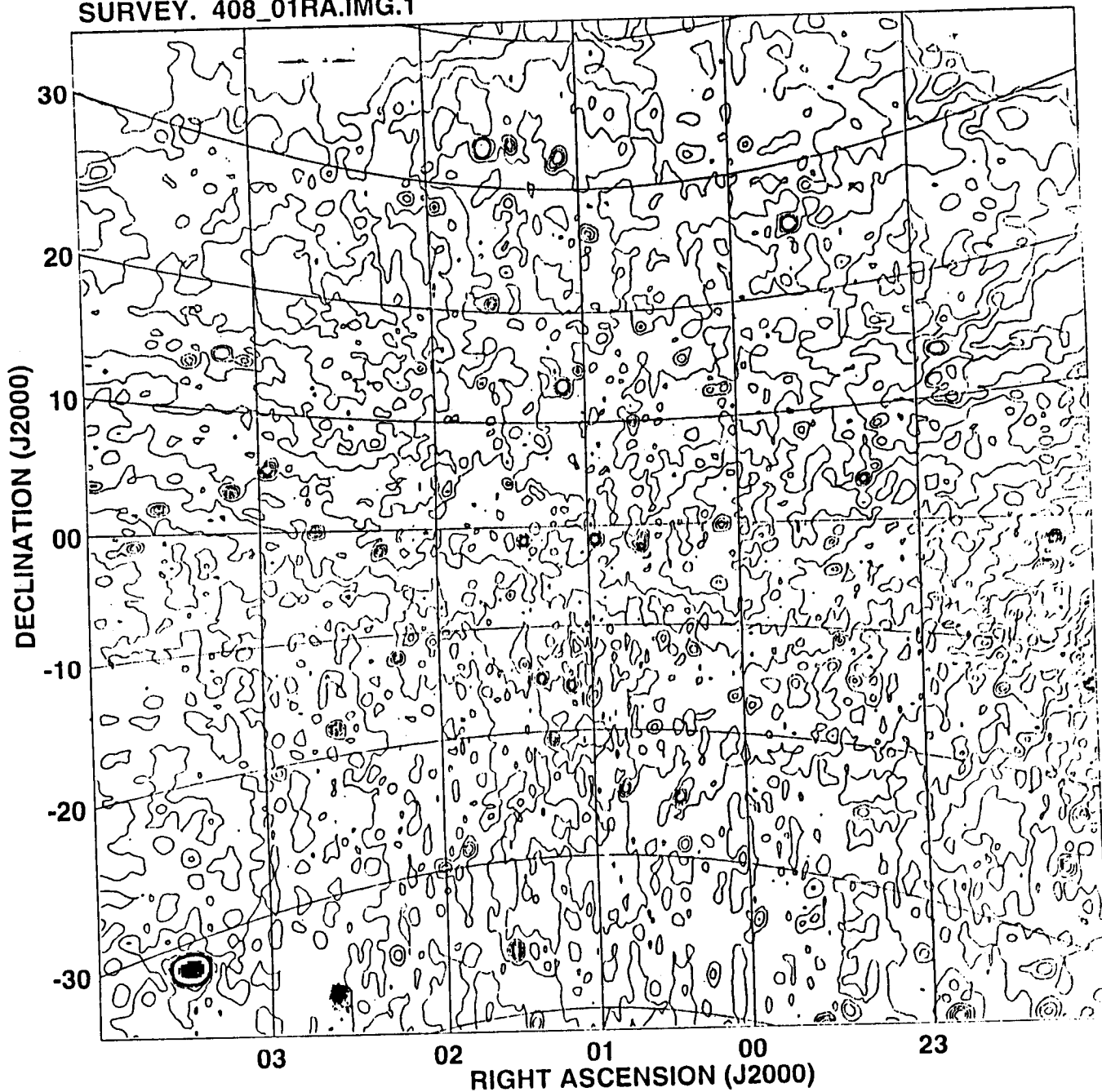
$$\alpha_p/2 = 0.031059 \pm 0.0016. \quad (3.27)$$

3.10 ESTIMATE OF THE GALACTIC CONTRIBUTION (T_{Gal})

The Galactic contribution to the sky signal is obtained from a 408 MHz all sky map (Haslam et al. 1981). Fig. 3.10.1 shows the all sky map at 408 MHz with the brightness temperature of the sky in the form of contours. The sky coordinates are in declination and right ascension; these are equatorial co-ordinates on the celestial sphere and are analogous respectively to latitude and longitude coordinates on the earth. Before estimating the temperature from 408 MHz map, the map is convolved with the beam (Fig. 3.3.3, section 3.3.1.1) of the modified 21 cm front end receiver. This was determined by measuring the radiation pattern of the corrugated plate+OMT combination. Fig. 3.10.2 shows the convolved map of all sky at 408 MHz.

The Galactic background brightness temperature T_{Gal} varies as $\nu^{-\alpha}$ with frequency ν where α is the spectral index. The temperature spectral index is approximately 2.7 (Platania et al.1997) and we assume that this adopted index may have an uncertainty of ± 0.2 . If T_ν is the Galactic brightness temperature at a frequency ν , then

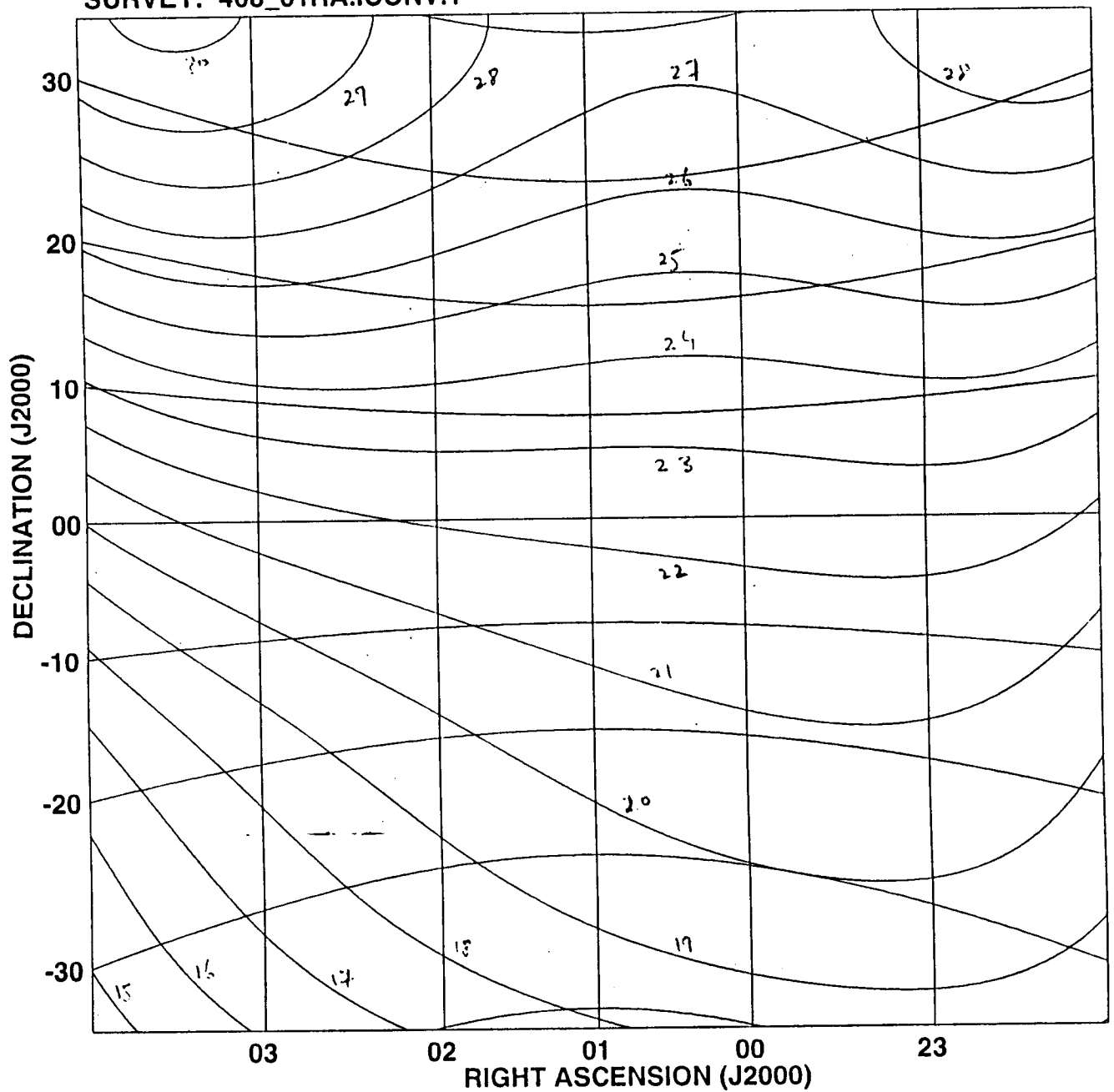
SURVEY. 408_01RA.IMG.1



Grey scale flux range= 120.0 1000.0
Peak contour flux = 1.7892E+03
Levs = 1.0000E+01 * (14.00, 16.00, 18.00,
20.00, 22.00, 24.00, 26.00, 28.00, 30.00)

**Fig. 3.10.1 : THIS PAGE CONTAINS THE 408 MHz SKY BRIGHTNESS DISTRIBUTION
AS MEASURED BY HASLAM et al. 1981**

SURVEY. 408_01RA.ICONV.1



Peak flux = $3.0214E+02$
 Levs = $1.0000E+01 * (15.00, 16.00, 17.00,$
 $18.00, 19.00, 20.00, 21.00, 22.00, 23.00,$
 $24.00, 25.00, 26.00, 27.00, 28.00, 29.00,$
 $30.00)$

**Fig. 3.10.2 : CONVOLVED MAP OF THE SKY AT 408 MHZ OVER
 THE DECLANATION (-30 TO 30) DEG. AND RIGHT ASCENSION
 (24 H TO 04 H)**

$$T_\nu \propto \nu^{-\alpha}, \quad \text{or}$$

$$T_\nu = K\nu^{-\alpha}. \quad (3.28)$$

Using the above relation, the brightness temperature at any two frequencies ν_1 and ν_2 can be written as

$$\frac{T_{\nu_1}}{T_{\nu_2}} = \left(\frac{\nu_1}{\nu_2}\right)^{-\alpha}. \quad (3.29)$$

For $\nu_1 = 408$ MHz, $\nu_2 = 1280$ MHz and $\alpha = 2.7$ we have

$$\frac{T_{408}}{T_{1280}} = \left(\frac{408}{1280}\right)^{-2.7} \quad \text{or} \quad (3.30)$$

$$T_{1280} = T_{408} \left(\frac{408}{1280}\right)^{-2.7}. \quad (3.31)$$

The sky background observations were made towards zenith from the radio observatory site at Gauribidanur which is at a latitude of $+13^\circ 5'$. The observations were made at night to avoid the Sun. The sky region observed was away from the Galactic plane and was at approximately RA:10–12^h and DEC: $+13^\circ 5'$. The value of the sky brightness T_{408} towards this region is 18 ± 2 K in the 408 MHz all sky map. Assuming that the CMBR temperature at 408 MHz is 2.7 K, the Galactic background temperature at 408 MHz may be 15.3 ± 2 K. From equation 3.30, the Galactic contribution at 1280 MHz is calculated to be

$$T_{Gal} = 0.9 \pm 0.3 \text{ K}. \quad (3.32)$$

The uncertainty in this estimate is because of the uncertainty in the 408-MHz absolute temperature scale and also the uncertainty in the spectral index of the Galactic background.

3.11 ESTIMATE OF THE ATMOSPHERIC CONTRIBUTION (T_{atm})

A multiple slab model for the atmosphere (Cernicharo et al.) has been used to estimate the contribution of the atmosphere to the sky temperature. The model relates the physical parameters of the atmosphere slabs to be consistent with the altitude and latitude of the site and the local temperature, pressure, and zenith column density of water vapour. A prediction is made for the atmospheric emission brightness temperature. The Gauribidanur observatory is at $13^\circ 36' 16''$ North latitude and at an elevation of 686 m; the ground temperature of the atmosphere is assumed to be 25°C , pressure to be 931 mB, and the zenith column density

of water vapour is assumed to be less than 10 mm. Using this model, the atmosphere contribution (T_{atm}) at zenith is estimated to be

$$T_{atm} = 1.55 \pm 0.2 \text{ K.} \quad (3.33)$$

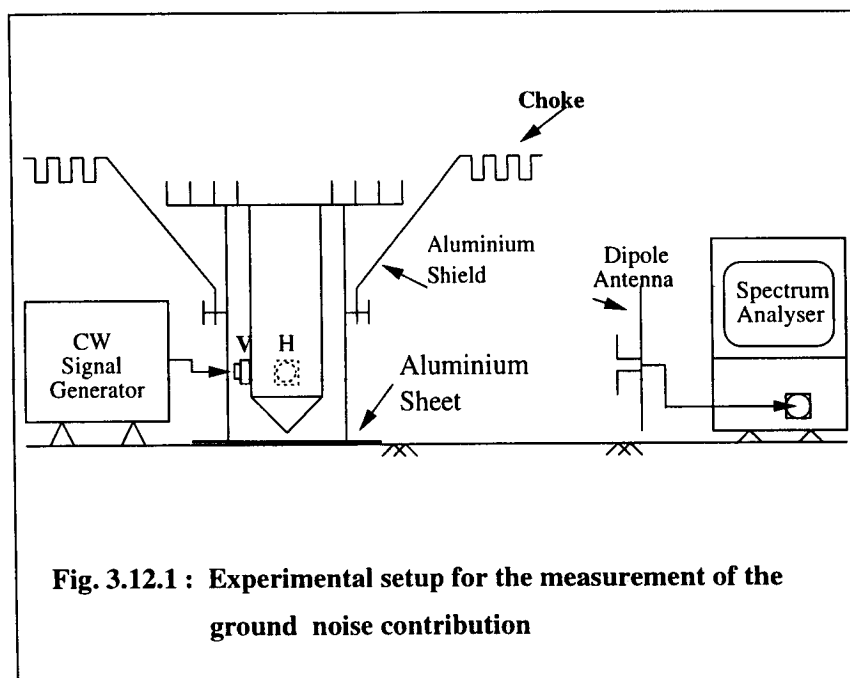


Fig. 3.12.1 : Experimental setup for the measurement of the ground noise contribution

3.12 ESTIMATE OF THE GROUND CONTRIBUTION (T_{gnd})

The amount of ground signal picked up by the receiver is measured by using the experimental setup shown in Fig. 3.12.1. The OMT is fed a 1280 MHz signal from a signal generator. A dipole, whose output is connected to a spectrum analyser is kept on the ground at various distances from the receiver. The power picked up by the dipole is noted at different positions. This experiment is carried out separately with and without the corrugated plate and the aluminium shield. The isolation between the ground and the receiver is calculated from the power measured by the dipole and the results obtained are given in Table 3.1. From the isolation measured, it is estimated that less than about 0.1% of the ground noise temperature gets into the receiver. The receiver box has a rectangular cross-section whereas the base of the shield has a square section: there are gaps on two sides between the receiver box and shield. Consequently, the measured ground leakage was greater close to the receiver box. To avoid this leakage, the ground close to the receiver was covered with aluminium sheets. With these ground sheets, ground shield and corrugated plate all in place, and assuming the temperature of the ground to be 30°C, the ground contribution is estimated to be

$$T_{gnd} = 0.3 \pm 0.3 \text{ K.} \quad (3.34)$$

Sl. No.	Isolation measured with	Isolation(dB) when Distance between receiver and the dipole is		
		1 m	3 m	5 m
1.	OMT	10	12.5	14.5
2.	OMT + Corrugated Plate	19	20.5	20.5
3.	OMT+ Shield	25.5	37.5	27.5
4.	OMT + Shield+ Corrugated plate	38.5	38.5	34.5

Table 3.1 : Isolation between the ground and the receiver under various experimental setups.

3.13 MEASUREMENT OF THE COSMIC MICROWAVE BACKGROUND TEMPERATURE (T_{CMB})

Measurement of the sky signal is made by pointing the receiver towards zenith. The time of observation is selected in such a way that during the period of observation the Galactic plane is far outside the primary beam of the receiver. The observations are also made at night to avoid the Sun.

Let P_1 and P_2 be the powers measured on the sky when the CAL is ON and OFF respectively. Therefore, we have

$$(T_a + T_R + T_{CAL}) \propto P_1 \quad (3.35)$$

$$T_a + T_R \propto P_2 \quad (3.36)$$

Taking the ratio of the two equations and equating it to a variable 'x', we get

$$x = \frac{P_1 - P_2}{P_2} = \frac{T_{CAL}}{T_a + T_R} \quad (3.37)$$

Measurement Parameter	Absolute Value	Uncertainty in the measurement \pm K
T_R	52.12 K	0.51
T_{cal}	70.166 K	0.215
T_{gal}	0.9 K	0.3
T_{atm}	1.55 K	0.2
T_{gnd}	0.3 K	0.3
αT_{amb}	10.0 K	0.5
Γ	0.13	0.01
T'_a	6.2 K	0.68
T_{cmb}	3.45 K	0.78

Table 3.2 : Tabular column showing the magnitude of various noise temperatures measured

$$T_a = \frac{T_{CAL}}{x} - T_R \quad (3.38)$$

But T_a can be written in the form (see Sec. 3.5)

$$T_a = T'_a(1 - \Gamma^2)(1 - \alpha) + \alpha T_{amb} \quad (3.39)$$

where $T'_a = T_{Gal} + T_{atm} + T_{CMB} + T_{gnd}$.

The value of sky temperature T'_a is measured to be 6.2 ± 0.68 K. The cosmic microwave background temperature T_{CMB} is determined by substituting the values of the required parameters as listed in Table 3.2 in the above equations and is found out to be

$$T_{CMB} = 3.45 \pm 0.78 \text{ K}. \quad (3.40)$$

3.14 COMPARISON WITH THE PREVIOUS MEASUREMENTS

The cosmic microwave background temperature has been measured by several groups around the world at various frequencies. Table 3.2 shows those measurements along with the groups involved. The results obtained in the two recent measurements made at 1400 MHz by Staggs et al.(1996) at Princeton and 1470 MHz by Bensadoun et al.(1993) at Berkeley are also tabulated in the table along with their error estimates.

Sl. No.	Frequency MHz	T_{CMB} K	Authors
1.	408	3.7 ± 1.2	Howel, T.F., Shakeshaft,J.R., (1967)
2.	610		
3.	411	3.0 ± 0.5	Stankevich et al. (1970)
4.	640		
5.	600	3.0 ± 1.2	Sironi et al.(1990)
6.	1400	2.65 ± 0.3	Staggs (1996)
7.	1470	2.26 ± 0.19	Bensadoun et al. (1993)

Table 3.3 : Tabular column showing the measurements of T_{CMB} at various frequencies

REFERENCES

- Bensadoun, M., Bersanelli, M., De Amici, G., Kogut, A., Levin, S. M., Limon, M., Smoot, G. F., Witebsky, C., 1993, Measurement of the Cosmic Microwave Background temperature at 1470 MHz, *Astrophys. J.*, 409, p 1.
- Cernicharo, J., Bremer, M., Atmospheric model code developed at IRAM.
- Haslam, C.G.T., Salter, C.J., Stoffel, H., Wilson, W.E., 1982, A 408 MHz All - Sky Continuum Survey.II. The Atlas of Contour Maps, A.A., Suppl. No.47.
- Howell, T.F., Shakeshaft, J.R., 1967, Spectrum of the 3 K Cosmic Microwave Radiation, *Nature*, 216.
- Partridge, R.B., 1995, 3 K : The Cosmic Microwave Background Radiation, Cambridge University Press, Cambridge.
- Platania, P., Bensadoun, M., Bersanelli, M., Amici, G.De., Kogut, A., Levin, S., Maino, D., Smoot, G.F., 1997, A Determination of the Spectral Index of Galactic Synchrotron Emission in the 1-10 GHz range, *Astrophys. J.*, 505, p473.
- Sironi, G., Limon, M., Marcellino, G., Bonelli, G., Bersanelli, M., Conti, G., Reif, K., The absolute temperature of the sky and the temperature of the Cosmic Background Radiation at 600 MHz, *Astrophys. J.*, 357, p 301.
- Staggs, S. T., Jarosik, N.C., Wilkinson, D. T., Wollack, E.J., 1996, An absolute measurement of the Cosmic microwave background radiation temperature at 20 cm , *Astrophys. J.*, 458, p 407.
- Stankevich, K.S., Wielebinski, R., Wilson, W.E., 1970, Radio Sky Background studies using the moon as a screen, *Aust. J. Phys.*, 23, p 529.
- Steven, W., 1978, The First three Minutes - A Modern View of the Origin of the Universe, The Trinity Press, Worcester and London.

CONCLUSIONS

The 21cm front end receivers have been built for the radio observation using GMRT dishes. The performances of these receivers are individually fully characterised. But the performance of the 21cm receiver system including both front end as well as back end is yet to be characterised on the antenna to see how well the receiver meets the required specifications like the cross polarisation level, linearity of the system etc. This receiver is mass produced and installed in all the 30 GMRT antennas.

Regarding the experiment conducted on cosmic microwave background radiation temperature measurement, the absolute value of the measured temperature happens to be slightly on the higher side when compared to the measurements made by several groups across the world. The reasons for this may be i) due to the calibration error or ii) the CMB temperature itself may be higher at the measurement frequency. It should be noted that the CMB temperature of 2.7 K as measured by other groups is within the expected errors of our experiment.